Lectures on thermal convection and turbulence of a stratified fluid

Third year bachelor course, "Turbulence in Fluids" (NS376B)
Department of Physics, Utrecht University.
By Aarnout van Delden (a.j.vandelden@uu.nl)
This version: April 2022

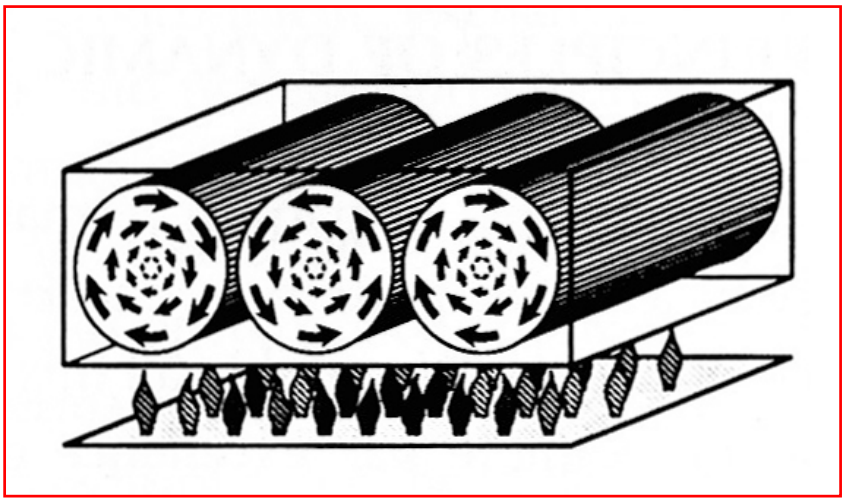

a

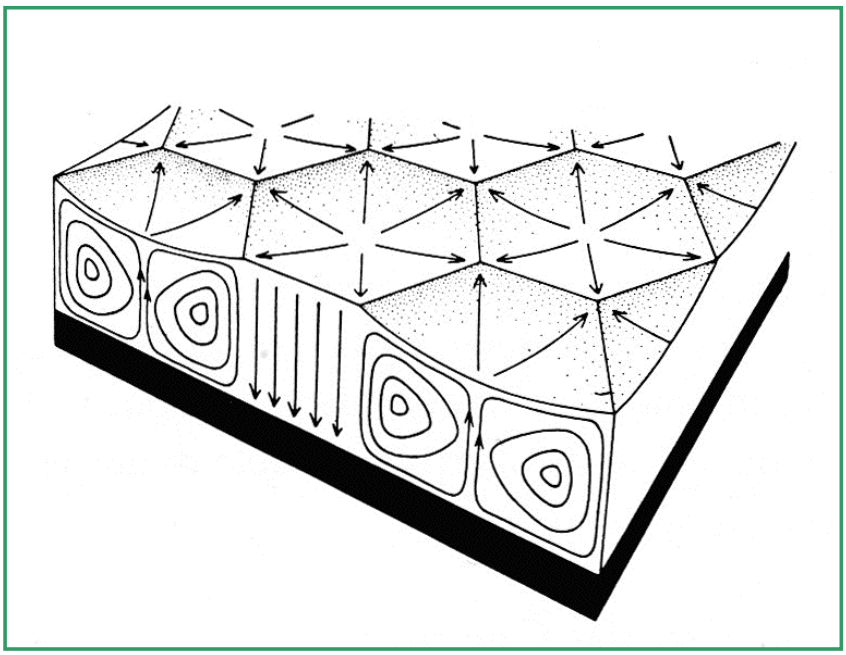

b

Figure 1. Schematic diagram illustrating (a) two-dimensional and (b) three-dimensional hexagonal convection patterns in a fluid, which is heated from below and cooled from above (see the text).

Contents

Part 1: Stability of a stratified fluid in rest

1. Introduction 4
2. Basic equations 4
3. Linear equations for the time-evolution of small perturbations 5
4. Boundary conditions 7
5. Analysis of the stability of the state of rest and the onset of convection 8
6. Exercises part 1 11
7. References part 1 12

Part 2: Spectral model of thermal convection

8. Finite amplitude convection 13
9. Fourier transformation of the governing equations 15
10. Spectral energy cascade in thermal convection 18
11. Lorenz (1963) model 19
12. Exercises part 2 21
13. References part 2 22

Part 3: Chaos and predictability in the Lorenz (1963) model

14. Finite amplitude convection according to the Lorenz model 23
15. Sensitive dependence on initial conditions 25
16. The "Strange Attractor" 26
17. Divergence of nearby trajectories (Lyapunov-exponent) 27
18. Dissipative system: volume contraction in phase space 27
19. Lorenz map: order in chaos? 28
20. Exercise, part 3 30
21. References part 3 31
22. Appendix to part 3: Runge-Kutta approximation to the time-derivative 32

Part 4: Scale selection and spectral energy transfer

23. The question of non-linear scale selection 33
24. Scale selection in a ten-component model of thermal convection 34
25. Upscale kinetic energy transfer in two-dimensional convection 37
26. Spectral blocking in two-dimensional flow 41
27. Exercises, part 4 43
28. References part 4 44

Part 5: Pattern formation in thermal convection

29. The horizontal pattern of thermal convection 45
30. Fourier representation in three spatial dimensions 48
31. The nonlinear equations for three-dimensional convection 49
32. The static temperature profile 50
33. Fourier transformation of the temperature equation 51
34. Three-dimensional poloidal flow 53
35. Boundary conditions and symmetry relations 54
36. A low-order model of poloidal convection: plan-form selection 55
37. A "down-hexagon" becomes an "open cell" in a higher order model 59
38. Exercises, part 5 61
39. References part 5 62
40. Appendix to part 5: Python-code of the spectral model of poloidal convection 63

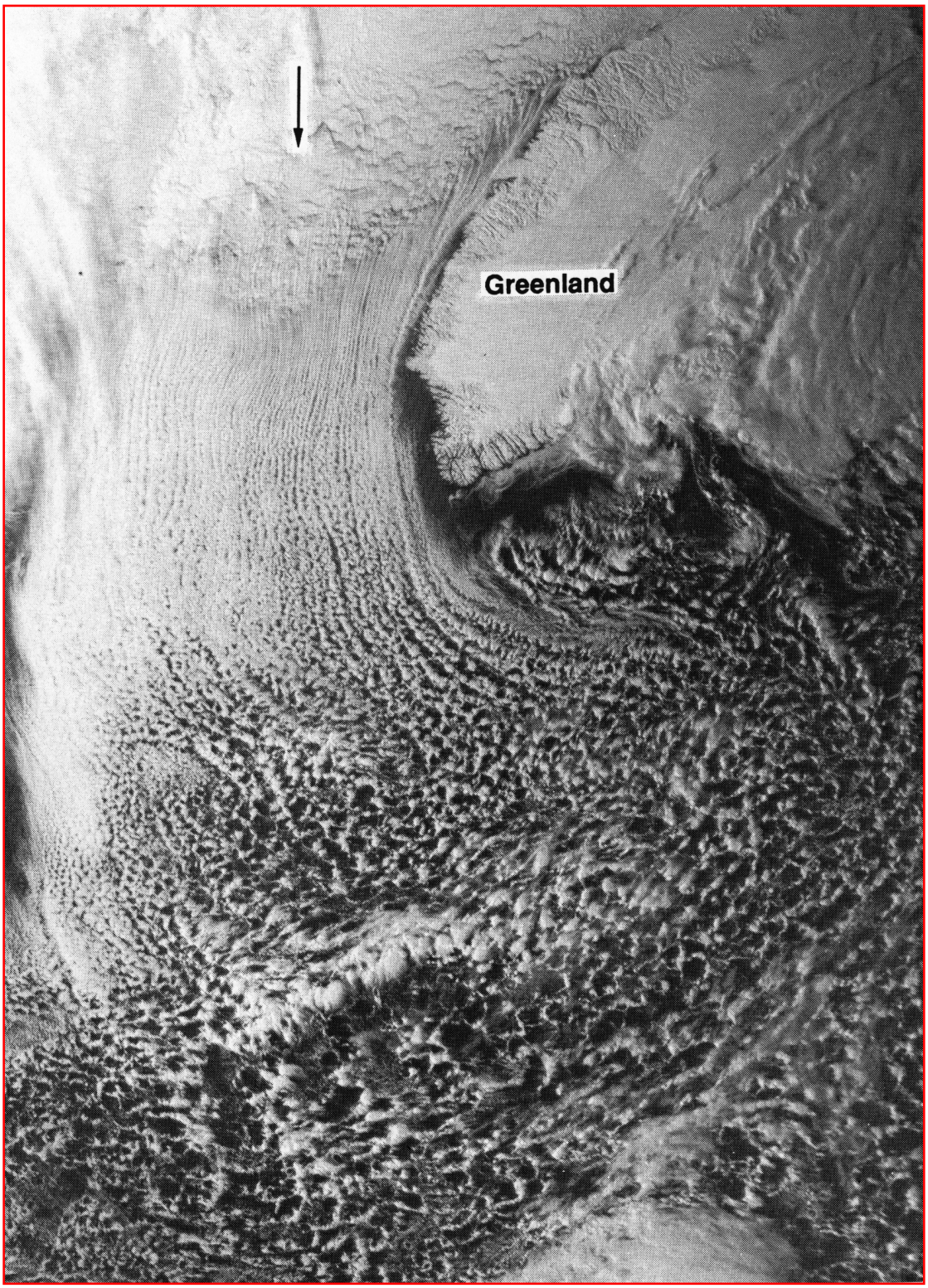

Figure 2. Two- and three-dimensional cloud patterns due to convection in the atmosphere over the North-West Atlantic Ocean and the Labrador Sea. The arrow indicates the direction of the average wind-vector. Cloud streets (two-dimensional convection) are observed in the Labrador Sea, while "open convection cells" (three-dimensional convection) are observed more towards the south over the Atlantic Ocean.

Part 1: Stability of a stratified fluid in rest

By Aarnout van Delden (http://www.staff.science.uu.nl/~delde102/TinF.htm)

1. Introduction

These lecture notes consist of five parts, intended for five two-hour lectures, as part of the third year physics bachelor course on "Turbulence in Fluids" at the University of Utrecht. The topic is the theory of thermal convection of a stratified fluid, under the influence of gravity, between rigid perfectly conducting horizontal boundaries, held at different temperatures (**figure 1**). If the temperature of the lower boundary is higher than the temperature of the upper boundary, a regular pattern of convection cells, consisting of areas of ascending and descending currents, emerges, as is illustrated in **figure 1**. **Figure 2** shows that this phenomenon occurs also in Earth's atmosphere. This prototype problem of fluid flow has been used to study the properties of predictability in, and chaotic solutions of, non-linear deterministic systems, as manifestations of "turbulence", both experimentally and numerically.

2. Basic equations

The basic equations that describe the evolution in time (t) of velocity (u, v, w), temperature (T) and pressure (p) in (x, y,z) space of a viscous fluid under the influence of gravity (g is the acceleration due to gravity) are (see lecture 1 by Anna von der Heydt):

$$\frac{\partial u}{\partial t}+u\frac{\partial u}{\partial x}+v\frac{\partial u}{\partial y}+w\frac{\partial u}{\partial z}=-\frac{1}{\rho}\frac{\partial p}{\partial x}+\nu\nabla^2 u \;; \tag{1}$$

$$\frac{\partial v}{\partial t}+u\frac{\partial v}{\partial x}+v\frac{\partial v}{\partial y}+w\frac{\partial v}{\partial z}=-\frac{1}{\rho}\frac{\partial p}{\partial y}+\nu\nabla^2 v \;; \tag{2}$$

$$\frac{\partial w}{\partial t}+u\frac{\partial w}{\partial x}+v\frac{\partial w}{\partial y}+w\frac{\partial w}{\partial z}=-\frac{1}{\rho}\frac{\partial p}{\partial z}+\nu\nabla^2 w-g \;; \tag{3}$$

$$\frac{\partial u}{\partial x}+\frac{\partial v}{\partial y}+\frac{\partial w}{\partial z}=0 \;; \tag{4}$$

$$\frac{\partial T}{\partial t}+u\frac{\partial T}{\partial x}+v\frac{\partial T}{\partial y}+w\frac{\partial T}{\partial z}=\kappa\nabla^2 T \;. \tag{5}$$

The "Laplace operator" is defined as

$$\nabla^2 \equiv \frac{\partial^2}{\partial x^2}+\frac{\partial^2}{\partial y^2}+\frac{\partial^2}{\partial z^2} \;.$$

The first three equations represent the three components of the equation of motion (**Navier-Stokes equation**). The fourth equation is derived from mass conservation, assuming incompressibility, which is an approximation to any fluid, but holds better for water than for air. Eq. 5 is an expression of Fourier's law applied to a fluid parcel. The temperature of a fluid parcel is conserved, except for the effect of molecular heat conduction (ν and κ are *constant* **molecular diffusion coefficients for momentum and heat**, respectively).

3. Linear equations for the time-evolution of small perturbations

Decompose all variables into a **background steady (static) state plus time-dependent perturbations**:

$$\begin{aligned} u &= 0 + u'(x,y,z,t) \\ T &= T_0(z) + T'(x,y,z,t) \\ p &= p_0(z) + p'(x,y,z,t) \\ \rho &= \rho_0(z) + \rho'(x,y,z,t) \end{aligned} \qquad (6)$$

Perturbations (deviations from the state of rest) are small. This means that e.g. $T' << T_0$, etc. The background state is in **hydrostatic balance**, i.e.

$$\frac{\partial p_0}{\partial z} = -\rho_0 g \qquad (7)$$

Substitute these assumptions into the equations and assume that products of perturbations are small.

$$\frac{\partial u'}{\partial t} = -\frac{1}{(\rho_0 + \rho')}\frac{\partial p'}{\partial x} + \nu\nabla^2 u' \qquad (8)$$

$$\frac{\partial v'}{\partial t} = -\frac{1}{(\rho_0 + \rho')}\frac{\partial p'}{\partial y} + \nu\nabla^2 u' \qquad (9)$$

$$\frac{\partial w'}{\partial t} = -\frac{1}{(\rho_0 + \rho')}\frac{\partial p_0}{\partial z} - \frac{1}{(\rho_0 + \rho')}\frac{\partial p'}{\partial z} + \nu\nabla^2 w' - g \qquad (10)$$

Note that

$$-\frac{1}{(\rho_0 + \rho')}\frac{\partial p_0}{\partial z} = \frac{\rho_0 g}{(\rho_0 + \rho')} = \frac{g}{(1 + \rho'/\rho_0)}$$

so that (10) becomes

$$(1 + \rho'/\rho_0)\frac{\partial w'}{\partial t} = g - \frac{(1 + \rho'/\rho_0)}{(\rho_0 + \rho')}\frac{\partial p'}{\partial z} + \nu(1 + \rho'/\rho_0)\nabla^2 w' - (1 + \rho'/\rho_0)g$$

Now assume that $1 + \rho'/\rho_0 \approx 1$, so that

$$\frac{\partial w'}{\partial t} \approx -\frac{1}{\rho_0}\frac{\partial p'}{\partial z} + \nu\nabla^2 w' - g\frac{\rho'}{\rho_0} \tag{11}$$

Likewise:

$$\frac{\partial u'}{\partial t} \approx -\frac{1}{\rho_0}\frac{\partial p'}{\partial x} + \nu\nabla^2 u' \tag{12}$$

$$\frac{\partial v'}{\partial t} \approx -\frac{1}{\rho_0}\frac{\partial p'}{\partial y} + \nu\nabla^2 v' \tag{13}$$

The approximate **equation of state** for a typical fluid is

$$\rho = \rho_0\left(1 - \alpha\left(T - T_0\right)\right) \tag{14}$$

(α is the coefficient of thermal expansion), so that

$$\rho' = -\alpha\rho_0 T' \tag{15}$$

The last term in eq. 11 (the "**buoyancy term**") becomes

$$-g\frac{\rho'}{\rho_0} = g\alpha T' \tag{16}$$

Further details of this linearisation of the equation of motion (commonly referred to as "**Boussinesq approximation**") can be found in the well-known paper by Spiegel and Veronis (1960) (see the list of references).

The temperature equation, linearised around the basic state of rest, is

$$\frac{\partial T'}{\partial t} + w'\frac{\partial T_0}{\partial z} = \kappa\nabla^2 T' \tag{17}$$

In the state of rest, the fluid possesses a vertical temperature gradient if the temperature of the lower boundary differs from the temperature of the upper boundary. The associated "**lapse rate**",

$$\frac{\partial T_0}{\partial z} = \frac{dT_0}{dz} \equiv -\Gamma\ , \tag{18}$$

is the constant vertical temperaure gradient which is sustained by molecular conduction when there is no macroscopic motion. Eq. 15 becomes

$$\frac{\partial T'}{\partial t} = \Gamma w' + \kappa\nabla^2 T' \tag{19}$$

Take the ∇^2 of eq. 11 and substituting (16) yields

$$\frac{\partial \nabla^2 w'}{\partial t} \approx -\frac{1}{\rho_{ref}} \frac{\partial \nabla^2 p'}{\partial z} + \nu \nabla^2 \nabla^2 w' + g\alpha \nabla^2 T' \tag{20}$$

For simplicity we have assumed that $\rho_0 \approx \rho_{ref} = \text{constant}$. Now, take $\partial/\partial x$ of (12), $\partial/\partial y$ of (13), $\partial/\partial z$ of (11) and add the results, and then use (4) and (16):

$$\nabla^2 p' = g\alpha\rho_{ref} \frac{\partial T'}{\partial z} \tag{21}$$

With this (20) becomes

$$\frac{\partial \nabla^2 w'}{\partial t} = \nu \nabla^2 \nabla^2 w' + g\alpha \nabla_H^2 T' \tag{22}$$

where

$$\nabla_H^2 \equiv \frac{\partial^2}{\partial x^2} + \frac{\partial^2}{\partial y^2} \ . \tag{23}$$

4. Boundary conditions

Eqs. (19) and (22) form a closed set of two equations governing the time evolution of small perturbations in a fluid with respect to the state of rest. We apply this set of equations to a fluid between horizontal, **perfectly conducting, stress-free** boundaries, which are maintained at different fixed temperatures. The lower plate is at z=0; the upper plate is at z=H. Therefore, we set

$$w' = 0 \text{ at } z = 0 \text{ and } z = H \tag{24}$$

Stress-free conditions implies

$$\frac{\partial u}{\partial z} = \frac{\partial v}{\partial z} = 0 \text{ at } z = 0 \text{ and } z = H \tag{25}$$

With (4) this implies that

$$\frac{\partial^2 w'}{\partial z^2} = 0 \text{ at } z = 0 \text{ and } z = H \tag{26}$$

A fixed temperature implies that

$$T' = 0 \text{ at } z = 0 \text{ and } z = H \tag{27}$$

In view of (19) this implies

$$\frac{\partial^2 T'}{\partial z^2} = 0 \text{ at } z = 0 \text{ and } z = H \tag{28}$$

5. Analysis of the stability of the state of rest and the onset of convection

We now simplify the problem by reducing it to a two-dimensional problem. If $\partial/\partial y=0$, the flow takes place in a two-dimensional vertical cross-section. Eqs. (19) and (22) become

$$\boxed{\frac{\partial T'}{\partial t} = \Gamma w' + \kappa \left(\frac{\partial^2}{\partial x^2} + \frac{\partial^2}{\partial z^2} \right) T'} \tag{29}$$

and

$$\boxed{\frac{\partial}{\partial t}\left(\frac{\partial^2}{\partial x^2} + \frac{\partial^2}{\partial z^2} \right) w' = g\alpha \frac{\partial^2 T'}{\partial x^2} + \nu \left(\frac{\partial^2}{\partial x^2} + \frac{\partial^2}{\partial z^2} \right)^2 w'} \tag{30}$$

On an infinite domain in the horizontal direction, the solution, which is consistent with the boundary conditions (24), (26), (27) and (28), corresponds to the *real part* of

$$w' = W \exp\{ilx + \sigma t\} \sin\left(\frac{\pi n z}{H}\right); \; T' = \Theta \exp\{ilx + \sigma t\} \sin\left(\frac{\pi n z}{H}\right). \tag{31}$$

Physically, this solution represent a wave-like, or cellular, fluid motion/temperature pattern. The parameters, l, n, σrepresent, respectively, the horizontal wave number, the vertical wave number and the **growth- or damping rate** of this wave-like motion- or temperature-pattern. The real solution of w' and T' consists of a superposition of these wave-like "**Fourier modes**". In the "linear phase", i.e. when the perturbations are very small, so that the linear equations (29) and (30) are valid, these Fourier modes do not interact. The growth or decay of each Fourier mode is independent of the growth or decay of all other Fourier modes.

We determine the fastest growing "mode", as follows. Substitute (31) into (29) and (30):

$$-\sigma k^2 W = -g\alpha l^2 \Theta + \nu k^4 W \; ;$$

$$\sigma \Theta = \Gamma W - \kappa k^2 \Theta \; . \tag{32}$$

Here

$$k^2 = l^2 + \left(\frac{\pi n}{H}\right)^2 . \tag{33}$$

Rewrite this linear homogeneous system of two equations as

$$MX = 0 \; , \tag{34}$$

where the vector, X, is

$$X = \begin{pmatrix} W \\ \Theta \end{pmatrix} \tag{35}$$

and the matrix, M, is

$$M = \begin{pmatrix} -\sigma k^2 - \nu k^4 & g\alpha l^2 \\ \Gamma & -\sigma - \kappa k^2 \end{pmatrix}. \tag{36}$$

A non-trivial solution exists if the determinant of M is zero, which yields

$$\left(\sigma k^2 + \nu k^4\right)\left(\sigma + \kappa k^2\right) - g\alpha l^2 \Gamma = 0 \ , \tag{37}$$

which yields a quadratic equation for the growth-rate, σ

$$\sigma^2 + (\nu + \kappa)k^2\sigma + \nu\kappa k^4 - \frac{g\alpha l^2 \Gamma}{k^2} = 0 \, . \tag{38}$$

The solution is

$$\sigma = -\frac{(\nu + \kappa)k^2}{2} \pm \frac{1}{2}\left((\nu + \kappa)^2 k^4 - 4\left(\nu\kappa k^4 - \frac{g\alpha l^2 \Gamma}{k^2}\right)\right)^{1/2} . \tag{39}$$

The **growth-rate**, σ, is positive , i.e. the state of rest is unstable to small perturbations, if

$$-4\left(\nu\kappa k^4 - \frac{g\alpha l^2 \Gamma}{k^2}\right) > 0 \, , \tag{40}$$

or if

$$\boxed{\Gamma > \frac{\nu\kappa k^6}{g\alpha l^2} = \frac{\nu\kappa}{g\alpha l^2}\left(l^2 + \left(\frac{\pi n}{H}\right)^2\right)^3}. \tag{41}$$

Evidently, the growth rate of the perturbations is positive if the lapse rate (vertical temperature gradient) exceeds a threshold value, which depends, among other, on the horizontal wave number, l, and on the vertical wave number, n. The lapse rate at which disturbances are marginally stable is designated as the "**critical lapse rate**":

$$\boxed{\Gamma_{crit} = \frac{\nu\kappa}{g\alpha l^2}\left(l^2 + \left(\frac{\pi n}{H}\right)^2\right)^3}. \tag{42}$$

The minimum value of Γ_{crit} occurs at the minimum value of n, which is n=1, and if

$$\frac{\partial \Gamma_{crit}}{\partial\left(l^2\right)} = 0 \ , \tag{43}$$

which corresponds to

$$l^2 = \frac{1}{2}\left(\frac{\pi}{H}\right)^2, \tag{44}$$

if n=1. Because

$$l = \frac{2\pi}{L} \ . \tag{45}$$

This corresponds to

$$L = 2\sqrt{2}H \ . \tag{46}$$

The *preferred horizontal wavelength* of an exponentially growing pattern of convection cells is $2\sqrt{2}\approx 2.8$ times the depth of the layer. One individual cell has an **aspect ratio** (horizontal scale divided by vertical scale= L/H) equal to $\sqrt{2}$. This is in reasonable agreement with the laboratory observations, shown in **figure 3**. One convection cell spans the full depth of the fluid, i.e. the solution (30) with n=1 is "selected" in reality, as is predicted in theory.

Lord Rayleigh (John William Strutt) (1842-1919), winner of the 1904 Nobel prize for Physics, published these theoretical results in 1916. Rayleigh was inspired by laboratory experiments due to Henri Bénard (1874-1939), which were published in 1900 (see list of references to part 1 in section 7). Thermal convection in stratified viscous fluids between horizontal boundaries under the influence of gravity is frequently referred to as "**Rayleigh-Bénard convection**".

Figure 3. Side-view (differential interferograms) of two-dimensional convection cells in silicone oil in a rectangular box of relative dimensions 10:4:1, which is heated from below. Uniform heating produces convection "rolls" parallel to the shorter side (Van Dyke, 1982). The flow pattern is remarkable orderly!

6. Exercises, part 1

(1)

The aspect ratio of observed convection cells (**figure 3**) is not exactly in agreement with the prediction made by Lord Rayleigh's theory. Give at least three likely reasons for this (slight) disagreement?

(2)

The instability criterion (41) is commonly expressed in terms of the so-called **Rayleigh number**, Ra, which is a non-dimensional number, defined as

$$\boxed{\mathrm{Ra} \equiv \frac{g\alpha\Gamma H^4}{\kappa\nu}}. \tag{47}$$

What is the critical value of the Rayleigh number at the preferred horizontal wavelength? Plot the marginal value of the Rayleigh number as a function of the aspect ratio, L/H, where the Rayleigh number is the ordinate. Identify the region of instability in this graph. Will this curve shift upwards or downwards if no-slip conditions are imposed on the upper and lower boundaries, instead of stress-free conditions (section 4)?

(3)

Each "mode" possesses a "critical modal Rayleigh number" at which linear stability sets in. At which minimum "critical modal Rayleigh number" is a "mode" with n=2 unstable.

(4)

Express eqs. (29) and (30),

$$\boxed{\frac{\partial T'}{\partial t} = \Gamma w' + \kappa\left(\frac{\partial^2}{\partial x^2} + \frac{\partial^2}{\partial z^2}\right)T'} \tag{29}$$

and

$$\boxed{\frac{\partial}{\partial t}\left(\frac{\partial^2}{\partial x^2} + \frac{\partial^2}{\partial z^2}\right)w' = g\alpha\frac{\partial^2 T'}{\partial x^2} + \nu\left(\frac{\partial^2}{\partial x^2} + \frac{\partial^2}{\partial z^2}\right)^2 w'} \tag{30}$$

in dimensionless form, in terms of the following units

$$\{L\} = H;\ \{t\} = \frac{H^2}{\kappa};\ \{T\} = \frac{\kappa\nu}{g\alpha H^3}\ . \tag{48}$$

Verify that $\{t\}$ has the unit of time (seconds) and that $\{T\}$ has the units of temperature (degrees Kelvin). The new (non-dimensional) unit of time, t^*, is

$$t^* \equiv \frac{\kappa}{H^2} t \ . \qquad (49)$$

The system of eqs. 29 and 30 contains 5 imposed parameters, which may determine the solution. In the non-dimensional form we discover that the solution depends on only two parameters: the Rayleigh number and a second non-dimensional number, which is commonly referred to as the "**Prandtl number**", Pr. Identify the Prandtl number.

7. References part 1

Aubin, D., 2008: "The memory of life itself": Bénard's cells and the cinematography of self-organization. **Stud.Hist.Phil.Sci., 39**, 359-369.

Getling A.V., 1998: **Rayleigh-Bénard Convection: Structures and Dynamics**. World Scientific Publishing, Singapore. 245 pp.

Lord Rayleigh, 1916: On convection currents in a horizontal layer of fluid when the higher temperature is on the under side. **Philosophical Magazine** S.6. vol 32, no. 192, pp. 529-546.

Spiegel, E.A., and G. Veronis, 1960: On the Boussinesq approximation for a compressible fluid. **The Astrophysical Journal**, vol. 131, pp. 442-447.

Van Dyke, M., 1982: **An Album of Fluid Motion**. The Parabolic Press, Stanford, California, 174 pp.

Part 2: Spectral model of thermal convection

By Aarnout van Delden (http://www.staff.science.uu.nl/~delde102/TinF.htm)

8. Finite amplitude convection

This section introduces the problem of *finite amplitude* thermal convection between horizontal, stress-free, perfectly conducting boundaries. At Rayleigh numbers above the minimum critical value many wave-like disturbances, or so-called "Fourier modes", grow to appreciable amplitudes, so that non-linear interactions between these modes cannot be neglected. The problem becomes very complicated, as we shall see in the following. Here, we restrict our attention to interactions between unstable waves and the horizontal mean state. **Figure 4** shows laboratory observations of the horizontal-mean steady temperature in a fluid layer undergoing convection at different Rayleigh numbers. Initially, when the fluid is in rest, the horizontal mean temperature is linear with height (eq. 18). After convection is initiated by hydrostatic instability, warm fluid is carried upward and cold fluid is carried downward. Temperature increases above mid-level, while it decreases below mid-level. This process reduces the potential energy of the fluid. The fluid layer becomes more stable around mid-level and less stable near the lower and upper boundaries.

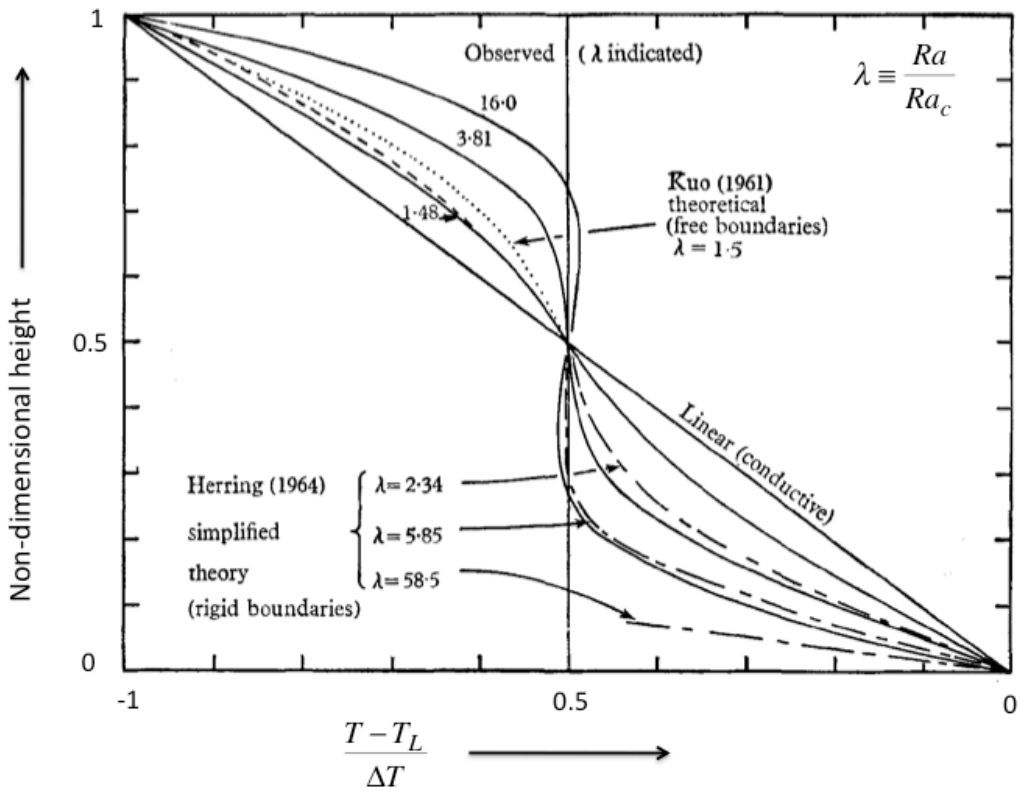

Figure 4. Horizontally averaged steady state temperature profiles at various normalised Rayleigh numbers, for sea-water with a salinity 3.5 %. T_L is the temperature of the lower boundary; ΔT is the temperature difference between upper and lower boundary. The height is scaled with the depth of the fluid layer, H. Note that convection warms the upper half of the fluid as much as it cools the lower half of the fluid. This is figure 8 in the paper by Gille, J., 1967: Interferometric measurement of temperature gradient reversal in a layer of convecting air. **J. Fluid Mech.**, **30**, 371- 384.

As in the linear analysis of the previous sections, we restrict our attention to two-dimensional flow in the *x*-*z* plane. The continuity eq. 4 now becomes

$$\frac{\partial u}{\partial x}+\frac{\partial w}{\partial z}=0\ . \tag{50}$$

We may then introduce a **stream function**, ψ, as follows

$$\boxed{u=-\frac{\partial \psi}{\partial z};\ w=\frac{\partial \psi}{\partial x}}\ , \tag{51}$$

so that the flow pattern is described by one variable, i.e. the stream function, ψ. The flow in the *x*-*z* plane is described by eqs. 1 and 3. Including the Boussinesq approximation (section 3), these are

$$\frac{\partial u}{\partial t}+u\frac{\partial u}{\partial x}+w\frac{\partial u}{\partial z}=-\frac{1}{\rho_{ref}}\frac{\partial p'}{\partial x}+\nu\nabla^2 u \tag{52}$$

$$\frac{\partial w}{\partial t}+u\frac{\partial w}{\partial x}+w\frac{\partial w}{\partial z}=-\frac{1}{\rho_{ref}}\frac{\partial p'}{\partial z}+\nu\nabla^2 w-g\alpha T' \tag{53}$$

By taking the *z*-derivative of (52) and subtracting the result from the *x*-derivative of (53) these two equations can easily be reduced to

$$\frac{d\nabla^2\psi}{dt}=\frac{\partial}{\partial t}\nabla^2\psi-\frac{\partial \psi}{\partial z}\frac{\partial}{\partial x}\nabla^2\psi+\frac{\partial \psi}{\partial x}\frac{\partial}{\partial z}\nabla^2\psi=\alpha g\frac{\partial T'}{\partial \mathrm{x}}+\nu\nabla^2\nabla^2\psi\ . \tag{54}$$

With the temperature equation (5), which is repeated here:

$$\frac{\partial T'}{\partial t}-\frac{\partial \psi}{\partial z}\frac{\partial T'}{\partial x}+\frac{\partial \psi}{\partial x}\frac{\partial T'}{\partial z}=\Gamma\frac{\partial \psi}{\partial x}+\kappa\nabla^2 T'\ , \tag{55}$$

this forms a closed set with two unknowns.

With the following non-dimensional units

$$\text{length}=H;\ \text{time}=\frac{H^2}{\kappa};\ \text{temperature}=\frac{\kappa\nu}{g\alpha H^3}\ , \tag{56}$$

eqs. (54) and (55) become, repectively

$$\boxed{\frac{\partial}{\partial t}\nabla^2\psi-\frac{\partial \psi}{\partial z}\frac{\partial}{\partial x}\nabla^2\psi+\frac{\partial \psi}{\partial x}\frac{\partial}{\partial z}\nabla^2\psi=\mathrm{Pr}\frac{\partial \theta}{\partial \mathrm{x}}+\mathrm{Pr}\nabla^2\nabla^2\psi} \tag{57}$$

$$\boxed{\frac{\partial \theta}{\partial t}-\frac{\partial \psi}{\partial z}\frac{\partial \theta}{\partial x}+\frac{\partial \psi}{\partial x}\frac{\partial \theta}{\partial z}=\mathrm{Ra}\frac{\partial \psi}{\partial x}+\nabla^2\theta}. \tag{58}$$

The symbol, θ, is used to indicate the non-dimensional temperature perturbation (in order to avoid the use of T', which looks ugly). We do not use a different symbol for all other variables and coordinates.

The **Rayleigh number** is defined as

$$\boxed{\mathrm{Ra} \equiv \frac{g\alpha\Gamma H^4}{\kappa\nu}} \tag{59}$$

The **Prandtl number** is defined as

$$\boxed{\mathrm{Pr} \equiv \frac{\nu}{\kappa}}\,. \tag{60}$$

9. Fourier transformation of the governing equations

If we allow only for two-dimensional flow in a vertical cross-section of the fluid layer, any variable, for instance the temperature, can be written as a Fourier series as follows

$$\boxed{\theta(x,z,t) = \sum_{\alpha} \Theta_\alpha(t) S_\alpha(x,z)} \tag{61}$$

where $\Theta_\alpha(t)$ is a complex amplitude and where

$$\boxed{S_\alpha(x,z) \equiv \exp\left\{i\pi\left(a_x l_\alpha x + n_\alpha z\right)\right\}}\,. \tag{62}$$

In this definition,

$$a_x = \frac{2H}{L}\,, \tag{63}$$

is a measure of the **aspect ratio** (L/H) of the domain. Because periodic boundary conditions are assumed in the horizontal direction, this domain may be repeated in the horizontal direction ad infinitum, so as to obtain a regular array of cells with prescribed wavelength. Furthermore, the **wave-vector**, α, is defined as,

$$\alpha \equiv \left(l_\alpha, n_\alpha\right), \tag{64}$$

in which l_α and n_α are *integer* wave numbers. The sum, $\sum_{\alpha}$, over all wave-vectors, α, corresponds to sum over all integer combinations of l_α and n_α, running from $-\infty$ to $+\infty$.

In view of the observations, shown in **figures 3** and **4**, a reasonable fit to the temperature distribution in a fluid layer filled with two-dimensional convection cells is

$$T'(x,y,t) = C_0(t)\sin\frac{2\pi z}{H} + C_1(t)\cos\frac{2\pi x}{L}\sin\frac{\pi z}{H}\,. \tag{65}$$

In other words, the temperature perturbation, θ, can, in principle, be represented as a sum of two Fourier modes with "wave-vectors", (l,n)=(0,2) and (l,n)=(1,1) and associated time-dependent amplitudes, C_0 and C_1. The first Fourier mode represents a modification of the initial linear temperature profile, while the second Fourier mode represents the perturbed temperature distribution, which is set up by rising warm fluid and cold sinking fluid.

The lowest-order model of finite amplitude convection that can be constructed is one in which the Fourier series in (61) is truncated to include only the two terms on the right hand side of (65).

Stress-free and perfectly conducting upper and lower boundaries imply the following boundary conditions:

$$w = \frac{\partial \psi}{\partial x} = 0;\ \frac{\partial u}{\partial z} = -\frac{\partial^2 \psi}{\partial z^2} = 0;\ \theta = \frac{\partial^2 \theta}{\partial z^2} = 0 \text{ at } z = 0 \text{ and } z = 1. \tag{66}$$

Let us now represent the stream function and the temperature by Fourier series as

$$\begin{pmatrix} \psi \\ \theta \end{pmatrix} = \sum_{\alpha} \begin{bmatrix} \Psi_\alpha \\ \Theta_\alpha \end{bmatrix} S_\alpha(x,z)\ , \tag{67}$$

where S is defined in (62).

The **orthonormality** of S_α is expressed in the form

$$\int S_\alpha S_\beta^* d\sigma = \delta_{\alpha,\beta}\ , \tag{68}$$

where the asterisk designates a complex conjugate, while $\delta$is the kronecker delta. The integration extends over the region

$$0 \le x \le \frac{2}{a_x},\ 0 \le z \le 2\ , \tag{69}$$

and dσ is an area element divided by the total area, $4/a_x$. Note that the integration is carried over a domain, which is two times as large as the domain of physical interest, which has its top boundary at z=1. This is no more than a mathematical trick.

The left hand side of eq. 58 consists of one linear term and two non-linear terms. If we substitute the Fourier series (67) into eq. 58, the non-linear terms become

$$\begin{aligned} &\sum_{\alpha,\beta} \left\{ -i\pi n_\alpha \Psi_\alpha i\pi a_x l_\beta \Theta_\beta + i\pi a_x l_\alpha \Psi_\alpha i\pi n_\beta \Theta_\beta \right\} S_\alpha S_\beta \\ &= \sum_{\alpha,\beta} \pi^2 a_x \left\{ n_\alpha l_\beta - n_\beta l_\alpha \right\} \Psi_\alpha \Theta_\beta S_\alpha S_\beta\ . \end{aligned} \tag{70}$$

Here, $\sum_{\alpha,\beta}$ is a double sum over all wave vectors, α and β. It is now very convenient to use the property of orthonormality of S (62) by substituting the Fourier series (67) into eq. 58 and

then multiplying the result by S_γ^* and integrating over the region indicated in (69). The spectral form of the temperature equation (58) thus becomes

$$\boxed{\frac{d\Theta_\gamma}{dt} = \sum_{\alpha,\beta} I_{\gamma\alpha\beta}\Psi_\alpha\Theta_\beta + i\mathrm{Ra}\pi a_x l_\gamma \Psi_\gamma - \pi^2 k_\gamma^2 \Theta_\gamma}\,, \tag{71}$$

where

$$k_\gamma^2 = a_x^2 l_\gamma^2 + n_\gamma^2 \tag{72}$$

and the **interaction coefficient**,

$$\boxed{I_{\gamma\alpha\beta} \equiv \pi^2 a_x \left(n_\alpha l_\beta - n_\beta l_\alpha\right)\delta_{\gamma,\alpha+\beta}}\,. \tag{73}$$

All interaction coefficients are zero unless the **selection rule** (in vector form),

$$\boxed{\alpha + \beta = \gamma}\,, \tag{74}$$

is satisfied. The selection rule determines whether the interaction of the waves with wave vectors, α and β, contributes to a change of the amplitude of the wave with wave vector, γ.

The Fourier transformed eq. 57 becomes

$$\boxed{\frac{d\Psi_\gamma}{dt} = \frac{1}{k_\gamma^2}\sum_{\alpha,\beta} k_\beta^2 I_{\gamma\alpha\beta}\Psi_\alpha\Psi_\beta - i\,\mathrm{Pr}\,\frac{a_x l_\gamma}{\pi k_\gamma^2}\Theta_\gamma - \mathrm{Pr}\,\pi^2 k_\gamma^2 \Psi_\gamma}\,, \tag{76}$$

The Fourier-coefficients (or amplitudes) are complex. Therefore, they may be expressed as a sum of a real part (superscript, R) and an imaginary part (superscript, I) as follows:

$$\Theta_\gamma = \Theta_\gamma^R + i\Theta_\gamma^I;\ \Psi_\gamma = \Psi_\gamma^R + i\Psi_\gamma^I\,. \tag{77}$$

The fields of temperature and stream function are real, so that

$$\Theta_\gamma = \Theta_{-\gamma}^*\,, \tag{78}$$

or

$$\Theta_{l,n}^R = \Theta_{-l,-n}^R \text{ and } \Theta_{l,n}^I = -\Theta_{-l,-n}^I \tag{79}$$

and analogous relations for Ψ.

The boundary conditions at the top and bottom of the layer imply a sine-dependence in the vertical for both $\theta$and ψ. Therefore,

$$\Theta^R_{l,n} = -\Theta^R_{l,-n} \text{ and } \Theta^I_{l,n} = -\Theta^I_{l,-n} \tag{80}$$

and analogous relations for Ψ. Because the temperature and the vertical velocity are in phase in the horizontal direction, we can, without loss of generality, assume that both these fields possess a cosine-dependence in the horizontal direction. This means that the stream function has a sine-dependence in the horizontal direction (eq. 51). We then have

$$\Psi^R_{l,n} = -\Psi^R_{-l,n} \text{ and } \Psi^I_{l,n} = -\Psi^I_{-l,n}; \tag{81}$$

$$\Theta^R_{l,n} = \Theta^R_{-l,n} \text{ and } \Theta^I_{l,n} = \Theta^I_{-l,n}. \tag{82}$$

The relations (79), (80) and (82) imply that

$$\Theta^R_{l,n} = 0 \ . \tag{83}$$

The relations (79), (80) and (81) imply that

$$\Psi^I_{l,n} = 0 \ . \tag{84}$$

The relations (79), (80) and (81/82) also imply that we need only explicitly solve the differential equations that govern the amplitudes pertaining to 1 quadrant in wave number space, for example the quadrant corresponding to $l \geq 0$ and $n \geq 0$.

10. Spectral energy cascade in thermal convection

Suppose that one so-called fundamental mode is **self-excited**, i.e. has a positive linear growth rate. Let this be $(l,n)=(1,1)$. The initial effect of the non-linear interactions is to distort the horizontal mean temperature profile in such a way as to stabilize it, making the temperature field more isothermal in the mid-region and enhancing the unstable temperature gradients near the upper and lower boundaries, thereby increasing the vertical heat transport. This is achieved through the interaction of (1,1) and (-1,1), which creates (0,2) in the temperature field (see the selection rule 74), but not in the stream function field (check this!). In the second instance the original symmetric cellular stream function pattern is distorted due to the interaction between (±1,1) and (0,2), which creates (±1,3). After that the interaction between (1,3) and (1,-1) will create (2,2), and so on. The energy flows up the spectrum to modes with wavelengths 1/2, 1/3, 1/4… of the wavelength of the fundamental self-excited (linearly unstable) mode. If this fundamental mode has even parity, i.e. $(l+n)$ is an even number, the selection rule leads to an important property of this cascade of energy, which limits the amount of wave vectors that are excited through the non-linear interactions, namely that only even parity modes are excited. This is the reason why odd-parity modes are usually neglected in studies on cellular convection (see e.g. Kuo, 1961). The idea behind these studies is that convection starts at the critical Rayleigh number in the form of a fundamental mode and proceeds to create higher harmonics (of even-parity) through the nonlinear cascade effect, described above, to reach the finite amplitude equilibrium state.

11. Lorenz (1963) model

Let us study only the first basic non-linear interaction in isolation. The temperature field is expanded into two Fourier components, as in eq. 65, while the stream function field is expanded into just one Fourier component, corresponding to the fundamental mode, $(l,n)=(1,1)$. In other words, we take into account only the following wave vectors in the sum on the r.h.s. of eq. 61:

$$\gamma = (1,1),\ (-1,1),\ (-1,-1),\ (1,-1),\ (0,2),\ (0,-2)\,. \tag{85}$$

We neglect all interactions with wave vectors outside this truncation. In view of the symmetry relations (79), (80) and (81/82), we need only to derive equations for the time-evolution of the Fourier coefficients,

$$\Psi^R_{1,1},\ \Theta^I_{1,1},\ \Theta^I_{0,2}\ . \tag{86}$$

The only non-linear interactions involved are the following: (1,1) and (-1,1) interact to contribute to (0,2) and (1,-1) and (0,2) interact to contribute to (1,1) (the feedback). If all interactions with wave vectors outside the truncation are neglected, **the non-linear terms are energy conserving**. The resulting equations are

$$\frac{dX}{dt} = \frac{a_x \,\mathrm{Pr}}{\pi\left(a_x^2+1\right)} Y - \pi^2\left(a_x^2+1\right)\mathrm{Pr}\, X\,; \tag{87}$$

$$\frac{dY}{dt} = -2\pi^2 a_x XZ + \pi a_x \mathrm{Ra} X - \pi^2\left(a_x^2+1\right)Y\,; \tag{88}$$

$$\frac{dZ}{dt} = 4\pi^2 a_x XY - 4\pi^2 Z\ , \tag{89}$$

where

$$X \equiv \Psi^R_{1,1},\ Y \equiv \Theta^I_{1,1} \text{ and } Z \equiv \Theta^I_{0,2}\,. \tag{90}$$

This coupled set of three ordinary first-order non-linear differential equations (87-89) represents the so-called **Lorenz (1963) low-order model of thermal convection**. Because Edward Lorenz used a different time unit (see eq. 56) to express the governing equations (54 and 55) in non-dimensional form, equations 87-89 differ from the original equations (i.e. eqs. 25-27 on page 135 of Lorenz, 1963), which also appear on page 58 of the book by Edward Ott (1993), or on page 311 of the book by Stephen Strogatz (1994).

In eqs .87-89 X represents the intensity of the macroscopic convective motion, Y is proportional to the temperature difference between the ascending and descending currents, while Z is a measure of the distortion of the horizontal mean vertical temperature profile from linearity (**figure 4**). A positive value of Z indicates that the horizontal mean temperature gradient is distorted such that it is enhanced at lower and upper boundaries, so that molecular heat transport across these boundaries is enhanced. In the middle of the fluid layer this heat transport is taken care of by the macroscopic convective motions.

The non-linear terms in eqs. 88 and 89 describe the interaction of the wave (or cellular motion) with the mean state (i.e with the horizontal mean temperature field).

The Lorenz model has three **steady state (equilibrium) solutions**, which are found by setting the time derivatives equal to zero. We see directly that one steady state solution is $\vec{A} \equiv (X,Y,Z) = (0,0,0)$, which corresponds to the state of rest. The stability of the state of rest can be investigated by linearising the equations around this steady state, which can then be written compactly as

$$\frac{d}{dt}\vec{A} = M\vec{A} \ , \tag{91}$$

with

$$\vec{A} \equiv \begin{pmatrix} X \\ Y \\ Z \end{pmatrix} \text{ and } M \equiv \begin{pmatrix} -\pi^2\left(a_x^2+1\right)\mathrm{Pr} & \dfrac{a_x \mathrm{Pr}}{\pi\left(a_x^2+1\right)} & 0 \\ \pi a_x \mathrm{Ra} & -\pi^2\left(a_x^2+1\right) & 0 \\ 0 & 0 & -4\pi^2 \end{pmatrix} . \tag{92}$$

A positive eigenvalue of the matrix, M, implies instability. This is the case if

$$\mathrm{Ra} = \frac{\pi^4\left(a_x^2+1\right)^3}{a_x^2} \ . \tag{93}$$

The critical Rayleigh number for the onset of convection is

$$\mathrm{Ra_c} = \frac{\pi^4\left(a_x^2+1\right)^3}{a_x^2} \ . \tag{94}$$

The minimum value of $\mathrm{Ra_c}$ occurs when $a_x = 1/\sqrt{2}$. The properties of the Lorenz model and its solutions are analysed in the exercises below. Exercises 5 to 8 will be done during the second tutorial. Exercise 9 is concerned with the two finite amplitude convective solutions and their stability to small-amplitude perturbations (homework).

12. Exercises, part 2

(5)

Figure 5 (next page) shows a regime diagram of laboratory convection as a function of Ra and Pr, demonstrating that time dependent flow emerges when Ra is sufficiently large. Time-dependent turbulent flow emerges for lower Ra when Pr is small than when Pr is large. Which non-linear terms are responsible for this "early" onset of time-dependent flow at low Pr: those in eq. 57 (momentum advection) or those in eq. 58 (temperature advection)? Is the Lorenz model more applicable to low Pr convection or to high Pr convection?

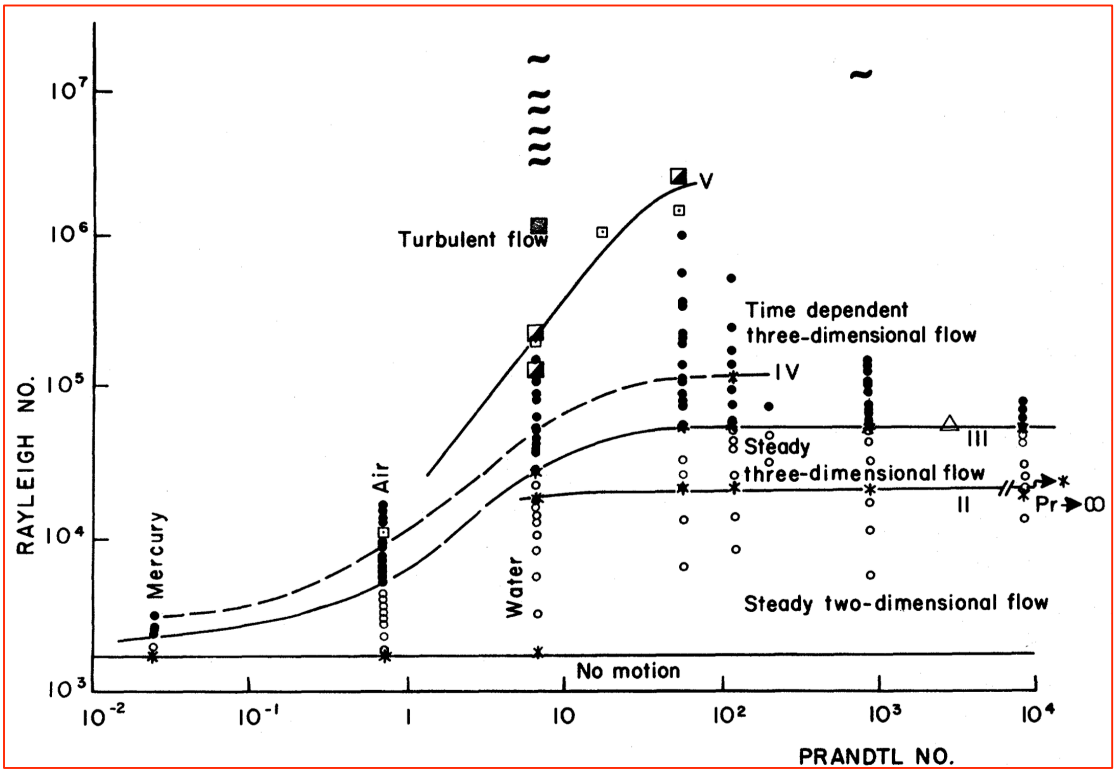

Figure 5 (exercise 7). Regime diagram of convection in fluids with different Prandtl numbers as a function of Rayleigh number for convection between rigid boundaries (not stress-free), distilled from laboratory experiments. Two-dimensional convection is observed at low Ra. As the Rayleigh number is increased, three-dimensional cells appear. If Ra is increased further, steady state regular cellular flow disappears and is replaced by a random array of transient plumes. Source: Krishnamurti and Howard (1981).

(6)

The Lorenz model has two other steady state solutions (next to the state of rest), corresponding to finite amplitude convection. Derive expressions for X, Y, and Z in these steady states. Write these expressions in terms of $r=\sqrt{(\text{Ra}-\text{Ra}_c)}$ and a_x (hint: the steady state values of X, Y, and Z do not depend on Pr). Convection modifies the horizontal mean temperature profile. In which way? Is this consistent with the observations shown in **figure 4**?

(7)

Show that the solution of the Lorenz model in phase space (i.e. as a function of X, Y and Z) for large t will either collapse to a point, to a line or to a two-dimensional surface (e.g. a torus) for all values of Ra, Pr and a_x. This means that the volume in phase space, spanned by the collection of trajectories corresponding to different initial states, will, as each point in phase space is displaced in accordance with eqs. 87-89, shrink to zero for large t. What is the associated e-folding time? In the words of Lorenz (1963) (p.135), *all trajectories ultimately become confined to a specific subspace having zero volume*. If the trajectories do not lie on a closed line or a torus in phase space, this subspace is referred as a "**strange attractor**", a term which was introduced by the Belgian mathematician, David Ruelle, and the Dutch mathematician, Floris Takens, in 1971 (see section 9.3 in Strogatz (1994)).

(8)

Derive expression for the growth-rate of small perturbations to the state of rest, similar to the expression in eq. 39, but now in the non-dimensional units of the Lorenz model (eqs. 87-89). You will find that perturbations grow at a rate, which depends on the Rayleigh number, Ra, and the aspect ratio (or a_x). Make a contour plot of the growth-rate as a function of Ra (vertical axis) and a_x (horizontal axis). HINT: the growth-rate corresponds to the positive eigenvalue of the matrix, M, in eq. 92.

(9) (homework)

Linearise the Lorenz equations (87-89) around the steady finite amplitude convective state and express this linearised system as in eqs. 91 and 92. Determine the linear stability of the finite amplitude steady states as a function of Ra and a_x, for Pr=10 (this is the value of Pr that was chosen by Lorenz in 1963) by determining the eigenvalues of the corresponding matrix, M. Draw a regime diagram, with Ra as the ordinate and a_x as the abscissa, indicating regions where finite amplitude convection is steady and stable and regions where finite amplitude convection is not steady and unstable. This can be done numerically. Determine the minimum value of Ra and the corresponding value of a_x for which all steady states are linearly unstable and for which the model only has time-dependent solutions (for Pr=10). This exercise is given as homework.

13. References part 2

Krishnamurti, R., and L.N. Howard, 1981: Large-scale flow generation in turbulent convection. **Proceedings National Academy of Science USA**, **78**, no. 4, pp. 1981-1985.

Kuo, H.L., 1961: Solution of the non-linear equations of cellular convection and heat transport. **J.Fluid Mech.**, 10, 611-634.

Lorenz, E.N., 1963: Deterministic non-periodic flow. **J.Atmos.Sci. 20**. 130-141.

Part 3: Chaos and predictability in the Lorenz (1963) model

By Aarnout van Delden (http://www.staff.science.uu.nl/~delde102/TinF.htm)

14. Finite amplitude convection according to the Lorenz model

When the Rayleigh number exceeds the critical value for onset of convection, convection currents in the form of convection cells grow in amplitude and start to modify the horizontal-mean temperature. This interaction between the convection cell (the "wave") and the horizontal mean thermal state is described by the nonlinear terms in the Lorenz model. The system evolves towards a new equilibrium (**figure 7**), which represents a state in which warm fluid is steadily transported upwards and cold fluid is steadily transported downwards on both sides of the upward current. Remember: side boundary conditions are periodic. **Figure 8** shows the temperature distribution in the state of rest (upper panel) and in the final new equilibrium state (lower panel), which is a linearly stable equilibrium at this Rayleigh number. The convective equilibrium state, however, looses its stability to small perturbations for all Rayleigh numbers above certain value (**exercise 8**). What is the character of the solution if the system does not possess a stable equilibrium? Edward Lorenz addressed this question in his famous paper, published in 1963. A tentative answer to this question can only be obtained by numerical methods. Lorenz trusted his numerical approximation to the time-derivatives, which in hindsight was not the best choice, and so discovered the chaotic solution of his equations.

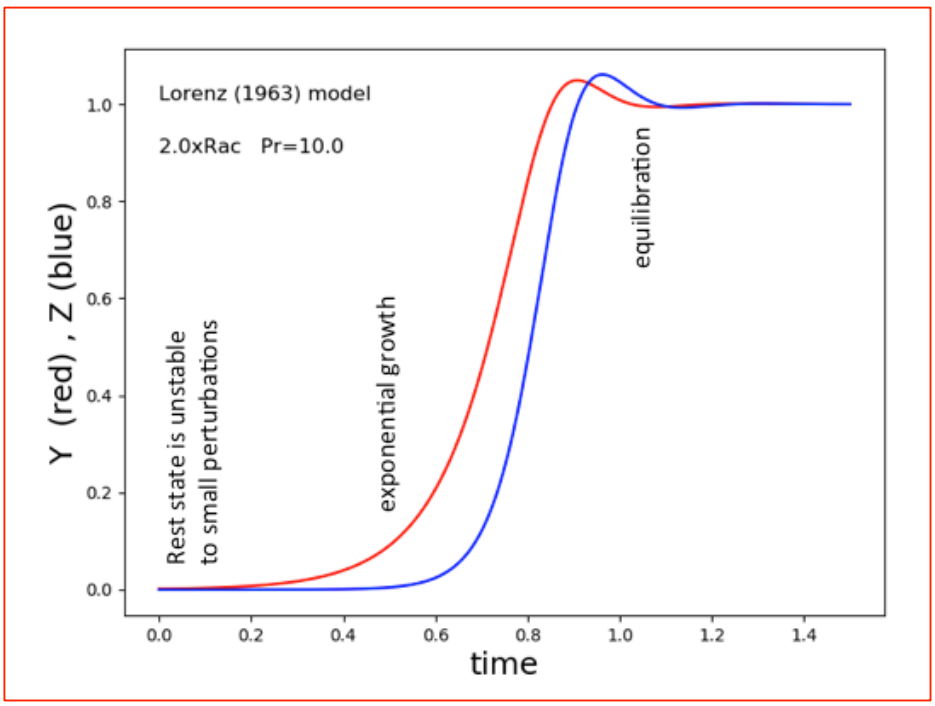

Figure 7. The evolution of Y and Z in a numerical integration of the Lorenz equations (87-89) with Pr=10, $a_x=1/\sqrt{2}$ and $Ra=2Ra_c$ (scaled with the steady state value). The initial state is the rest state, which is perturbed slightly. Because the rest state is unstable to small perturbations at $Ra=2Ra_c$, the initial perturbation to Y grows exponentially (red curve). The blue curve represents the Fourier amplitude, $Z=\Theta_{0,2}$, which grows due to nonlinear interactions, leading to an equilibration and an adjustment to a new equilibrium state (lower panel of **figure 8**). The numerical approximation to the time derivative employs the Runge Kutta fourth order scheme.

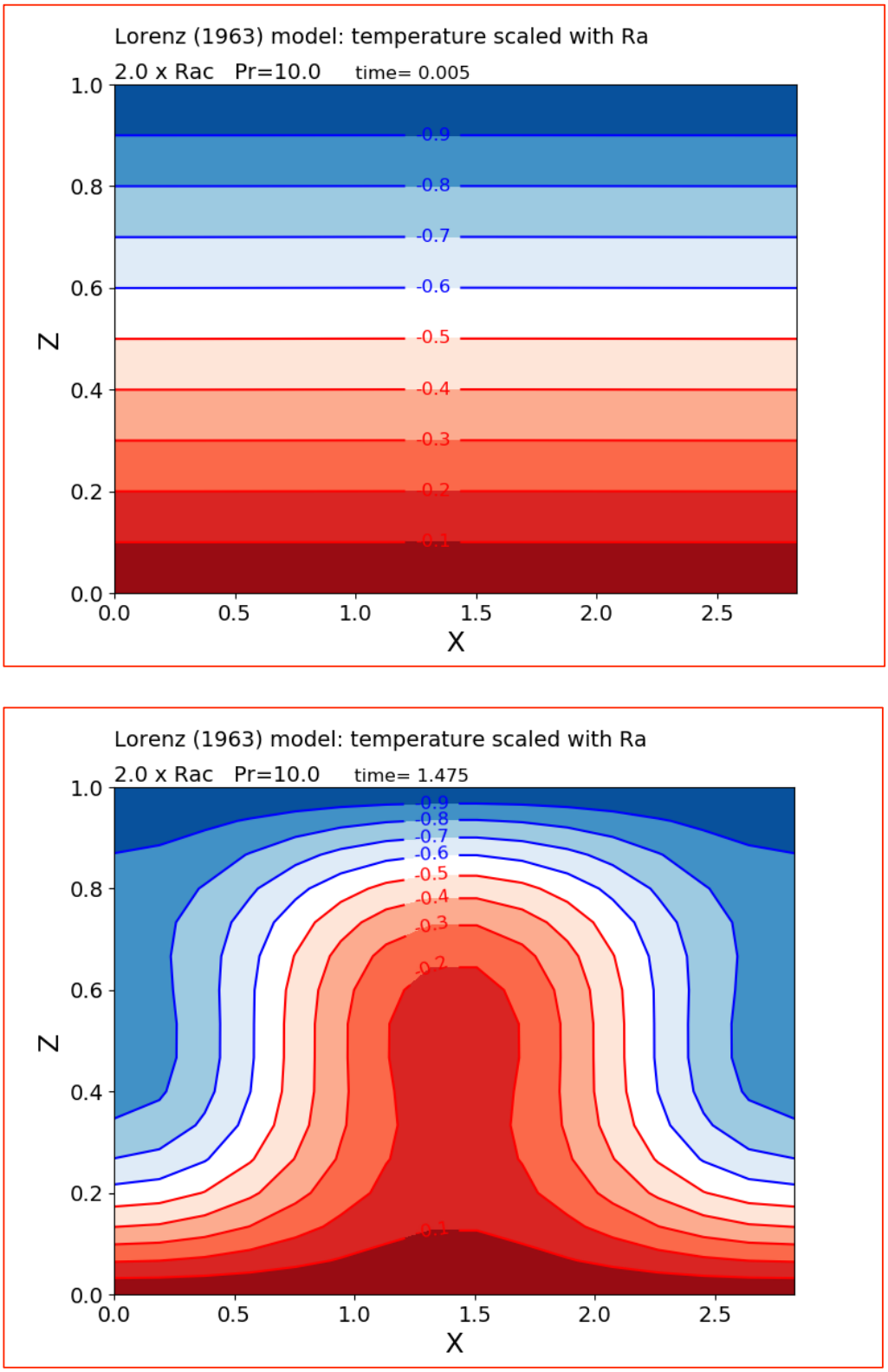

Figure 8. The temperature at t=0 (upper panel) and at t=1.5 (lower panel), scaled with the imposed value of Ra (=2Ra$_c$). The state of rest is an ***unstable*** equilibrium at Ra=2Ra$_c$, while the finite amplitude convective equilibrium is a ***stable*** equilibrium at this Rayleigh number. The Prandtl number, Pr=10 and the aspect ratio is $2\sqrt{2}$. The temperature distribution in "physical space", shown here, is reconstructed from two Fourier coefficients, Y and Z. Animation: http://www.staff.science.uu.nl/~delde102/LorenzModelTemp_2Rac.mov . (see exercise 14).

15. Sensitive dependence on initial conditions

Lorenz studied numerical approximations of the time-dependent solutions of his model and discovered that these solutions are very sensitive to the initial state for certain combinations of values of the Rayleigh number and Prandtl number. At Ra=28Ra$_c$, Pr=10 and a_x=1/√2, Lorenz (1963) obtained a solution which looks very much like the solution shown in **figure 9**. This solution will never be exactly the same. A slight difference in the initial condition leads to a different solution. In other words, small causes can have large effects, an idea that is known by the metaphor, "**Butterfly Effect**", which has its origin in Lorenz's question: *can the flap of a butterfly's wings be instrumental in generating a tornado*?

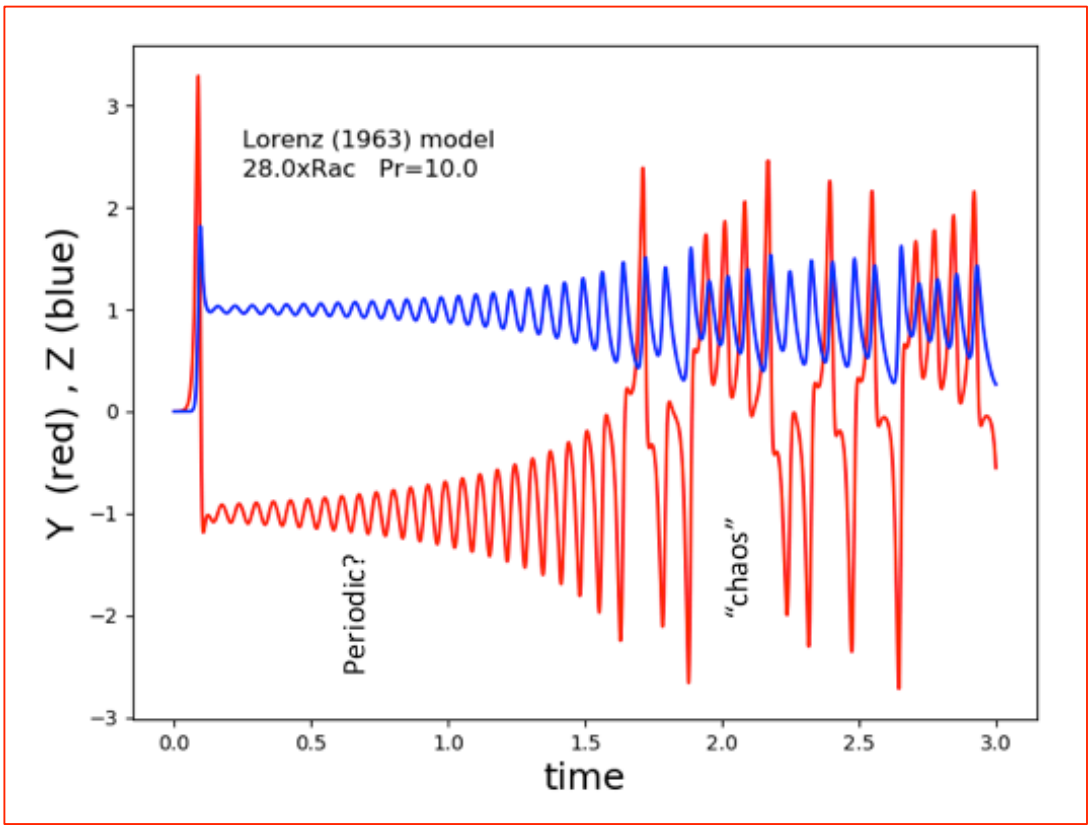

Figure 9. The evolution of *Y* and *Z* in a numerical integration of the Lorenz equations (87-89) with Pr=10, a_x=1/√2 and Ra=28Ra$_c$ (scaled with the steady state value). Initially the state of rest is perturbed slightly by putting *Y*=0.1 while *X* and *Z* are equal to zero. Because the rest state is unstable to small perturbations at Ra=28Ra$_c$, the initial perturbation to *Y* (red curve) grows exponentially. The blue curve represents the Fourier amplitude, *Z*=$\Theta_{0,2}$, which grows due to nonlinear interaction with *Y*, leading to an adjustment to a new equilibrium. However, this equilibrium is also unstable to small perturbations. The system has no stable equilibrium state. The solution appears periodic initially, but this solution also seems unstable. The numerical approximation to the time derivative employs the Runge Kutta fourth order scheme.

Sensitive dependence on initial conditions means that the trajectories in phase space of two solutions, which are very close to each other initially, ultimately diverge in time, which makes the evolution "unpredictable". The predictability aspect of his model was the main interest of Edward Lorenz in 1960's. The message of his 1963-paper was an inconvenient one for the weather and climate modeling community, which was at the beginning of the huge, still ongoing, project of developing numerical models to predict weather and climate. Lorenz's message was practically ignored for nearly 10 years, being cited only 25 times in the first 10

years after publication. In 1971 two mathematicians: David Ruelle and Floris Takens, published a paper, entitled "On the Nature of Turbulence", which became very influential. This paper connected Lorenz's ideas about "predictability" to the problem of the nature or definition of turbulence. After its discovery by mathematicians in the early 1970's, Lorenz's 1963-paper became a "seminal paper". Now (in 2021) it is no doubt the most cited paper in Meteorology (more than 25 thousand times until Jnaury 2022)! The history of research on the topic of Lorenz's 1963-paper is sketched in a book entitled, "The Essence of Chaos", published in 1993. Chapter 3 ("Our Chaotic Weather") and chapter 4 ("Encounters with Chaos") are highly recommended.

16. The "Strange Attractor"

The solution, shown in **figure 9**, is shown again in **figure 10**, but now as a trajectory projected on the *Y*-*Z* plane in phase space. The trajectory wanders through phase space at random, leaving and entering the "basins of attraction" of the two fixed points representing the steady convective equilibria on either side of the *Z*-axis (the line *Y*=0). In fact, the trajectory never returns to the same point in phase space and is therefore referred to as "chaotic". The chaotic trajectory, seen in **figure 10**, forms an object, which is called a "**Strange Attractor**". This term was used first by David Ruelle in 1971 in a talk at a meeting in La Jolla (California), in the presence of Edward Lorenz. The title of Ruelle's talk was, "Strange Attractors as a Mathematical Explanation of Turbulence". The Strange Attractor in **figure 10** also resembles the wings of a Butterfly. This, probably, was the inspiration for Lorenz's question on the effect of a flap of a butterfly's wings, cited in the previous section.

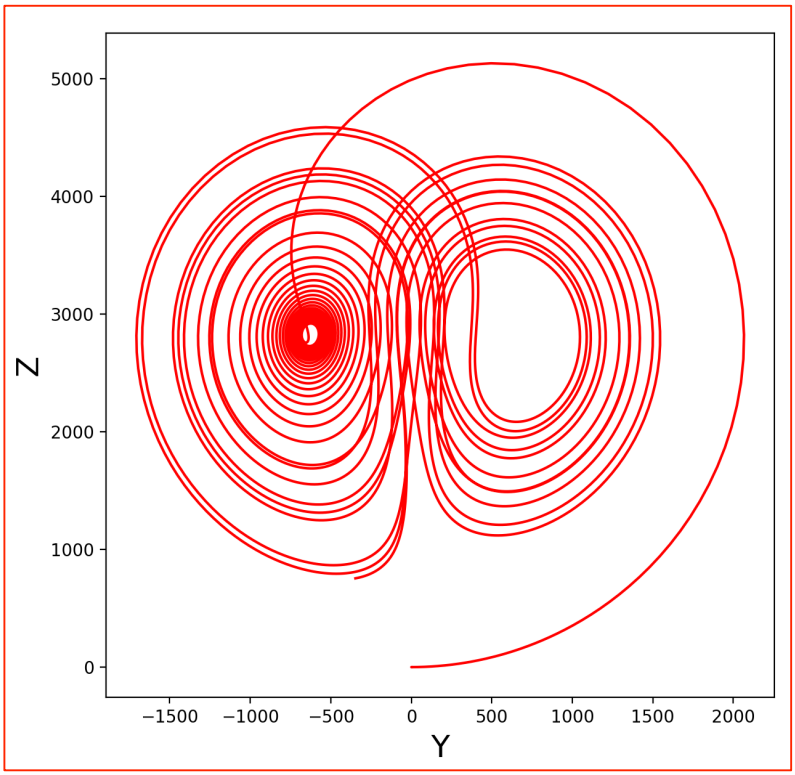

Figure 10. The solution, shown in figure 9, in a two-dimensional (*Y*,*Z*) section of phase space. Note: *Y* and *Z* are not scaled, as in **figure 9**.
Animation: https://webspace.science.uu.nl/~delde102/LorenzModelTemp_28Rac.mov.

17. Divergence of nearby trajectories

Suppose that we measure the temperature in an experimental system with an error, $|\delta_0|$. We then use this measured value as an initial condition to make a forecast with a numerical model of the experimental system. If the system is non-linear it may have a chaotic solution. This means that the initial error will amplify with time. How fast is this amplification?

Following ideas suggested first by the Russian mathematician, Aleksandr Lyapunov (1857-1918), it is hypothesized that the amplification of the error is exponential in time. In other words, after a time, t, the absolute value of the error, δ, is

$$|\delta(t)| \approx |\delta_0| \exp(\lambda t) . \qquad (95)$$

The growth-rate of the error, λ, is called "**Lyapunov exponent**".

How far in time will we accept the prediction? This depends on our "**tolerance**". Let a be a measure of the tolerance. In other words, the prediction is not accepted if $|\delta(t)| > a$. This occurs after a time in the order of

$$t_{\text{horizon}} \approx \frac{1}{\lambda} \ln \frac{a}{|\delta_0|} . \qquad (96)$$

This implies an **error-doubling time**, equal to $\ln(2)/\lambda$, which only depends on the Lyapunov exponent. We can increase t_{horizon} by accepting a larger error, or, better, by reducing the initial error. Let us reduce the initial error, $|\delta_0|$, by a factor 10^{-n}, where n is a positive integer. How much longer can we predict? For the same tolerance, the increase of t_{horizon} is

$$\Delta t_{\text{horizon}} \approx \frac{n}{\lambda} \ln 10 . \qquad (97)$$

Therefore, t_{horizon} increases only *linearly* by a *constant* factor $\ln 10/\lambda \approx 2.3/\lambda$ for each factor of 10 in the reduction of the error (see **exercise 13d**).

18. Dissipative system: volume contraction in phase space

The Lorenz model is "dissipative". This has an interesting consequence for the dimension of the attractor in phase space. The solution of the Lorenz model travels along a trajectory in phase (X, Y, Z)-space with a "velocity",

$$(U,V,W) \equiv \left(\frac{dX}{dt}, \frac{dY}{dt}, \frac{dZ}{dt} \right) . \qquad (98)$$

The divergence of this "velocity" vector is proportional to the change of the volume, $V=\Delta X \Delta Y \Delta Z$, of a "fluid parcel" in phase space. We can write,

$$\frac{1}{V}\frac{dV}{dt} = \frac{1}{\Delta X}\frac{d\Delta X}{dt} + \frac{1}{\Delta Y}\frac{d\Delta Y}{dt} + \frac{1}{\Delta Z}\frac{d\Delta Z}{dt} \qquad (99)$$

The distance, ΔX, represents the distance in the X-direction of two trajectories (solutions), labeled "1" and "2", so that we can write:

$$\frac{1}{\Delta X}\frac{d\Delta X}{dt}=\frac{1}{\Delta X}\frac{d}{dt}\left(X_1-X_2\right)=\frac{1}{\Delta X}\left(\frac{dX_1}{dt}-\frac{dX_2}{dt}\right)=\frac{\Delta U}{\Delta X}\approx\frac{\partial U}{\partial X}=\frac{\partial}{\partial X}\frac{dX}{dt}\ . \qquad (100)$$

Applying this idea also to ΔY and ΔZ leads to

$$\frac{1}{V}\frac{dV}{dt}=\frac{\partial}{\partial X}\left(\frac{dX}{dt}\right)+\frac{\partial}{\partial Y}\left(\frac{dY}{dt}\right)+\frac{\partial}{\partial Z}\left(\frac{dZ}{dt}\right)=-\pi^2\left(a_x^2+1\right)\mathrm{Pr}-\pi^2\left(a_x^2+1\right)-4\pi^2<0\ . \qquad (101)$$

(Lorenz (1963), p. 135). This means that the volume of a collection of trajectories in phase space *decreases* in time at a rate, which is proportional to $(\pi^2((a_x^2+1)(\mathrm{Pr}+1))+4)$. This implies that all trajectories will ultimately become confined to a subspace in phase space having zero volume! (page 135, Lorenz (1963)). If the solution is a stable fixed point, the "trajectory" becomes confined to one point in space. This is trivial. If the solution is chaotic, the associated "trajectory" becomes confined to a two dimensional object. The butterfly (**figure 10**) is such a two-dimensional object. It is, in fact, an extremely complicated two-dimensional surface in three-dimensional phase space.

19. Lorenz map: order in chaos?

Although the non-periodic solution of the Lorenz (1963) model, shown in **figure 9**, is chaotic, in the sense that it is sensitively dependent on initial conditions, it does possess a certain degree of "order". Referring to his **figure 2** (our **figure 10**), Lorenz (1963) (p. 138) states

"we find that the trajectory apparently leaves one spiral only after exceeding some critical distance from the centre. Moreover, the extent to which this distance is exceeded appears to determine the point at which the next spiral is entered; this in turn seems to determine the number of circuits to be executed before changing spiral again.

It therefore seems that some single feature of a given circuit should predict the same feature of the following circuit. A suitable feature of this sort is the maximum value of Z, which occurs when a circuit is nearly completed."

Schematically, the chaotic solution in terms of Z looks as is drawn in **figure 11**. The period and amplitude of the oscillations in Z seem totally erratic. Nevertheless Lorenz (1963) measured the amplitude of successive peaks and made a scatter plot of this amplitude as function of the amplitude of the previous peak and found a remarkable result, which is shown in **figure 12** (his figure 4 on page 139). This scatter plot is known as the "**Lorenz map**". There is almost no "thickness" to the curve represented by the dots in **figure 12**.

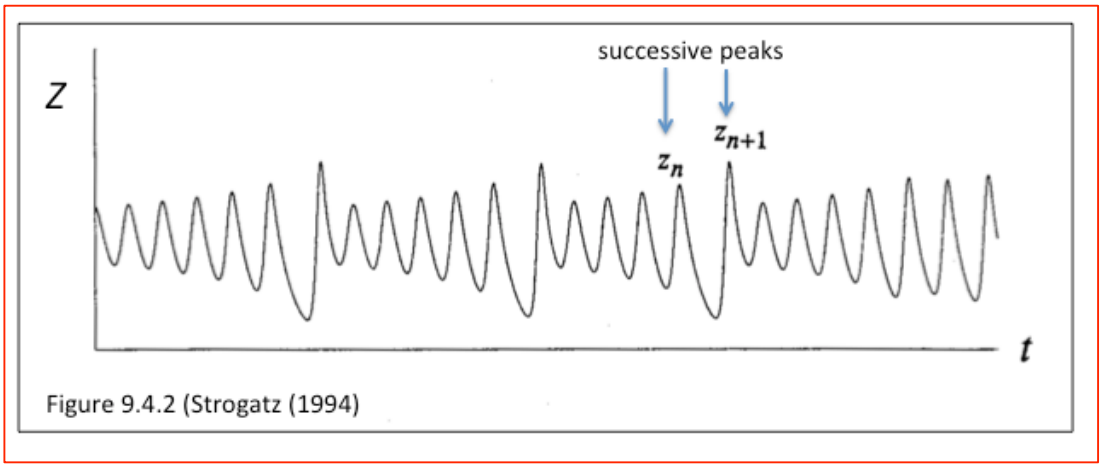

Figure 11. A schematic graph of the chaotic solution of the Lorenz (1963) model (the blue curve in **figure 9**). The amplitudes of successive peaks are related as is shown in **figure 12**.

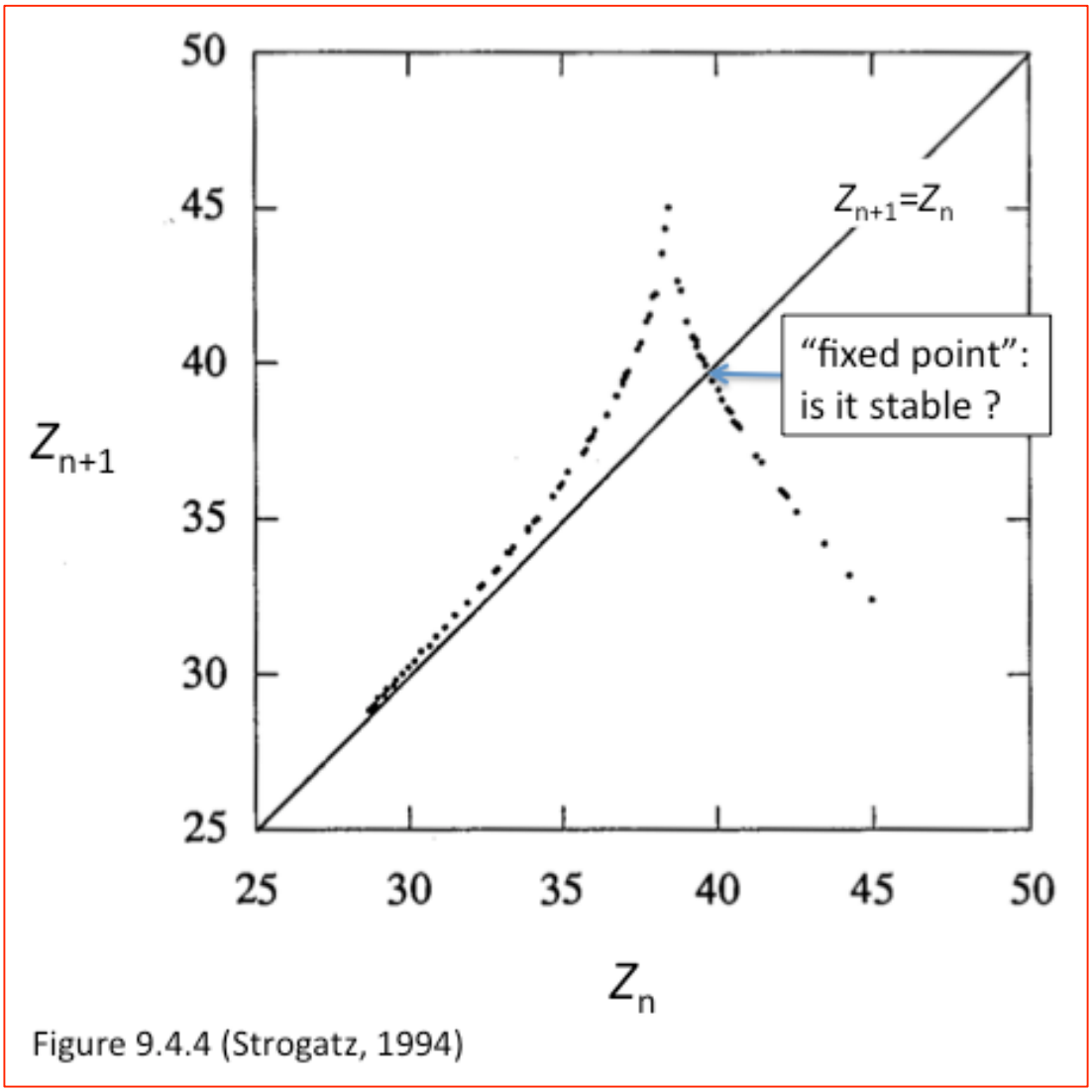

Figure 12. Scatter plot of the height of successive peaks in the graph shown in **figure 11**, which is a schematic representation of the blue curve in **figure 9**. This scatter plot is now known as the "Lorenz map" (page 327, Strogatz, 1994). See May (1976).

Lorenz (1963) (p. 139) states that

"an investigator, unaware of the nature of the governing equations, could formulate an empirical prediction scheme from the "data" pictured in figures 10 and 12. From the value of the most recent maximum of Z, values at future maxima may be obtained by repeated applications of figure 12".

Unfortunately, the time between successive peaks in **figure 11** is very erratic (**exercise 13c**) and therefore not predictable! The paper by Robert May (1976) is recommended for an interesting discussion on discrete maps.

20. Exercises, part 3

(10)

The total kinetic energy (K) and the total potential energy (P), associated with the perturbations (eq. 6) in two-dimensional convection (in which v=0) are, respectively,

$$K = \frac{1}{2}\int\left(u^2 + w^2\right)d\sigma\ ; \qquad (102)$$

$$P = -\frac{1}{2}\mathrm{Pr}\int\theta^2 d\sigma\,. \qquad (103)$$

Express K and P in spectral space and show that K+P is **conserved by the non-linear terms in the Lorenz model**.

(11)

Use the expression for kinetic energy in spectral space, derived in exercise 10, to derive an expression for the kinetic energy in the steady state of finite amplitude convection in the Lorenz model. At which aspect ratio will the kinetic energy be a maximum if Ra=10000 and if Ra=20000? Is the equilibrium state of finite amplitude convection stable to small perturbations at these two combinations of values of the aspect and the Rayleigh number (use the result of exercise 8)? Is this aspect ratio at which kinetic energy is maximized larger or smaller than the preferred aspect ratio for onset of convection at the minimum critical Rayleigh number? What does this imply?

(12)

The graph in **figure 12** (the "Lorenz map") represents a scatter plot of the value of Z_{n+1} as a function of Z_n in an integration of the Lorenz model when all three equilibrium states are linearly unstable, where Z_n is the n-th local maximum value of $Z(t)$. The straight line represents the line, Z_{n+1}=Z_n . According to the Lorenz map, the value of the next maximum (next peak in Z) is predictable. Suppose that Z_0=40. For which value of n is Z_n>Z_0? For which value of n is Z_n<Z_0? A fixed point is found at the intersection of the Lorenz map and the line, Z_{n+1}=Z_n. Is this a stable fixed point? How can you deduce this from **figure 12**?

(13) (homework)

For this exercise you need to know how to program a computer (in Python, MATLAB, Mathematica, C or any other suitable language).

(a) Integrate the Lorenz (1963) equations (eqs. 87-89) in time numerically through at least 5 non-dimensional time units. Approximate the time-derivatives with the fourth order (RK-4) Runge-Kutta scheme (**section 22**). Do this for the exact same values of a_x, Ra and Pr, which Lorenz used to illustrate the chaotic solution of his model, i.e. $a_x=1/(2^{1/2})$, Pr=10 and Ra=28Ra$_c$ (Ra$_c$ is defined in eq. 94). The initial condition should lie close to steady state of rest, $(X,Y,Z) = (0,0,0)$, which is perturbed by putting $Y=0.1$ at $t=0$, while assuming that X and Z are equal to zero at $t=0$.

(b) Locate local maxima of $Z(t)$, Z_n. Plot Z_{n+1} as a function of Z_n, in other words reproduce the *Lorenz map* (**figure 12**; see also page 139 of Lorenz (1963), or p. 326-328 of Strogatz (1994)).

(c) Now, plot the time between local maxima of $Z(t)$ as a function of time (e.g. the time half-way between two maxima). Discuss the plot.

(d) Perform a second integration with a slightly different initial condition, by weakly perturbing X initially. Plot a measure of the separation in phase space between the two solutions and estimate the associated Lyapunov-exponent, defined in eq. 95 (see also p. 320-323 of Strogatz (1994)).

(e) Compare the "climate" of the two solutions, i.e. the time average of X, Y, and Z. You may have to extend your integration in time by many more than 5 non-dimensional time units to get a "stable" answer. What conclusions can you draw? Now, compare the "climate" of the absolute values of the two solutions, i.e. the time average of $|X|$, $|Y|$, and $|Z|$. What do you conclude from this?

(f) Model climate can also be characterised by the so-called "probability distribution function" ("pdf"). A plot of the "pdf" as a function of X and Y gives the probability of finding the Lorenz model state vector in any point in X-Y plane of phase space. Plot this "pdf" and interpret your result in the light of **(e).**

(14)

What is the mathematical relation between C_0 and C_1 in equation 65 and Y and Z in equations 87-89 (the Lorenz model)? This information can be used to reconstruct and visualize (animate) the temperature field of a numerical integration of the Lorenz model (see **figure 8** and http://www.staff.science.uu.nl/~delde102/LorenzModelTemp_2Rac.mov).

(15)

The Lorenz model represents the lowest order model of convection. It describes the growth, when the Rayleigh exceeds the critical Rayleigh, of the amplitude of one Fourier mode in both the stream function and the temperature, and the interaction of this Fourier mode with one additional Fourier mode, which represents the modification of the horizontal-mean temperature field by convection.

If the Rayleigh number exceeds the critical value for onset of convection for two Fourier modes $(l,n)=(1,1)$ and $(l,n)=(2,1)$: what will happen? The Lorenz model does **not** describe this situation in which more than one Fourier mode or wave is linearly unstable, or "self-excited".

If two modes grow, will this lead to a less ordered flow pattern? Observations indicate that this is mostly not the case (**figure 3**). It appears as if one Fourier mode predominates. Why is one discrete scale of motion selected?

These questions might be answered with an extension of Lorenz's (1963), in which two linearly unstable (self-excited) modes (or waves) with wave vectors, $(l,n)=(1,1)$ and $(l,n)=(2,1)$, are included inside the truncation. Which other modes would you include in this truncated model? How many first order ordinary differential equations would this model have?

21. References part 3

Lorenz, E.N., 1963: Deterministic non-periodic flow. **J.Atmos.Sci. 20**. 130-141.

Lorenz, E.N., 1993: **The Essence of Chaos**. University of Washington Press.

May, R.M., 1976: Simple mathematical models with very complicated dynamics. **Nature**, 261, 459-467.

Ruelle, D. and F. Takens, 1971: On the nature of turbulence. **Communications in Mathematical Physics. 20** (3): 167–192.

Ruelle, D., 1991: **Chance and Chaos**. Princeton University Press. 195 pp.

Strogatz, S.H., 1994: **Non-linear Dynamics and Chaos**. Perseus Books. 498 pp. (sections 9.2-9.4)

22. Appendix to part 3: Runge-Kutta approximation to the time-derivative

Suppose we have an ordinary differential equation of the type, $dX(t)/dt=F(X)$. We then find $X(t+\Delta t)$ by following the following recipe.

$$
\begin{aligned}
X_0 &= X(t) \\
X_1 &= X_0 + \left(F(X_0)\Delta t/2\right) \\
X_2 &= X_0 + \left(F(X_1)\Delta t/2\right) \\
X_3 &= X_0 + \left(F(X_2)\Delta t\right) \\
X_4 &= X_0 - \left(F(X_3)\Delta t/2\right) \\
X(t+\Delta t) &= \left(X_1 + 2X_2 + X_3 - X_4\right)/3
\end{aligned}
$$

This fourth order "Runge-Kutta" (RK-4) approximation to the time derivative is very accurate for sufficiently small time step. This scheme is also recommended and used by Lorenz in his 1993-book on "The Essence of Chaos" (p. 190).

Part 4: Scale selection and spectral energy transfer in thermal convection

By Aarnout van Delden (http://www.staff.science.uu.nl/~delde102/TinF.htm)

23. The question of non-linear scale selection

The analysis of the stability to small perturbations of the state of rest of a stratified fluid indicates that, when the Rayleigh number *just* exceeds a minimum critical value, there is one ("preferred") Fourier mode with a well-defined aspect ratio, which grows exponentially in time, i.e. has a positive linear growth-rate. At Rayleigh numbers relatively far above the minimum critical value for onset of convection many Fourier modes are self-excited simultaneously. Non-linear interactions between self excited modes and higher harmonics will become important. Will the aspect ratio of the convections cells be the same as predicted by linear theory? This section investigates the role of nonlinearity in scale selection by studying the transfer of kinetic energy between Fourier modes due to non-linear interactions.

The Lorenz model describes the growth of one Fourier mode in both the stream function and the temperature, and the interaction of this Fourier mode with another Fourier mode, which represents the modification of the horizontal-mean linear static temperature profile by convection, such that heavy cold fluid moves down, while warm light fluid moves up, thereby lowering the **centre of gravity** of the fluid layer (**figure 4**).

The Lorenz model is not able to describe the deformation, or change of form, of the finite amplitude convection cell, by transfer of energy to higher harmonics. Nor is it able to describe the transfer of energy between different scales of motion, or Fourier modes. The aspect ratio of the cellular motion in the Lorenz model is fixed and imposed by the value of the parameter, $a_x = 2H/L$ (eq. 69).

In part 4 of these notes we construct a more complex, but still low-order, model of thermal convection, which consists of several Fourier modes, which may simultaneously be **self-excited**, i.e. have positive linear growth-rates. These modes are unstable when the amplitude of this mode is nearly zero. With this model we can study the following questions. If the Rayleigh number exceeds the critical value for onset of convection for two modes, e.g. for $(l,n)=(1,1)$ and $(l,n)=(2,1)$, what will happen? If two modes are self-excited, hence grow spontaneously, will this lead to a less ordered, chaotic or turbulent flow pattern? Observations indicate that this is mostly not the case (**figure 3**). It appears as if one mode predominates. Why is one mode selected over others?

The low-order model under study here simulates the interaction of two modes with neighbouring horizontal wave numbers, equal to j and $j+1$ ($j \geq 1$), which may both be self-excited at sufficiently high Rayleigh number. The stream function patterns, corresponding to these two Fourier modes, are drawn in **figure 13** for $j=1$.

Which other modes would you include in this truncated model so that the two chosen modes interact? How many first order ordinary differential equations would this model consist of?

According to the selection rule (74) two modes or waves with wave vectors, $(l,n)=(j,1)$ and $(l,n)=(j+1,1)$, cannot interact without the mediation of another mode or wave. Let us suppose that $j=1$ and that the modes, $(l,n)=(j,1)=(1,1)$ and $(l,n)=(j+1,1)=(2,1)$, are both self-excited. The interaction of these modes and their mirror images in wave number space will excite the modes, (1,2) and (3,2). The mode (1,2) is excited through the interaction of (-1,1) and (2,1), while the model (3,2) is excited through the interaction of (1,1) and (2,1). Negative

wave number modes will also be excited, but, because of the symmetry relations, summarized in eqs. 79-82 at the end of **section 9**, equations describing the time-evolution of these modes do not have to be made explicit.

Some nomenclature: modes with n=1 are termed "**single vertical modes**" and modes with n=2 are termed "**double vertical modes**". The interaction of two single vertical modes excites a double vertical mode, which, in turn, interacts with a single vertical mode to contribute to the growth or decay of other single vertical modes, but also to contribute to the growth or decay of "**triple vertical modes**" (n=3). Since triple vertical modes have relatively high critical modal Rayleigh numbers (the critical modal Rayleigh number increases with n^6; see eq. 42 and **exercise 3**), the amplitude of these modes is so quickly reduced (by the effect of viscosity and molecular conduction) that interactions with triple vertical modes and even higher-order modes, with n>3, can be neglected.

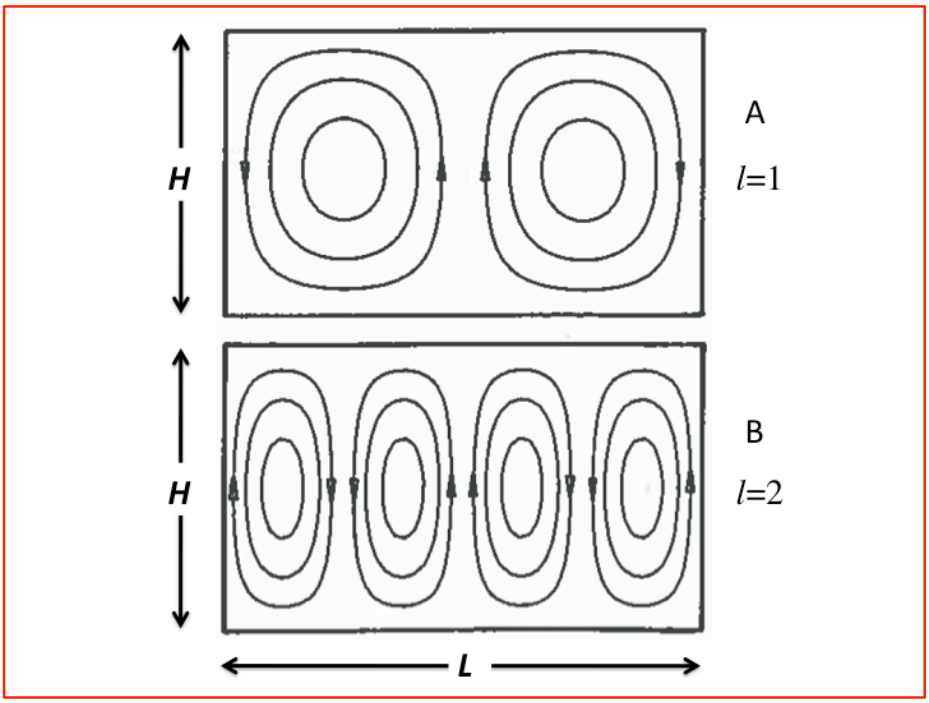

Figure 13. The stream function fields corresponding to cellular convection-patterns with horizontal wave number, l=1 (upper panel) and l=2 (lower panel). Both patterns are referred to in the text as "single vertical modes", because they have vertical wave number n=1.

24. Scale selection in a ten-component model of thermal convection

The above arguments are the basis for ignoring all modes with $n\geq 3$ in a low-order model for the interaction of two single vertical modes with "neighbouring" horizontal wave numbers, j and j+1 ($j\geq 1$).

All modes with $n\geq 3$ are excluded except the mode, $J \equiv \Theta_{04}^{I}$, which is included to give a slightly more realistic representation of the horizontal-mean temperature as a function of z. The (0,4) mode is excited through the interaction of double vertical modes with their mirror images around the l-axis. **Table 1** lists all possible interactions between wave modes, which are included inside the truncation of the 10-component model.

γ	α	β
(0,2)	(-j,1)	(j,1)
(0,2)	(-j-1,1)	(j+1,1)
(0,4)	(-1,2)	(1,2)
(0,4)	(-2j-1,2)	(2j+1,2)
(j,1)	(j+1,-1)	(-1,2)
(j,1)	(-j-1,-1)	(2j+1,2)
(j+1,1)	(j,-1)	(1,2)
(j+1,1)	(-j,1)	(2j+1,2)
(1,2)	(-j,1)	(j+1,1)

(2j+1,1)	(j,1)	(j+1,1)
(j,1)	(j,-1)	(0,2)
(j+1,1)	(j+1,-1)	(0,2)
(1,2)	(1,-2)	(0,4)
(2j+1,2)	(2j+1,-2)	(0,4)

Table 1: Non-zero interactions taken inside the truncation in the ten-coefficient model. The interaction of wave vectors, α and β, contributes to wave vector, γ.

The model consists of 10 nonlinear ordinary differential equations describing the time-evolution of the following Fourier coefficients:

$$
\begin{aligned}
&A \equiv \Psi^R_{j,1};\ E \equiv \Theta^I_{j,1};\ I \equiv \Theta^I_{0,2};\\
&B \equiv \Psi^R_{j+1,1};\ F \equiv \Theta^I_{j+1,1};\ J \equiv \Theta^I_{0,4};\\
&C \equiv \Psi^R_{1,2};\ G \equiv \Theta^I_{1,2};\\
&D \equiv \Psi^R_{2j+1,2};\ H \equiv \Theta^I_{2j+1,2}.
\end{aligned}
\tag{104}
$$

With the information in **table 1** it is straightforward, but tedious, to derive (from equations 71, 73 and 76) the ten first-order ordinary differential equations that govern the time-evolution of the amplitudes of each of the ten Fourier coefficients, listed in 104. These ten equations are referred to in the text as **equation set 105**:

$$
\begin{aligned}
\frac{dA}{dt} &= \frac{a_x j \Pr}{\pi k_A^2} E - \pi^2 \Pr k_A^2 A - (2j+1)\pi^2 a_x \frac{k_B^2 - k_C^2}{k_A^2} BC - \pi^2 a_x \frac{k_D^2 - k_B^2}{k_A^2} BD\\
\frac{dB}{dt} &= \frac{a_x (j+1) \Pr}{\pi k_B^2} F - \pi^2 \Pr k_B^2 B - (2j+1)\pi^2 a_x \frac{k_C^2 - k_A^2}{k_B^2} AC + \pi^2 a_x \frac{k_D^2 - k_A^2}{k_B^2} AD\\
\frac{dC}{dt} &= \frac{a_x j \Pr}{\pi k_C^2} G - \pi^2 \Pr k_C^2 C + (2j+1)\pi^2 a_x \frac{k_B^2 - k_A^2}{k_C^2} AB\\
\frac{dD}{dt} &= \frac{a_x (2j+1) \Pr}{\pi k_D^2} H - \pi^2 \Pr k_D^2 D - \pi^2 a_x \frac{k_B^2 - k_A^2}{k_D^2} AB\\
\frac{dE}{dt} &= \pi a_x j \mathrm{Ra} A - \pi^2 k_A^2 E - (2j+1)\pi^2 a_x BG - (2j+1)\pi^2 a_x CF - \pi^2 a_x BH - \pi^2 a_x DF - 2j\pi^2 a_x AI\\
\frac{dF}{dt} &= \pi a_x (j+1) \mathrm{Ra} B - \pi^2 k_B^2 F - (2j+1)\pi^2 a_x AG + (2j+1)\pi^2 a_x CE + \pi^2 a_x AH + \pi^2 a_x DE - 2(j+1)\pi^2 a_x BI\\
\frac{dG}{dt} &= \pi a_x j \mathrm{Ra} C - \pi^2 k_C^2 G + (2j+1)\pi^2 a_x AF + (2j+1)\pi^2 a_x BE - 4\pi^2 a_x CJ\\
\frac{dH}{dt} &= \pi a_x (2j+1) \mathrm{Ra} D - \pi^2 k_D^2 H - \pi^2 a_x AF + \pi^2 a_x BE - 4(2j+1)\pi^2 a_x DJ\\
\frac{dI}{dt} &= -4\pi^2 I + 4j\pi^2 a_x AE + 4(j+1)\pi^2 a_x BF\\
\frac{dJ}{dt} &= -16\pi^2 J + 8\pi^2 a_x CG + 8(2j+1)\pi^2 a_x DH\ ,
\end{aligned}
\tag{105}
$$

where the **total wave number** of each mode is defined as

$$k_A^2 \equiv a_x^2 j^2 + 1;\; k_B^2 \equiv a_x^2 (j+1)^2 + 1;\; k_C^2 \equiv a_x^2 + 4;\; k_D^2 \equiv a_x^2 (2j+1)^2 + 4\ . \qquad (106)$$

The set of ten equations (105) are solved numerically applying a fourth order Runge-Kutta approximation to the time derivatives (**section 22**). **Figure 14** shows the result of an integration, in terms of the evolution in time of the Fourier coefficients of the streamfunction, A, B, C and D, for an integration with j=1, a_x=1/2√2 and Pr=1, in which the Rayleigh number, Ra, is increased linearly in time from 0 to 25 times the critical value, Ra_c in the first 2.5 time units, and held constant at $25\mathrm{Ra}_c$ after t=2.5. The initial state is the state of rest, which is perturbed by introducing small perturbations to A and B.

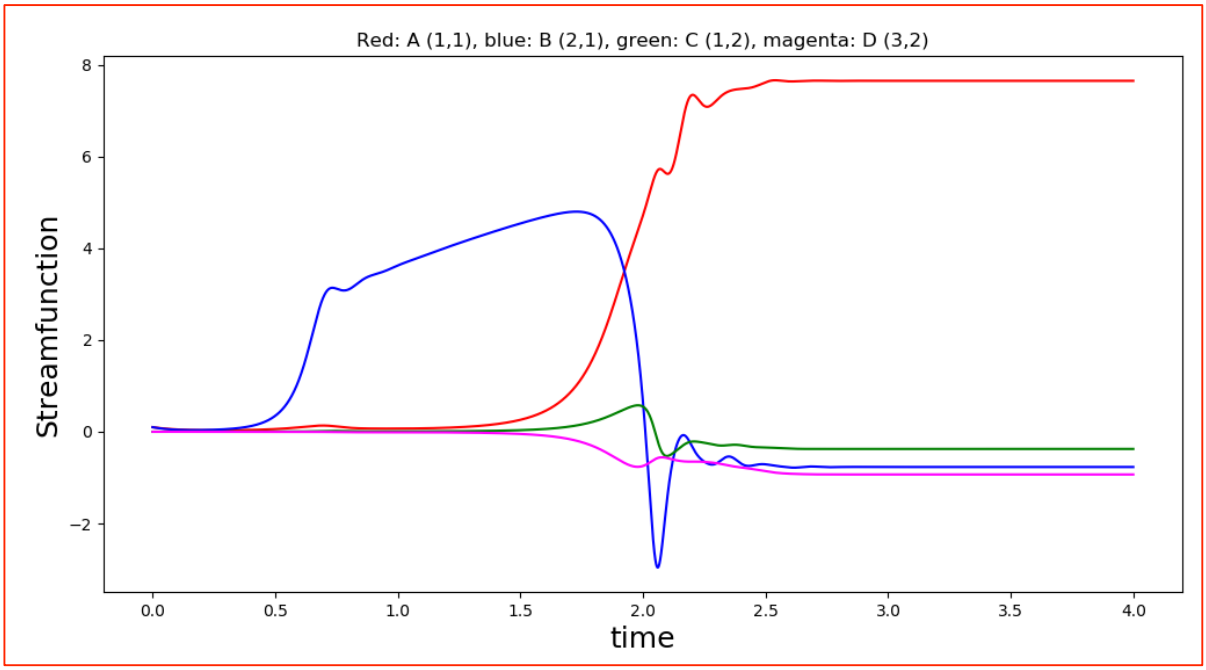

Figure 14. Time-evolution of the Fourier coefficients, A (blue), B (red), C (green) and D(magenta) of the ten-component model (eqs. 105), with a_x=1/2√2 and Pr=1, in a numerical integration with the state of rest as initial condition. During the first 2.5 time units the Rayleigh number increases linearly from 0 to 25 times the critical value for onset of instability of the mode corresponding to wave vector, (2,1), corresponding to B (streamfunction) and F (temperature). Ra is constant after t=2.5. The domain has an aspect ratio of 4√2, so that the mode (i.e. (2,1)) has an aspect ratio of 2√2. The mode with wave vector (2,1) is the fastest growing mode near the state of rest. Units are non-dimensional.

The minimum critical value of Ra for onset of instability of the fastest growing mode, in this case B, is $\mathrm{Ra}_c \approx 657$ (eq. 94). Indeed, we see, that B grows fastest initially (blue curve in **figure 14**). However, after t=0.17 the larger-scale mode, (1,1) (i.e. A), which has a critical Rayleigh number of about 1110, should grow exponentially also, at least "linearly". This does not seem to materialize until after t=1.5. However, the growth of A after t=1.5 seems to go at the cost of B. This implies that there is transition to a larger scale of motion. The stream function field before and after this transition is shown in **figure 15**. The "transfer of kinetic energy to larger scales", observed in this numerical example, is in fact typical for two-dimensional flow. In the next section we will study this phenomenon in a little more detail.

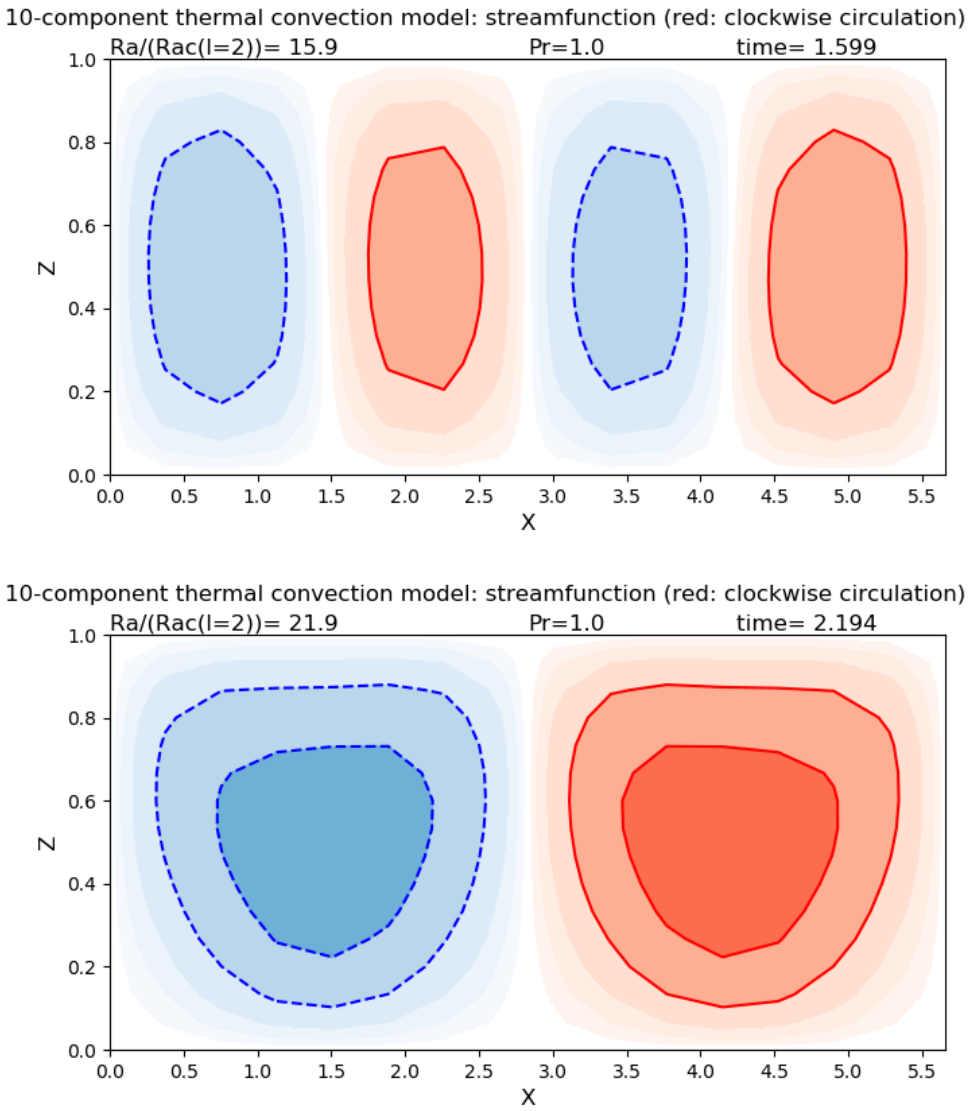

Figure 15. Streamfunction, at t=1.6 (above) and at t=2.2 (below) in the simulation, illustrated also in **figure 14**. Red shading corresponds to a clockwise circulation. The streamfunction is scaled with the steady state value of X at Ra=25Ra$_c$, in the Lorenz model (**exercise 6**). The contour interval is 1. The coefficient, B in the 10 component model corresponds to X in the Lorenz model with $a_x=1/\sqrt{2}$. See the animation: https://webspace.science.uu.nl/~delde102/10-ComponentModel(Converted).mov.

25. Upscale kinetic energy transfer in two-dimensional convection

The increase of the wavelength of two-dimensional convection cells with increasing Ra is consistently observed in reality. **Figure 16** shows the non-dimensional wavelength (or aspect ratio) of convection rolls as a function of Rayleigh number for different Prandtl numbers, as observed in the laboratory.

This section demonstrates that the increase of the aspect ratio in two-dimensional convection is likely due to the nonlinear terms that describe the transfer of kinetic energy between different scales of motion. In the ten-component model, the transfer of kinetic energy through the "spectrum", which consists of only four modes, is governed by the nonlinear terms in the first four equations in the set of equations, 105. These equations are repeated below.

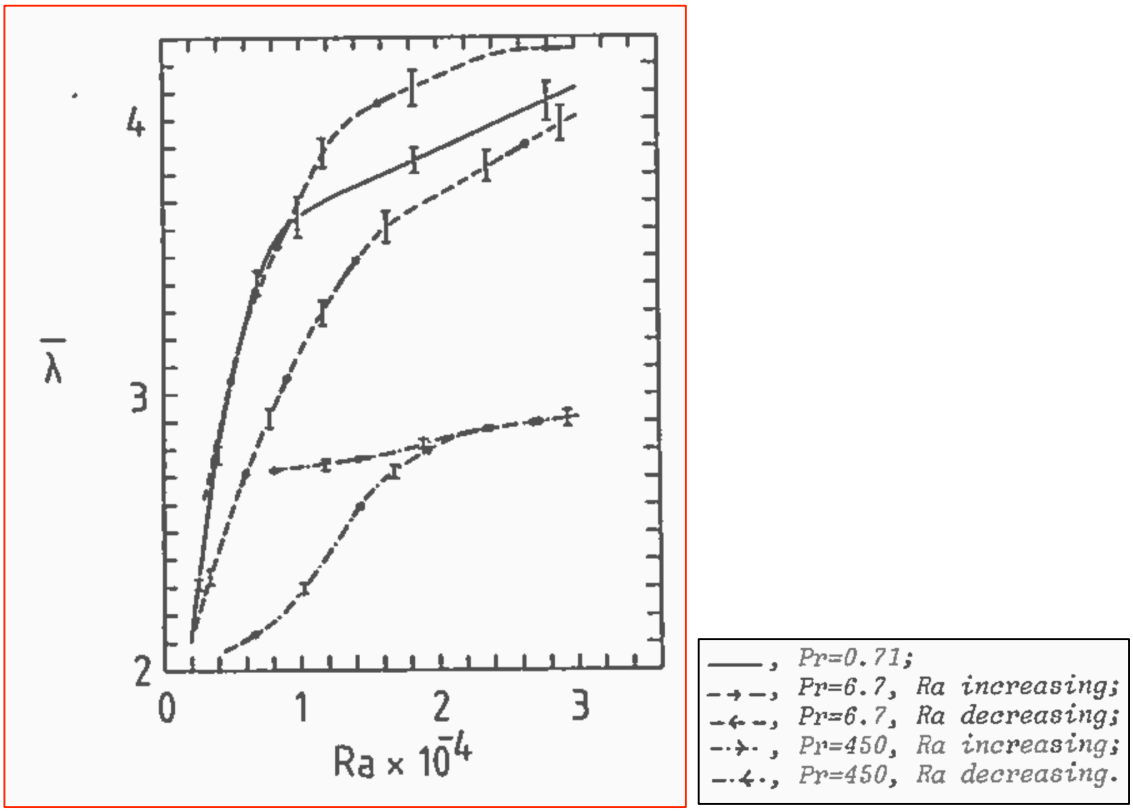

Figure 16. Smoothed values of the aspect ratio, $\bar{\lambda}$, of two-dimensional convection cells, with error limits, as measured by Willis et al. (1972). Note the dependence of the state of the system on its history. This typical property of non-linear systems is called **hysteresis**.

$$\frac{dA}{dt} = \frac{a_x j \mathrm{Pr}}{\pi k_A^2} E - \pi^2 \mathrm{Pr}\, k_A^2 A - (2j+1)\pi^2 a_x \frac{k_B^2 - k_C^2}{k_A^2} BC - \pi^2 a_x \frac{k_D^2 - k_B^2}{k_A^2} BD$$

$$\frac{dB}{dt} = \frac{a_x (j+1) \mathrm{Pr}}{\pi k_B^2} F - \pi^2 \mathrm{Pr}\, k_B^2 B - (2j+1)\pi^2 a_x \frac{k_C^2 - k_A^2}{k_B^2} AC + \pi^2 a_x \frac{k_D^2 - k_A^2}{k_B^2} AD$$

$$\frac{dC}{dt} = \frac{a_x j \mathrm{Pr}}{\pi k_C^2} G - \pi^2 \mathrm{Pr}\, k_C^2 C + (2j+1)\pi^2 a_x \frac{k_B^2 - k_A^2}{k_C^2} AB$$

$$\frac{dD}{dt} = \frac{a_x (2j+1) \mathrm{Pr}}{\pi k_D^2} H - \pi^2 \mathrm{Pr}\, k_D^2 D - \pi^2 a_x \frac{k_B^2 - k_A^2}{k_D^2} AB \qquad (107)$$

The importance of the non-linear terms in this set of equations, relative to the linear terms, increases with decreasing Prandtl number, Pr.

We simplify the linear terms by introducing relaxation coefficients, λ_A, λ_B, λ_C, and λ_D, which serve as a parametrisation of the linear terms, i.e. the effect of viscosity and the linear effect of the temperature field on the velocity field. Hence we rewrite these equations as

$$\frac{dA}{dt} = \lambda_A A + (2j+1)\pi^2 a_x \frac{k_C^2 - k_B^2}{k_A^2} BC - \pi^2 a_x \frac{k_D^2 - k_B^2}{k_A^2} BD$$

$$\frac{dB}{dt} = \lambda_B B - (2j+1)\pi^2 a_x \frac{k_C^2 - k_A^2}{k_B^2} AC + \pi^2 a_x \frac{k_D^2 - k_A^2}{k_B^2} AD$$

$$\frac{dC}{dt} = \lambda_C C + (2j+1)\pi^2 a_x \frac{k_B^2 - k_A^2}{k_C^2} AB$$

$$\frac{dD}{dt} = \lambda_D D - \pi^2 a_x \frac{k_B^2 - k_A^2}{k_D^2} AB \qquad (108)$$

The relaxation coefficients correspond to the linear **growth rate**, σ, of eq. 39, which is also the subject of **exercise 8**. A negative relaxation coefficient implies linear damping (a linearly stable mode), while and positive relaxation coefficient implies linear growth (a linearly unstable mode or **self-excited mode**, which grows exponentially in time).

The wave numbers k_A, k_B, k_C, and k_D, of each mode are defined in (106). For $a_x \approx 1/8$ and $j \approx 1$ (**figures 14 and 15**), the wave numbers are ordered from large scale (small wave number) to small scale (large wave number) according to

$$k_A^2 < k_B^2 < k_C^2 < k_D^2 \qquad (109)$$

Kinetic energy is "injected" into the spectrum through the self-excited modes. At modest Raleigh numbers this happens through the modes, *A* and *B*. The kinetic energy is then transferred to smaller scales of motion by triad interactions. This is in accord with "Richardson's notion that large eddies are unstable (self-excited) and break up, transferring their energy to somewhat smaller eddies" (Pope, section 6.1.1):

Big whorls have little whorls,
Which feed on their velocity;
And little whorls have lesser whorls,
And so on to viscosity…

The 10-component model includes only two triad interactions. The first interaction is between *A*, *B* and *C*. The second interaction is between *A*, *B* and *D*.

Let us assume that *A* and *B* are self-excited (i.e. $\lambda_A > 0$ and $\lambda_B > 0$), while *C* and *D* are damped (i.e. $\lambda_C < 0$ and $\lambda_D < 0$). The amplitudes of the damped modes, *C* and *D*, will in general remain small, as can be verified in **figure 14**. Then it is possible to apply a so-called **adiabatic elimination technique**, an idea introduced by Hermann Haken (1978). This consists of eliminating the damped variables, assuming that they follow the self-excited variables "adiabatically". In the system under study here, this means that *C* and *D* are always in equilibrium with *A* and *B*, which implies that the time-derivatives of *C* and *D* are zero, so that

$$C = -(2j+1)\pi^2 a_x \frac{k_B^2 - k_A^2}{\lambda_C k_C^2} AB \,. \tag{110}$$

and

$$D = \pi^2 a_x \frac{k_B^2 - k_A^2}{\lambda_D k_D^2} AB \,. \tag{111}$$

Substituting (107) and (108) into the equations for time-evolution of A and B yields

$$\boxed{\frac{dA}{dt} = \left(\lambda_A + \mu_1 B^2\right) A}\,, \tag{112}$$

with

$$\mu_1 = \pi^4 a_x^2 \frac{\left(k_B^2 - k_A^2\right)}{k_A^2} \left((2j+1)^2 \frac{k_B^2 - k_C^2}{\lambda_C k_C^2} + \frac{k_B^2 - k_D^2}{\lambda_D k_D^2} \right) > 0 \,,$$

and

$$\boxed{\frac{dB}{dt} = \left(\lambda_B + \mu_2 A^2\right) B}\,, \tag{113}$$

with

$$\mu_2 = \pi^4 a_x^2 \frac{k_B^2 - k_A^2}{k_B^2} \left((2j+1)^2 \frac{k_C^2 - k_A^2}{\lambda_C k_C^2} + \frac{k_D^2 - k_A^2}{\lambda_D k_D^2} \right) < 0 \,.$$

Remember: $\lambda_C<0$ and $\lambda_D<0$.

We have thus reduced the system of four equations, which describe the streamline pattern in the 10-component model, to a closed system of two equations (112 and 113). Note that, because $\mu_1>0$ and $\mu_2<0$, A can grow at the cost of B. In Haken's words, mode A "**enslaves**" mode B. This implies that all kinetic energy goes to the larger scale of motion (mode A). This is indeed what happens in the simulation illustrated in **figures 14** and **15**. This is in contrast to Richardson's hypothesis, that there should be a "cascade of energy to smaller scales". The absence of a downscale transfer of energy is related to the impossibility of "vortex-stretching" in two-dimensional flow, or the conservation of vorticity by the non-linear terms (**section 26**).

The surprising degree of order, frequently exhibited by complex non-linear systems, as the one studied here, is the subject of the relatively new discipline, called "**Synergetics**" by Haken (1978). Synergetics is the science explaining the formation of patterns and ordered structures in open non-linear systems, consisting of interacting sub-systems. These structures are called "**dissipative structures**. "**Open**" means that energy (heat or matter) is exchanged with the outside world. "**Dissipative**" means that the system is subject to friction or some other form of dissipation, such as viscosity or molecular diffusion of heat.

26. Spectral blocking in two-dimensional flow

This section investigates the nonlinear **triad interactions** in the 10-component model describing spectral transfer of kinetic energy and shows that there is tendency to inhibit the net transfer of energy both to smaller *and* to larger scales in the 10-component model under study. This tendency, in fact, is generic and is consequence of the absence of vortex stretching in two-dimensional flow.

Let us go back to the set of equations (108) and assume that the relaxation coefficients are all equal to zero, which means that the system is frictionless and is isolated (no contact with the outside world), and should conserve kinetic energy, K.

The kinetic energy, K_γ, in a mode corresponding to wave vector, γ, is given by (**exercise 10**)

$$K_\gamma = \frac{1}{2} k_\gamma^2 \Psi_\gamma^2 .$$

The total kinetic energy, K, is equal to the sum of the contributions of all modes in all four quadrants of wave vector space. In view of the symmetry relations listed in **section 9**, we can restrict out attention to the contributions from wave vectors in one quadrant. Therefore, we define K as follows:

$$K \equiv K_A + K_B + K_C + K_D = \frac{1}{2}\left(k_A^2 A^2 + k_B^2 B^2 + k_C^2 C^2 + k_D^2 D^2\right)$$

Let us isolate the two triad interactions in the 10-component model , i.e. the interaction between A, B and C and the interactions between A, B and D, which we write as two sets of three equations as follows.

$$\begin{aligned}
\frac{dK_A}{dt} &= (2j+1)\pi^2 a_x \left(k_C^2 - k_B^2\right) ABC - \pi^2 a_x \left(k_D^2 - k_B^2\right) ABD \\
\frac{dK_B}{dt} &= -(2j+1)\pi^2 a_x \left(k_C^2 - k_A^2\right) ABC + \pi^2 a_x \left(k_D^2 - k_A^2\right) ABD \\
\frac{dK_C}{dt} &= (2j+1)\pi^2 a_x \left(k_B^2 - k_A^2\right) ABC \\
\frac{dK_D}{dt} &= -\pi^2 a_x \left(k_B^2 - k_A^2\right) ABD .
\end{aligned}$$

It can easily be seen that $dK/dt=0$. **Kinetic energy is conserved by the non-linear terms**. If we separate the equations governing the spectral exchange of kinetic energy in the two triad interactions we find for the first triad, $(j,1)$, $(j+1,1)$ and $(1,2)$,

$$\begin{aligned}
\frac{dK_A}{dt} &= (2j+1)\pi^2 a_x \left(k_C^2 - k_B^2\right) ABC \\
\frac{dK_B}{dt} &= -(2j+1)\pi^2 a_x \left(k_C^2 - k_A^2\right) ABC \\
\frac{dK_C}{dt} &= (2j+1)\pi^2 a_x \left(k_B^2 - k_A^2\right) ABC
\end{aligned}$$

and for the second triad $(j,1)$, $(j+1,1)$ and $(2j+1,2)$

$$\frac{dK_A}{dt} = -\pi^2 a_x \left(k_D^2 - k_B^2\right) ABD$$
$$\frac{dK_B}{dt} = \pi^2 a_x \left(k_D^2 - k_A^2\right) ABD$$
$$\frac{dK_D}{dt} = -\pi^2 a_x \left(k_B^2 - k_A^2\right) ABD.$$

Using the inequality (109) it is easily seen that the middle scale (*B*) in both triad interactions either looses or gains energy from the both larger scale (*A*) and the smaller scale (*C* or *D)*. This phenomenon is called "**spectral blocking**". Note that, for a_x=1/2√2, the ordering of the total wave numbers differs from the ordering given in (109) if *j*>4. This has no consequences for the second triad, but does have consequences, because k_C^2 is be smaller than k_B^2.

In the year 1953 R. Fjortoft and G.K. Batchelor independently showed that spectral blocking is due to the simultaneous conservation of kinetic energy and vorticity by the non-linear advection terms in two-dimensional flow. **Vorticity** is defined as the curl of the velocity vector:

$$\vec{\omega} \equiv \vec{\nabla} \times \vec{v} = \begin{vmatrix} \hat{i} & \hat{j} & \hat{k} \\ \frac{\partial}{\partial x} & \frac{\partial}{\partial y} & \frac{\partial}{\partial z} \\ u & v & w \end{vmatrix} = \left(\frac{\partial w}{\partial y} - \frac{\partial v}{\partial z}\right)\hat{i} + \left(\frac{\partial u}{\partial z} - \frac{\partial w}{\partial x}\right)\hat{j} + \left(\frac{\partial v}{\partial x} - \frac{\partial u}{\partial y}\right)\hat{k} \qquad (114)$$

Here, $\hat{i}, \hat{j}$ and $\hat{k}$ are unit vectors in the *x, y* and *z* directions, respectively. In the case treated in this section the flow restricted to the *x*-*z* plane. The associated vorticity, η, is

$$\eta \equiv \frac{\partial u}{\partial z} - \frac{\partial w}{\partial x} = -\left(\frac{\partial^2 \psi}{\partial x^2} + \frac{\partial^2 \psi}{\partial z^2}\right) \qquad (115)$$

According to eq. 54 and in the absence of buoyancy-forcing and dissipation due to viscosity, vorticity is conserved by fluid parcels:

$$\frac{d\nabla^2 \psi}{dt} = \frac{d\eta}{dt} = 0 .$$

27. Exercises, part 4

(16)

The **total enstrophy** (E) (the area integrated square-vorticity) in two-dimensional flow is

$$E = \frac{1}{2}\int\left(\eta^2\right)d\sigma$$

(see **lecture 9**). Express E in terms the Fourier coefficients of the stream function (see **exercise 10**). In **section 26** it is shown that kinetic energy is conserved in the two triad interactions in the 10-component model. Show that enstrophy is also conserved in these two triad interactions. Assume that mode B in this model possesses the lowest critical Rayleigh number. Show that the middle scale in both triad interactions in the 10-component model looses/gains more kinetic energy to/from larger scale than to/from the smaller scale

(17)

For this exercise you are given the python-code of the 10-component model of two-dimensional convection, which integrates the twelve equations (105), and asked to install and run this code on your computer. Oscillations with a period in the range between 1 and 10 non-dimensional viscous time-units (H^2/ν) are observed in a layer of fluid with low Pr and Rayleigh numbers which are just super-critical to several times super-critical (Krishnamurti, 1973). The 10-component model also exhibits oscillations at low Pr (=0.1), with $a_x=1/2\sqrt{2}$ and for Rayleigh number 1.5 times supercritical.

(a) Can you qualitatively foresee the existence of these oscillations from eqs. 112 and 113?
(b) Investigate these oscillations in the 10-component model (105). Are the oscillations qualitatively in accord with your predictions based on eqs. 112 and 113?
(c) Do you get oscillations with periods similar to periods observed by Krishnamurti?
(d) Is this solution "chaotic"? If so, why?
(e) Make a scatter plot ("map") of the peak-values of A as a function of the previous peak-value of A. Compare this "map" with the Lorenz map (**figure 12**).
(f) Plot the time between successive peaks as a function of time half-way these peaks. What do you conclude from this?

28. References part 4

Batchelor, G.K. 1953: **Theory of homogeneous turbulence**. Cambridge University Press. 186 pp.

R. Fjortoft, 1953: On the changes in the spectral distribution of kinetic energy for two-dimensional, non-divergent flow. **Tellus**, **5**, 225-230.

Haken, H., 1977: **Synergetics**. Springer Verlag, Heidelberg. 325 pp.

Krishnamurti, R., 1973: Some further studies on the transition to turbulent convection. **J.Fluid Mech**., **60**, 285-303.

Pope, S.B., 2000: **Turbulent Flows**. Cambridge University Press. 771 pp.

Willis, G.E., J.W. Deardorff and R.C.J. Somerville, 1972: Roll-diameter dependence in Rayleigh convection and its effect upon heat flux. **J.Fluid Mechanics**, **54**, 351-367.

Part 5: Pattern formation in thermal convection

By Aarnout van Delden (http://www.staff.science.uu.nl/~delde102/TinF.htm)

29. The horizontal pattern of thermal convection

Our attention up to this point has been restricted to two-dimensional thermal convection, or convection in the form of rolls (upper panel of **figure 1**). Three-dimensional convection patterns, such as hexagons, are observed just as frequently as rolls. Therefore, it is important to address the interesting question of convection pattern selection. Can we reproduce observed three-dimensional convection patterns with the model equations, which are introduced in **sections 2 and 3**? Can we use these equations to understand why and under which circumstances a particular highly ordered flow pattern appears in the fluid system under study here? Thermal convection between parallel horizontal rigid boundaries is a prototype problem in studies addressing the question of growth and form in physical, chemical and biological systems with many degrees of freedom. See for example the seminal book, entitled "*On Growth and Form*", by D'Arcy Wentworth Thompson (1942) or the popular book by Philip Ball, entitled "*Shapes: Natures Patterns*", published in 2009. We will take a peek at this field of study in this part of these lecture notes.

Thermal convection is observed to take place mostly in the form of regular cellular patterns. **Figure 2**, for example, demonstrates that convection in the atmosphere is observed mostly as *cloud streets* (rolls), *open convection cells*, with clouds (upward motion) at the edge of the cell and downward motion in the middle, and *closed convection cells* with clouds in the middle and downward motion at the edges.

The question of convective pattern selection is very difficult because it cannot be solved by linearising the governing equations. It is an intrinsically non-linear mathematical problem. Nevertheless, with some simplifications we can get a long way.

First we discuss some phenomenological aspects of this question. For simplicity we begin by assuming that the fluid layer undergoing convection is tessellated into a regular array of identical convection cells. There are many possible vertical velocity fields that are periodic in both horizontal directions. The horizontal field of vertical velocity in the fluid layer can be organised into parallel strips, triangles, squares, rectangles and hexagons. A convection pattern consisting of equilateral triangles is pretty unlikely, except if it is forced to be this way by the boundaries of a triangular domain. A square convection pattern will be preferred over a rectangular convection pattern, except if boundary conditions impose otherwise. But even squares do not seem to be very probable, as is explained in the following.

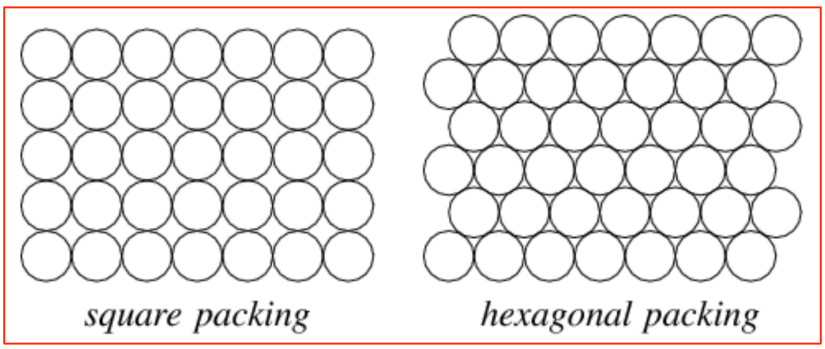

Figure 17. An arrangement of circles inside a given boundary such that no two circles overlap and some (or all) circles are mutually tangent. The hexagonal packing is closest (most efficient) because the area covered by circles divided by the total area is a minimum ($=\pi/(2\sqrt{3})=0.91$). This ratio in the case of square packing ($\pi/4=0.79$).

Let us assume that convection starts as a series of updraughts and compensating downdraughts. The updraughts will probably be circular in the horizontal plane. This is because a circle has a minimum circumference for a given area. Circular updraughts, therefore, are probably less susceptible to diffusive dissipation. Suppose, for simplicity, that all circular updraughts in the fluid layer are identical, having a fixed radius and intensity. How will these updraughts be organised? Probably as closely packed as possible. The densest packing of circles in the plane is the hexagonal lattice of the bee's honeycomb (**figure 17**). One must of course allow for downward motion in between the circular upward motion to satisfy mass balance. The intensity of the compensating downward motion decreases with increasing spacing of the circular updraughts. An optimal spacing of circular updraughts might exist, which depends on minimizing the difference between the maximum updraught velocity and the minimum downdraught velocity, again in order to minimize diffusive dissipation. In any case, the result is a series of hexagonal convections cells with upward motion in the middle and downward motion in the periphery. This convection pattern would, in meteorology, be referred to as a closed convection cell, or "*l*-cell" in physics. The sense of the circulation can also be the reverse, which would result in a so-called "open convection cell" in meteorology, or "*g*-cell" in physics.

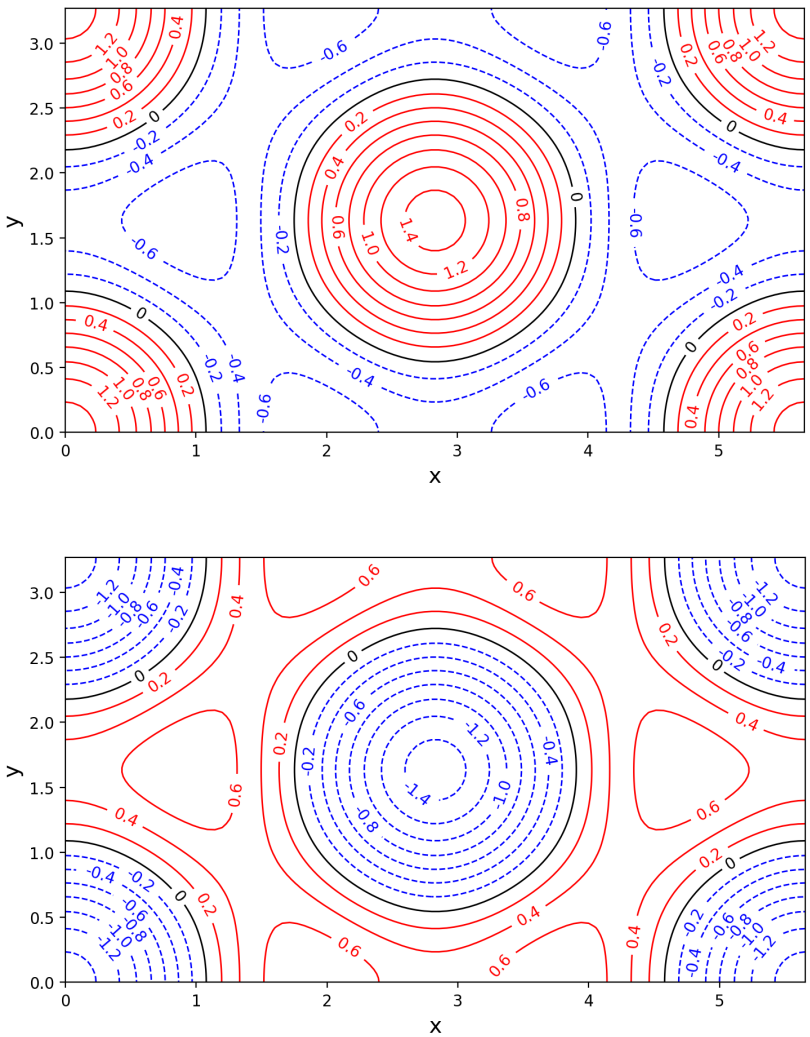

Figure 18. The hexagonal pattern of w according to eq. 116, with l=m=1, and a plus sign in front of the second term $a_y=\sqrt{3}a_x$. The upper panel shows an **up-hexagon** (eq. 116a). The area covered by circular updraught divided by the total area is equal to 0.4. The lower panel shows a **down-hexagon** (eq. 116b).

A hexagonal pattern of the vertical velocity, which fulfils continuity, is described by

$$w = \cos\pi a_x lx \cos\pi a_y my + \frac{1}{2}\cos 2\pi a_x lx \quad \text{(up-hexagon)} \tag{116a}$$

$$w = -\cos\pi a_x lx \cos\pi a_y my - \frac{1}{2}\cos 2\pi a_x lx \quad \text{(down-hexagon)} \; . \tag{116b}$$

$$w = -\cos\pi a_x lx \cos\pi a_y my + \frac{1}{2}\cos 2\pi a_x lx \quad \text{(up-hexagon)} \tag{116c}$$

$$w = \cos\pi a_x lx \cos\pi a_y my - \frac{1}{2}\cos 2\pi a_x lx \quad \text{(down-hexagon)} \; . \tag{116d}$$

with

$$a_y = \frac{2H}{L_y} = \sqrt{3}a_x \text{ and } a_x = \frac{2H}{L_x} = \frac{1}{2\sqrt{2}} \; , \tag{117}$$

so that $L_y = \sqrt{3}L_y$ (Palm, 1960). Note that the sign in front of the second term (the roll pattern) determines whether the result is an up-hexagon (+) or a down-hexagon (-).

Figure 18 shows up- and down-hexagons for l=1 and m=1, according to eq.116a,b. While the updraught is circular, the downdraughts in between appear triangular.

The hexagonal convection pattern consists of a superposition of two Fourier modes with identical total horizontal wave numbers, representing two patterns: a chequerboard convection pattern (**figure 19**, left panel), with alternating square up- and down draughts (the first term on the right hand side of 116), and two rolls aligned along the y-axis (**figure 19**, right panel). The first step to tackle the question of plan-form-selection in thermal convection is to formulate a low order-model of hexagonal convection, which includes the two Fourier modes in eq. 116.

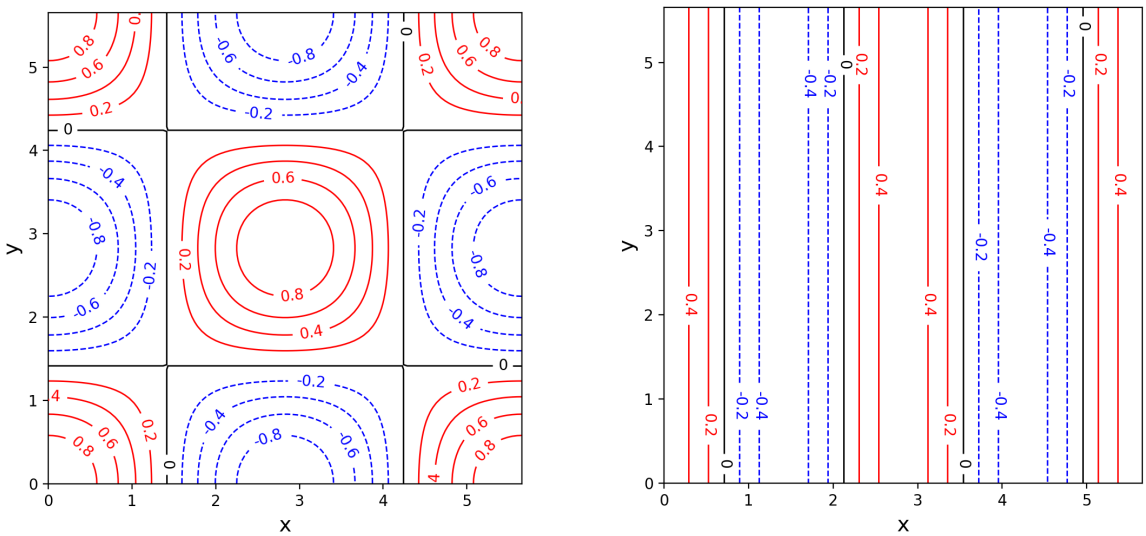

Figure 19. Left panel: a square (chequerboard) pattern of w, according to the first term on the r.h.s. of eq. 116, with l=m=1. Note that the pattern of squares does not correspond to the square packing shown in **figure 17**. Right panel: a two-dimensional pattern of w, according to the second term on the r.h.s. of eq. 116, with l=2 and m=0 . In both cases the domain is a square ($a_x = a_y = 1/2\sqrt{2}$). Updraughts and downdraughts cover equal areas. In **figure 18** the domain is rectangular, out of necessity to fit in a hexagon.

30. Fourier representation in three spatial dimensions

The three-dimensional field vertical velocity field can be expanded in a Fourier series as in eq. 61:

$$w(x,y,z,t) = \sum_{\alpha} W_{\alpha}(t) S_{\alpha}(x,y,z) \ . \tag{118}$$

Here W_{α} is a time-dependent complex Fourier coefficient, and the basis-functions,

$$S_{\alpha}(x,y,z) = \exp\left\{ i\pi\left(a_x l_{\alpha} x + a_y m_{\alpha} y + n_{\alpha} z \right) \right\} \ . \tag{119}$$

$\sum_{\alpha}$ means a sum over all integral lattice-points in the volume, $\alpha = (l_{\alpha}, m_{\alpha}, n_{\alpha})$. The parameters a_x and a_y are a measures of the aspect ratio of the three-dimensional domain of computation:

$$0 \le x \le L_x / H;\ 0 \le y \le L_y / H, \tag{120}$$

so that

$$a_x = \frac{2H}{L_x};\ a_y = \frac{2H}{L_y}. \tag{121}$$

Because boundary conditions are periodic, this domain may be repeated in both horizontal directions ad infinitum, so as to obtain a regular array of cells with a prescribed wavelength.

The orthonormality of the basis functions, S_{α}, is expressed as

$$\int S_{\alpha} S_{\beta}^{*} d\sigma = \delta_{\alpha,\beta}, \tag{122}$$

where the asterisk designates a complex conjugate, while δ is the Kronecker delta. The integration extends over the region

$$0 \le x \le \frac{2}{a_x},\ 0 \le y \le \frac{2}{a_y},\ 0 \le z \le 2, \tag{123}$$

and dσ is a volume element divided by the total volume, $\sigma = 8/(a_x a_y)$.

If the following wave vectors are taken inside the truncation of the low-order model:

$(\pm 1, \pm 1, \pm n)$, $(0, \pm 2, \pm n)$ with n=1,2,3…N_{max}. (124)

A hexagonal pattern is obtained if $a_y = \sqrt{3} a_x$. A square pattern is obtained if $a_y = a_x$ while ignoring the wave vector, $(0, \pm 2, \pm n)$. A roll convection pattern is obtained by ignoring $(\pm 1, \pm 1, \pm n)$. An important property of the model in the case that $a_y = \sqrt{3} a_x$ is that the two Fourier modes, $(\pm 1, \pm 1, \pm n)$ and $(0, \pm 2, \pm n)$, have identical horizontal wave numbers. This implies that both Fourier modes have the same critical Rayleigh number for onset of convection and will therefore grow with the same linear growth rates.

31. The nonlinear equations for three-dimensional convection

The fundamental equations for shallow convection, including the Boussinesq approximation, are (sections 2 and 3)

$$\frac{\partial u}{\partial t}+u\frac{\partial u}{\partial x}+v\frac{\partial u}{\partial y}+w\frac{\partial u}{\partial z}=-\frac{1}{\rho_{ref}}\frac{\partial p'}{\partial x}+\nu\nabla^2 u \ ; \tag{125a}$$

$$\frac{\partial v}{\partial t}+u\frac{\partial v}{\partial x}+v\frac{\partial v}{\partial y}+w\frac{\partial v}{\partial z}=-\frac{1}{\rho_{ref}}\frac{\partial p'}{\partial y}+\nu\nabla^2 v \ ; \tag{125b}$$

$$\frac{\partial w}{\partial t}+u\frac{\partial w}{\partial x}+v\frac{\partial v}{\partial y}+w\frac{\partial w}{\partial z}=-\frac{1}{\rho_{ref}}\frac{\partial p'}{\partial z}+g\alpha T'+\nu\nabla^2 w \ ; \tag{125c}$$

$$\frac{\partial T'}{\partial t}+u\frac{\partial T'}{\partial x}+v\frac{\partial T'}{\partial y}+w\frac{\partial T'}{\partial z}=\Gamma w+\kappa\nabla^2 T' \tag{126}$$

$$\frac{\partial u}{\partial x}+\frac{\partial v}{\partial y}+\frac{\partial w}{\partial z}=0 \ \text{(continuity equation);} \tag{127}$$

From (125a,b,c) and (126) it is possible to derive two new governing equations, one for the vertical component of the vorticity-vector (see eq.114),

$$\zeta=\frac{\partial v}{\partial x}-\frac{\partial u}{\partial y} \ , \tag{128}$$

and one for the vertical velocity, w, thereby eliminating p'. The latter equation is the (non-linear) version of equation 22.

The vorticity equation is found by taking the partial derivative with respect to y of (125a) and subtracting the result from the partial derivative with respect to x of (125b). In terms of the following units of length $\{L\}$, time $\{t\}$ and temperature $\{T\}$,

$$\{L\}=H;\ \{t\}=\frac{H^2}{\kappa};\ \{T\}=\frac{\kappa\nu}{g\alpha H^3} \ , \tag{129}$$

the equations are

$$\frac{d\zeta}{dt}=\zeta\frac{\partial w}{\partial z}-\frac{\partial w}{\partial x}\frac{\partial v}{\partial z}+\frac{\partial w}{\partial y}\frac{\partial u}{\partial z}+\mathrm{Pr}\nabla^2\zeta \ , \tag{130}$$

and

$$\frac{d\nabla^2 w}{dt} = \left(2\frac{\partial^2 u}{\partial z^2} - 2\frac{\partial^2 u}{\partial x \partial z} - \nabla^2 u\right)\frac{\partial w}{\partial x} + \left(2\frac{\partial^2 v}{\partial z^2} - 2\frac{\partial^2 w}{\partial x \partial z} - \nabla^2 v\right)\frac{\partial w}{\partial y} - \nabla^2 w \frac{\partial w}{\partial z}$$
$$+2\left(\frac{\partial^2 u}{\partial y \partial z} - \frac{\partial^2 w}{\partial x \partial y}\right)\frac{\partial v}{\partial x} + 2\left(\frac{\partial^2 v}{\partial y \partial z} - \frac{\partial^2 w}{\partial y^2}\right)\frac{\partial v}{\partial y}$$
$$+2\left(\frac{\partial^2 u}{\partial x \partial z} - \frac{\partial^2 w}{\partial x^2}\right)\frac{\partial u}{\partial x} + 2\left(\frac{\partial^2 v}{\partial x \partial z} - \frac{\partial^2 w}{\partial x \partial y}\right)\frac{\partial u}{\partial y} + \Pr \nabla_H^2 \theta + \Pr \nabla^4 w \qquad (131)$$

The Prandtl number (Pr) is defined in (60). Equation 131 is the full non-linear version of equation 22. ∇_h^2 is defined in eq. 23.

The three-dimensional non-dimensional version of the temperature equation is (see eq. 17 and 58)

$$\frac{d\theta}{dt} = Raw + \nabla^2\left(\theta - \bar{\theta}(z)\right) \qquad (132)$$

Ra is the Rayleigh number (eq. 59). The parameter, $\bar{\theta}(z)$, is new, and is explained in **section 32**.

Note that

$$\frac{d}{dt} = \frac{\partial}{\partial t} + u\frac{\partial}{\partial x} + v\frac{\partial}{\partial y} + w\frac{\partial}{\partial z}. \qquad (133)$$

The top and bottom horizontal boundaries are assumed to be rigid, stress-free and perfectly conducting, as in **section 4**:

$$w = 0;\ \frac{\partial u}{\partial z} = \frac{\partial v}{\partial z} = 0;\ \theta = \frac{\partial^2 \theta}{\partial z^2} = 0. \qquad (134)$$

32. Introducing vertical asymmetry

In **section 31**we have secretly introduced a z-dependent **static temperature distribution** $\bar{\theta}(z)$, which may deviate from linearity, such as imposed by eq. 18 when Γ=constant, thus making the static reference state (the state of rest) vertically asymmetric. Enok Palm (1960) discovered that such an asymmetry plays a leading role in convection pattern selection.

The static state obeys the following equation:

$$\nabla^2(\theta - \bar{\theta}(z)) = 0 \text{ or } \theta = \bar{\theta}(z). \qquad (135)$$

Remember that θ is the temperature perturbation relative to a static state in which temperature depends linearly on height (eq. 18). In other words, $\bar{\theta}(z)$ represents the deviation from linearity of the static state temperature profile. In the atmosphere this might be due to net absorption or emission of radiation, latent heat release in the convective layer due to condensation of water vapour in the updraught. The static state temperature profile may also deviate from linearity due to non-stationary temperature at the boundary. In the example

shown in **figure 2**, the layer of air undergoing convection flows southward over a sea surface, which becomes progressively warmer. *For simplicity* this effect can be modeled by assuming that the temperature at the lower *and* upper boundary increases at a constant rate, Q, according to $\theta = Qt$. The deviation of the static temperature profile from linearity will be governed by,

$$\frac{\partial \theta}{\partial t} = \frac{\partial^2 \theta}{\partial z^2} \text{ with } \theta = Qt \text{ at } z=0 \text{ and } z=1. \tag{136}$$

The solution is

$$\theta = Qt + \frac{Q}{2} z(z-1). \tag{137}$$

The deviation from linearity of θ is determined by the quadratic dependence on z. **If $Q>0$ the static temperature profile is concave**, while **if $Q<0$ the static temperature profile is convex**. Concave means that the θ decreases most strongly with z at $z=0$.

We do not want to be too specific about the process which maintains the static temperature profile. Hence we will simplify matters by just prescribing the nonlinear dependence of the static temperature profile by a function of z as

$$\bar{\theta}(z) = C \sin \pi z, \tag{138}$$

so that, the static temperature profile is concave if $C<0$, while the static temperature profile is convex if $C>0$. This approach can easily be assimilated with the Fourier decomposition of the variables (**sections 30** and **33**).

33. Fourier transformation of the temperature equation

The method of transforming the equations to normal mode form will be illustrated in detail in this section with the temperature equation (132). The variables are written in Fourier series as follows.

$$\begin{Bmatrix} u \\ v \\ w \\ \zeta \\ \theta \end{Bmatrix} = \sum_\alpha \begin{Bmatrix} U_\alpha(t) \\ V_\alpha(t) \\ W_\alpha(t) \\ Z_\alpha(t) \\ \Theta_\alpha(t) \end{Bmatrix} S_\alpha(x,y,z) \ , \tag{139}$$

as in eq. 118. U_α, V_α, W_α, Z_α, and Θ_α are a time-dependent complex Fourier coefficients, or amplitudes, and $S_\alpha(x,y,z)$ is defined by eq. 119.

The definition of the vertical component of the vorticity (eq. 128) and the continuity equation (eq. 127) are linear equations. The Fourier transformation of these equations is easy, resulting in the following diagnostic relations.

$$U_\alpha = \frac{-a_x n_\alpha l_\alpha}{q_\alpha^2} W_\alpha + \frac{a_y m_\alpha}{\pi q_\alpha^2} i Z_\alpha ; \tag{140}$$

$$V_\alpha = \frac{-a_y n_\alpha m_\alpha}{q_\alpha^2} W_\alpha - \frac{a_x l_\alpha}{\pi q_\alpha^2} iZ_\alpha , \tag{141}$$

where

$$q_\alpha^2 = a_x^2 l_\alpha^2 + a_y^2 m_\alpha^2 \tag{142}$$

is the total horizontal wave number. The total vertical wave number is

$$k_\alpha^2 \equiv \pi^2 q_\alpha^2 + \pi^2 n_\alpha^2 \ . \tag{143}$$

Making the temperature eq. 126 non-dimensional, using the units of time, length and temperature given in (129), yields

$$\frac{\partial \theta}{\partial t} = -u\frac{\partial \theta}{\partial x} - v\frac{\partial \theta}{\partial y} - w\frac{\partial \theta}{\partial z} + \mathrm{Ra}w + \nabla^2\left(\theta - \bar{\theta}\right) \tag{144}$$

Fourier transforming this equation entails that we first substitute 139 and then make use of the orthonormality of the basis functions ($S_\alpha(x,y,z)$) (eq. 122). The advection terms (the first three terms on the r.h.s. of eq.144) can expressed as

$$\sum_{\alpha,\beta} \left\{ -i\pi a_x l_\alpha U_\beta \Theta_\alpha - i\pi a_y m_\alpha V_\beta \Theta_\alpha - i\pi n_\alpha W_\beta \Theta_\alpha \right\} S_\alpha S_\beta \ , \tag{145}$$

where $\sum_{\alpha,\beta}$ is a double sum over all wave vectors, α and β. Substitution of (140) and (141) in (145), so as to eliminate U_β and V_β, yields

$$\sum_{\alpha,\beta} \pi \left\{ \frac{n_\beta\left(l_\alpha l_\beta a_x^2 + m_\alpha m_\beta a_y^2\right)}{q_\beta^2} - n_\alpha \right\} iW_\beta \Theta_\alpha S_\alpha S_\beta + \frac{a_x^2 a_y^2}{q_\beta^2}\left(l_\alpha m_\beta - l_\beta m_\alpha\right) Z_\beta \Theta_\alpha S_\alpha S_\beta \, . \tag{146}$$

We now use the property of orthonormality of S_α (122). Multiplying both sides of (144) by S_γ^* and integrating over the volume $\mathrm{d}\sigma$, using (122), we obtain the spectral form of the temperature equation, which consists of a system of prognostic quations for the Fourier coefficients (amplitudes) of the temperature for each wave vector, $\gamma = (l_\gamma, m_\gamma, n_\gamma)$:

$$\frac{d\Theta_\gamma}{dt} = \sum_{\alpha,\beta} \left\{ \pi L_{\gamma\alpha\beta} iW_\alpha \Theta_\beta + M_{\gamma\alpha\beta} iZ_\alpha \Theta_\beta \right\} + \mathrm{Ra}W_\gamma - k_\gamma^2\left(\Theta_\gamma - \bar{\Theta}_\gamma\right), \tag{147}$$

where the **coupling coefficients** (or **interaction coefficients**) are defined as

$$L_{\gamma\alpha\beta} \equiv \left\{ \frac{n_\beta\left(l_\alpha l_\beta a_x^2 + m_\alpha m_\beta a_y^2\right)}{q_\beta^2} - n_\alpha \right\} \delta_{\alpha,\beta} \ , \tag{148}$$

and

$$M_{\gamma\alpha\beta} \equiv \frac{a_x^2 a_y^2}{q_\beta^2}\left(l_\alpha m_\beta - l_\beta m_\alpha\right)\delta_{\alpha,\beta} \ . \tag{149}$$

The coupling coefficients are zero unless the following **selection rule** (in vector form) is satisfied.

$$\alpha+\beta=\gamma \ . \tag{150}$$

34. Three-dimensional poloidal flow

The spectral form of the vorticity equation (130) can also be found, following the method described in the previous section. The result will not be written out in full here because, for simplicity and on good grounds, it is easily observed that the transformed vorticity equation does not contain a linear term, which may lead to spontaneous growth of the spectral amplitudes of the vorticity. In other words, the Fourier coefficients of the vorticity, Z_α (eq. 139), are never self-excited. The coefficients, Z_α, can grow only through nonlinear interactions. Therefore, we will henceforth neglect the coefficients, Z_α, i.e. assume they remain equal to zero. This approximation, which greatly reduces the number of degrees of freedom in the system, represents an extreme application of **adiabatic elimination** (**section 25**). It implies that the fluid motion is fixed completely by the vertical velocity, *w*. The other two velocity components, *u* and *v*, can be retrieved from the following two diagnostic spectral equations, which are derived from eqs. 140 and 141, assuming that $Z_\alpha = 0$.

$$U_\alpha = \frac{-a_x n_\alpha l_\alpha}{q_\alpha^2} W_\alpha \ \text{and} \ V_\alpha = \frac{-a_y n_\alpha m_\alpha}{q_\alpha^2} W_\alpha \, . \tag{151}$$

This type of flow is called "**poloidal**".

For poloidal flow, i.e. with $Z_\alpha = 0$, the spectral form of the temperature equation (147) becomes

$$\frac{d\Theta_\gamma}{dt} = \sum_{\alpha,\beta}\left\{\pi L_{\gamma\alpha\beta} i W_\alpha \Theta_\beta\right\} + \mathrm{Ra} W_\gamma - k_\gamma^2\left(\Theta_\gamma - \overline{\Theta}_\gamma\right), \tag{152}$$

while the spectral form of the vertical velocity equation (131) is

$$\frac{dW_\gamma}{dt} = \sum_{\alpha,\beta}\left\{\pi N_{\gamma\alpha\beta} i W_\alpha W_\beta\right\} + \mathrm{Pr}\frac{\pi^2 q_\gamma^2}{k_\gamma^2}\Theta_\gamma - \mathrm{Pr}\, k_\gamma^2 W_\gamma \, , \tag{153}$$

with the interaction coefficient,

$$N_{\gamma\alpha\beta} \equiv \frac{k_\beta^2}{k_\gamma^2 q_\alpha^2 q_\beta^2}\left\{2n_\alpha\left(a_x^2 l_\alpha l_\beta - a_y^2 m_\alpha m_\beta\right)^2 + \left(q_\beta^2 n_\alpha - q_\alpha^2 n_\beta\right)\left(a_x^2 l_\alpha l_\beta - a_y^2 m_\alpha m_\beta\right) - n_\gamma q_\alpha^2 q_\beta^2\right\}\delta_{\alpha,\beta} \, . \tag{154}$$

35. Boundary conditions and symmetry relations

In order to satisfy the upper and lower boundary conditions on temperature and vertical velocity (66), the Fourier coefficients have to satisfy the following symmetry relations.

$$W^R_{l,m,-n} = -W^R_{l,m,n};\ W^I_{l,m,-n} = -W^I_{l,m,n}; \tag{155a}$$

$$\Theta^R_{l,m,-n} = -\Theta^R_{l,m,n};\ \Theta^I_{l,m,-n} = -\Theta^I_{l,m,n}; \tag{155b}$$

This means that all coefficients with n=0 are zero.

The fields in "physical space" are real, of course, which means that (see eqs. 78 and 79)

$$W^R_{l,m,n} = W^R_{-l,-m,-n};\ W^I_{l,m,n} = -W^I_{-l,-m,-n}; \tag{156a}$$

$$\Theta^R_{l,m,n} = \Theta^R_{-l,-m,-n};\ \Theta^I_{l,m,n} = -\Theta^I_{-l,-m,-n}; \tag{156b}$$

These expressions imply the following additional symmetry relations:

$$W^R_{l,m,n} = -W^R_{-l,-m,n};\ W^I_{l,m,n} = W^I_{-l,-m,n}; \tag{157a}$$

$$\Theta^R_{l,m,n} = -\Theta^R_{-l,-m,n};\ \Theta^I_{l,m,n} = \Theta^I_{-l,-m,n}; \tag{157b}$$

From this it can be deduced that

$$W^R_{0,0,n} = 0;\ \Theta^R_{0,0,n} = 0 \tag{158}$$

As a result of the above symmetry relations, only the equations for the evolution of the coefficients in one quarter of the wave vector volume have to be explicitly integrated. Furthermore, if the horizontal dependence of w and θ is represented by a cosine series, as in eq, 116, we have

$$W^R_{l,m,n} = W^R_{l,-m,n} = W^R_{-l,m,n};\ W^I_{l,m,n} = -W^I_{l,-m,n} = -W^I_{-l,m,n}, \tag{159}$$

and analogous relations for Θ^R_γ and Θ^I_γ. All this implies that

$$W^R_\gamma = 0 \text{ and } \Theta^R_\gamma = 0. \tag{160}$$

This means that we only need to explicitly solve the equations for one octant of wave vector space. We choose: $l \geq 0$, $m \geq 0$ and $n > 0$.

36. A low-order model of poloidal convection: plan-form selection

In this section we study plan-form selection in thermal convection between rigid perfectly conducting horizontal plates in a highly truncated low-order model of poloidal convection. The model is based on eqs. 152 and 153.

Let us take the following wave vectors inside the truncated Fourier series of w and θ,

$$(\pm1,\pm1,\pm1) \text{ and } (0,\pm2,\pm1) \tag{161}$$

so that a hexagonal pattern is obtained if $a_x=\sqrt{3}a_y$ (eqs. 116-117), a square pattern is obtained if $a_x=a_y$ while neglecting $(0,\pm2,1)$ (**figure 19**), and a roll pattern is obtained by neglecting $(\pm1,\pm1,\pm1)$.

An important property of the hexagonal pattern is that it is the result of superposing two Fourier modes with identical horizontal wave number, $q^2=a_x^2l^2+a_y^2m^2$. These modes, therefore, have identical critical modal Rayleigh numbers (see **exercise 3**). Hence these modes will grow with identical linear growth-rates.

Let us construct a low-order model of poloidal convection, which consists of the following wave vectors

$$(\pm1,\pm1,\pm1) \text{ and } (0,\pm2,\pm1) \text{ with } n=1,2 \qquad (162)$$

This means that the field of motion is described with only 4 wave vectors. In addition to this, we take $(0,0,\pm n)$, with $n=1,2,3,4$, inside truncation of the Fourier expansion of the temperature, in order to represent the horizontal average temperature distribution (the thermal stratification and its modification by convection). All interactions with waves outside the truncation are neglected.

All possible wave vector interactions are listed in **table 2**.

Class 1 interactions			Class 2 interactions			Class 3 interactions		
γ	α	β	γ	α	β	γ	α	β
(0, 0, 1)	(1, 1, −1)	(−1, −1, 2)	(1, 1, 1)	(1, 1, 2)	(0, 0, −1)	(0, 2, 1)	(1, 1, −1)	(−1, 1, 2)
(0, 0, 1)	(−1, −1, −1)	(1, 1, 2)	(1, 1, 1)	(1, 1, −1)	(0, 0, 2)	(0, 2, 1)	(−1, 1, −1)	(1, 1, 2)
(0, 0, 1)	(−1, 1, −1)	(1, −1, 2)	(1, 1, 1)	(1, 1, −2)	(0, 0, 3)	(1, 1, 1)	(1, −1, −1)	(0, 2, 2)
(0, 0, 1)	(1, −1, −1)	(−1, 1, 2)	(0, 2, 1)	(0, 2, 2)	(0, 0, −1)	(1, 1, 2)	(1, −1, 1)	(0, 2, 1)
(0, 0, 2)	(1, 1, 1)	(−1, −1, 1)	(0, 2, 1)	(0, 2, −1)	(0, 0, 2)	(0, 2, 2)	(−1, 1, 1)	(1, 1, 1)
(0, 0, 2)	(−1, 1, 1)	(1, −1, 1)	(0, 2, 1)	(0, 2, −2)	(0, 0, 3)	(1, 1, 1)	(1, −1, 2)	(0, 2, −1)
(0, 0, 3)	(1, 1, 1)	(−1, −1, 2)	(1, 1, 2)	(1, 1, 1)	(0, 0, 1)			
(0, 0, 3)	(−1, −1, 1)	(1, 1, 2)	(1, 1, 2)	(1, 1, −1)	(0, 0, 3)			
(0, 0, 3)	(−1, 1, 1)	(1, −1, 2)	(1, 1, 2)	(1, 1, −2)	(0, 0, 4)			
(0, 0, 3)	(1, −1, 1)	(−1, 1, 2)	(0, 2, 2)	(0, 2, 1)	(0, 0, 1)			
(0, 0, 4)	(1, 1, 2)	(−1, −1, 2)	(0, 2, 2)	(0, 2, −1)	(0, 0, 3)			
(0, 0, 4)	(−1, 1, 2)	(1, −1, 2)	(0, 2, 2)	(0, 2, −2)	(0, 0, 4)			
(0, 0, 1)	(0, 2, −1)	(0, −2, 2)						
(0, 0, 1)	(0, −2, −1)	(0, 2, 2)						
(0, 0, 2)	(0, 2, 1)	(0, −2, 1)						
(0, 0, 3)	(0, 2, 1)	(0, −2, 2)						
(0, 0, 3)	(0, −2, 1)	(0, 2, 2)						
(0, 0, 4)	(0, 2, 2)	(0, −2, 2)						

Table 2: Non-zero interactions taken inside the truncation in the low order model of poloidal convection. The interaction of wave-vectors α and β contributes to the wave-vector γ. Interactions fall into the following 3 classes. (1) Wave-wave interactions, which contribute to the horizontal mean state; (2) wave-mean interactions, which contribute to the waves; (3) wave-wave interactions, which contribute to the waves (van Delden, 1988).

It is straightforward, but admittedly tedious, to derive the model equations explicitly from eqs 152 and 153, using the definitions of the interaction- or coupling coefficients 148 and 154 If it is assumed that $a_x^2 = 3a_y^2 = 3a^2$, the twelve first order ordinary differential equations are given below.

$$\frac{d\Theta_{111}}{dt} = -\frac{3}{2}\pi W_{111}\Theta_{022} - \frac{3}{2}\pi W_{021}\Theta_{112} + \pi\Theta_{001}W_{112} - 2\pi\Theta_{002}W_{111} - 3\pi\Theta_{003}W_{112} + \mathrm{Ra}W_{111} - \pi^2\left(4a^2+1\right)\Theta_{111}$$

$$\frac{d\Theta_{021}}{dt} = -3\pi W_{111}\Theta_{112} + \pi\Theta_{001}W_{022} - 2\pi\Theta_{002}W_{021} - 3\pi\Theta_{003}W_{022} + \mathrm{Ra}W_{021} - \pi^2\left(4a^2+1\right)\Theta_{021}$$

$$
\begin{aligned}
\frac{d\Theta_{112}}{dt} &= \frac{3}{2}\pi W_{021}\Theta_{111} + \frac{3}{2}\pi W_{111}\Theta_{021} + \pi\Theta_{001}W_{111} - 3\pi\Theta_{003}W_{111} - 4\pi\Theta_{004}W_{112} + \mathrm{Ra}W_{112} - \pi^2\left(4a^2+4\right)\Theta_{112}\\
\frac{d\Theta_{022}}{dt} &= 3\pi W_{111}\Theta_{111} + \pi\Theta_{001}W_{021} - 3\pi\Theta_{003}W_{021} - 4\pi\Theta_{004}W_{022} + \mathrm{Ra}W_{022} - \pi^2\left(4a^2+4\right)\Theta_{022}\\
\frac{d\Theta_{001}}{dt} &= -4\pi W_{111}\Theta_{112} - 4\pi W_{112}\Theta_{111} - 2\pi W_{021}\Theta_{022} - 2\pi W_{022}\Theta_{021} - \pi^2\left(\Theta_{001} - \overline{\Theta}_{001}\right)\\
\frac{d\Theta_{002}}{dt} &= 8\pi W_{111}\Theta_{111} + 4\pi W_{021}\Theta_{021} - 4\pi^2\Theta_{002}\\
\frac{d\Theta_{003}}{dt} &= 12\pi W_{111}\Theta_{112} + 12\pi W_{112}\Theta_{111} + 6\pi W_{021}\Theta_{122} + 6\pi W_{022}\Theta_{021} - 9\pi^2\Theta_{003}\\
\frac{d\Theta_{004}}{dt} &= 16\pi W_{112}\Theta_{112} + 8\pi W_{022}\Theta_{022} - 16\pi^2\Theta_{004}\\
\frac{dW_{111}}{dt} &= -\frac{3}{2}\pi W_{022}W_{111} - \frac{3}{2}\pi W_{021}W_{112} + \frac{4a^2\,\mathrm{Pr}}{4a^2+1}\Theta_{111} - \pi^2\,\mathrm{Pr}(4a^2+1)W_{111}\\
\frac{dW_{021}}{dt} &= -3\pi W_{112}W_{111} + \frac{4a^2\,\mathrm{Pr}}{4a^2+1}\Theta_{021} - \pi^2\,\mathrm{Pr}\left(4a^2+1\right)W_{021}\\
\frac{dW_{112}}{dt} &= 3\pi\frac{4a^2+1}{4a^2+4}W_{111}W_{021} + \frac{4a^2\,\mathrm{Pr}}{4a^2+4}\Theta_{112} - \pi^2\,\mathrm{Pr}(4a^2+4)W_{112}\\
\frac{dW_{022}}{dt} &= 3\pi\frac{4a^2+1}{4a^2+4}W_{111}^2 + \frac{4a^2\,\mathrm{Pr}}{4a^2+4}\Theta_{022} - \pi^2\,\mathrm{Pr}\left(4a^2+4\right)W_{022}
\end{aligned}
\qquad \textbf{(163)}
$$

The commas in the subscripts and the superscripts have been omitted to save space. The hexagonal solution is equivalent to having,

$$\Theta_{111} = \Theta_{021};\ \Theta_{112} = \Theta_{022};\ W_{111} = W_{021};\ W_{112} = W_{022}. \qquad (164)$$

When substituting these equalities into the equation set (163) it is found that,

$$\frac{d\Theta_{111}}{dt} = \frac{d\Theta_{021}}{dt};\ \frac{d\Theta_{112}}{dt} = \frac{d\Theta_{022}}{dt};\ \frac{dW_{111}}{dt} = \frac{dW_{021}}{dt};\ \frac{dW_{112}}{dt} = \frac{dW_{022}}{dt}. \qquad (165)$$

This implies that (164) is a solution of the model. Unfortunately, it is not possible to obtain a general analytical expression for the coefficients, belonging to this solution, as a function of the parameters, a, Ra, Pr and $\overline{\Theta}_{001}$.

In this model the system can "choose" between a hexagon with upward flow in the centre (called "up-hexagon" or "*l*-cell") or downward flow in the centre (called "down-hexagon" or "*g*-cell"), or a roll, both with a non-dimensional wavelength (aspect ratio) equal to a^{-1}.

The horizontal-mean temperature, which depends only on height and time, is determined by the coefficients, $\Theta_{001}, \Theta_{002}, \Theta_{003}$ and Θ_{004}, which depend on time, and the constant value of the imposed, or prescribed, coefficient, $\overline{\Theta}_{001}$, as follows.

$$\theta(t,z) = -2\left\{(\Theta_{001} + \overline{\Theta}_{001})\sin\pi z + \Theta_{002}\sin 2\pi z + \Theta_{003}\sin 3\pi z + \Theta_{004}\sin 4\pi z\right\}. \qquad (166)$$

While the model itself can generate a horizontal mean temperature profile with vertical gradient which is vertically asymmetric about mid-level, such a temperature profile can also be imposed, by specifying the value of $\overline{\Theta}_{001}$. A positive value of $\overline{\Theta}_{001}$ will make the static horizontal-mean temperature profile hydrostatically most unstable at the lower boundary, while a negative value of $\overline{\Theta}_{001}$ will make the static horizontal-mean temperature profile hydrostatically most unstable at the upper boundary. The adjective, "static" stands for "in the absence of convection".

The model equations are integrated in time with the fourth order Runge-Kutta scheme (**section 22**). The basic version of the script is given in **section 40**. A large number of

integrations (`nrun_len=250` in the script), lasting 25 time units, are performed for nearly identical initial conditions. The values of $\overline{\Theta}_{001}$(=0), Ra, Pr and a are identical in the first set of 250 runs (see the caption of **figure 19**). Subsequently, another two set of 250 runs are performed for $\overline{\Theta}_{001}$=500 and for $\overline{\Theta}_{001}$=-500, respectively, with identical values of Ra, Pr and a.

The initial condition is a perturbed state of rest. The perturbation consists of a random number between -0.1 and +0.1 (negative or positive!) added to the initial values (=zero) of the amplitudes, W_{111} and W_{021}, using the *Numpy* random number generator. In meteorology this technique is called "**ensemble forecasting**" [1].

For Pr=5, Ra=5000 and a=1/(2√2), for example, the model finds a steady state solution well within the prescribed length of time of the run (25 time units). When $\overline{\Theta}_{001}$=0 the set of 250 solutions consists of a collection of the following three basic steady solutions: rolls, down hexagons and up-hexagons, which are approximately equally probable. The roll solution in the case $\overline{\Theta}_{001}$=0 is identical to the finite amplitude solution of the Lorenz (1963) model (**exercise 9**). The probability of up-hexagons increases with increasing $\overline{\Theta}_{001}$>0, at the cost of the probability of down-hexagons. This result implies that a static temperature profile with the largest hydrostatic instability at the lower boundary promotes up-hexagons! Why is this? We do not know (yet).

It appears that the "volume" of the "basin of attraction" of up-hexagons in the low-order model increases with increasing positive $\overline{\Theta}_{001}$. This idea might be tested by plotting the position of the random initial state in phase space, while using colours to distinguish between the three possible final steady state solutions: rolls (green), up-hexagons (blue) and down-hexagons (red). Because the initial condition depends only on W_{111} and W_{021}, such a scatter plot can be restricted to the plane, W_{111} versus W_{021}. This is left as an exercise (**exercise 22**).

Figure 20 shows the steady state horizontal-mean temperature distribution at the end of a run corresponding to (a) rolls, (b) up-hexagons and (c) down-hexagons for Ra=5000, Pr=5, a=1/(2√2) and $\overline{\Theta}_{001}$=0. Henceforth "the horizontal-mean temperature distribution" is referred to, in short, as the "**temperature profile**".

At initial time the temperature profile is linear. Convection, which consists of upward warm currents and downward cold currents, distorts this temperature profile. As expected, warming occurs above mid-level, while cooling occurs below mid-level. The intensity of the warming versus the intensity of the cooling is symmetric about mid-level only in the case of a flow pattern consisting of two-dimensional convection cells, i.e. convection rolls. The average temperature of the fluid layer at the end of the run in the case of convection rolls is identical to the imposed average temperature of the fluid layer in the initial state of rest, i.e. -2500 non-dimensional temperature units.

In the case of steady three-dimensional convection, however, the intensity of warming and cooling is not symmetric about mid-level. Steady down-hexagons warm the upper half the fluid layer *more* than they cool the lower half of the fluid layer, while steady up-hexagons warm the upper half the fluid layer *less* than they cool the lower half of the fluid layer. This leads to a very remarkable conclusion. The **flow pattern determines the average temperature of the fluid**. Net warming occurs if the flow-pattern consists of down hexagons and net cooling occurs if the flow-pattern consists of up hexagons!

At Ra=5000, Pr=5 and a=1/(2√2), the average temperature in the final steady state is equal to -2796 units in the case of steady convection in form of up-hexagons, 296 units lower than the initial average temperature (-2500 units). In the case of steady convection in the form of a down-hexagon the average temperature is equal to -2204 units, 296 units higher than the

[1] Instead of making a single weather forecast, a set (or "ensemble") of weather forecasts is produced. This set of forecasts aims to give an indication of the range of possible future states of the atmosphere.

initial average temperature. In both cases, heat transport into the fluid at the lower boundary and heat transport out of fluid at the upper boundary are identical! This conclusion leads to an important question in connection to the problem of climate change prediction: in how far does future global warming of earth's atmosphere depend on the circulation?

An asymmetric temperature profile is imposed, by specifying that $\overline{\Theta}_{001} \neq 0$. A value of $\overline{\Theta}_{001}$ greater than zero will generate a concave static temperature profile, which is most unstable at the lower boundary, and a fluid layer which, in the static state, is colder than the fluid layer in the static state when $\overline{\Theta}_{001}$=0. This should promote the formation of up-hexagon. We have just seen that this is indeed the case.

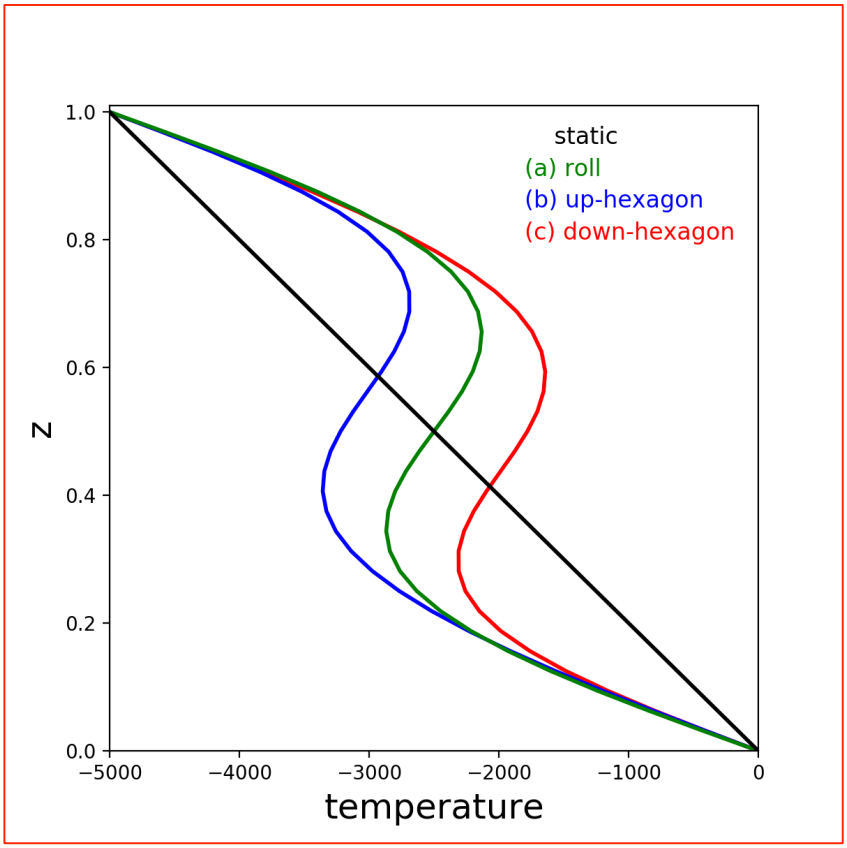

FIGURE 20 showing the horizontal mean **temperature profile** (eq. 166) for the state of rest (black), steady convection in the form of rolls (green), up-hexagons (blue) and down-hexagons (red) for Ra=5000, Pr=5, a=1/(2√2) and $\overline{\Theta}_{001}$=0. Units are non-dimensional (eq. 48). Note that steady convection may cool or warm the fluid! Compare this figure with **figure 4**, which shows observations of the steady temperature profile.

A drawback of the 12-component model is the fixed difference in the intensity of the upward motion relative the intensity of the downward motion in the hexagonal convection cell. This property of the hexagon is also reflected in a fixed ratio, indicated by the letter, R, of the area covered by the vertical motion in the middle of the cell relative to the total area. In the 12-component model, R=0.4. This may have a decisive influence on the net cooling or warming of the fluid layer by convection. The next section provides a short look into this aspect of convection. A solution of a higher order version of the 12-component model (eq.163), demonstrates that R increases in the case of hexagonal convection when more Fourier modes are included.

37. A "down-hexagon" becomes an "open cell" in a higher order model

Because of the restriction on the number of modes inside the truncation of the Fourier series, hexagonal convection cells, according to the low-order convection model of the previous section, are constrained to look like the pattern shown in **figure 18**. The updraught/downdraught in the middle of the convection cell covers only 40% of the total area, i.e. R=0.4. The question now is, how strongly will this ratio change if we include more modes (higher harmonics) inside the truncation of the Fourier series of the temperature and the vertical velocity?

To answer this question we return to the full equations (152-153). It is relatively easy to write a computer program to integrate these equations by again applying the Runge-Kutta scheme of **section 22** to approximate the time-derivatives. Such a *spectral* numerical model is fairly accurate because it is practically free of numerical diffusion and numerical dispersion. Unfortunately, a spectral model, based on the explicit computation of interaction coefficients (eqs. 148-149), quickly becomes very computationally expensive with increasing resolution. Nevertheless, a truncation, which includes all combinations of wave numbers, such that $|l|<4$ and $|l|<6$ and $0<|n|<4$, is feasible on a laptop computer, while possessing substantially more degrees of freedom compared to the low-order model of the previous section. For the horizontal mean state (wave numbers with l=0, m=0) the Fourier series of the temperature is truncated at n=6, i.e. all wave vectors with l=m=0, with n<7, are included in the truncation. A higher resolution is feasible on a "super-computer", but for the purpose here, it is sufficient to show the result of a model-integration for the above-mentioned truncation.

As an example, the model with this truncation is initialised with a steady state solution of the low-order model of the previous section. In this particular case, this solution corresponds to a "down-hexagon" (see the lower panel of **figure 18**), at parameter values, Ra=5000, Pr=5, $a=1/(2\sqrt{2})$ and $\overline{\Theta}_{001}$=2500. The integration is continued for 0.3 time units.

Figure 21 shows the intensity of the vertical velocity halfway the convective layer at the beginning of this integration, at t=0 (left panel), and at the end of this integration, at t=0.3 non-dimensional time units (right panel). The down-hexagon at t=0 is still a down-hexagon at t=0.3, but with a very different ratio, R. R increases from 0.4 at t=0 to 0.58 at t=0.3. The hexagonal convection cell with downward motion in the middle at t=0.3 can rightly be called an "**open convection cell**, as these convection cells are called by meteorologists to designate cellular cumulus cloud patterns, which are cloud-free in the middle. Open cells in the atmosphere are observed regularly on satellite images of the earth (**figure 22**). The average cloud cover fraction of the open cells, seen in **figure 22**, is about 0.4.

In the present numerical experiment the maximum upward velocity in the periphery of the convection cell, where we would expect clouds, increases from slightly more than 20 to 47 units! The maximum downward velocity in the centreof the cell decreases from about -40 to -30 units.

In closing, let me make a personal note. In my opinion, the following question is the most enigmatic and fascinating within the domain of turbulence theory. How and why does order so easily arise in complex systems with innumerable degrees of freedom? Research on this perhaps esoteric question, which was the topic of my PhD-research in the 1980's, is receiving less attention in recent decades than in the 1960's to 1990's, a time which saw the appearance of books about order and self-organisation in complex systems, such as Hermann Haken's "**Synergetics**" (**section 28**). **Figure 21** is one of the most important figures of my PhD thesis. After finishing my PhD, I decided, partially out of necessity, but unfortunately, to discontinue research on this topic and to devote my time as a researcher to other maybe more pressing research topics in Climate Science and Meteorology. By writing these lecture notes in the final phase of my official career as a scientist, I have come to realise that this fascinating research question deserves renewed and more attention.

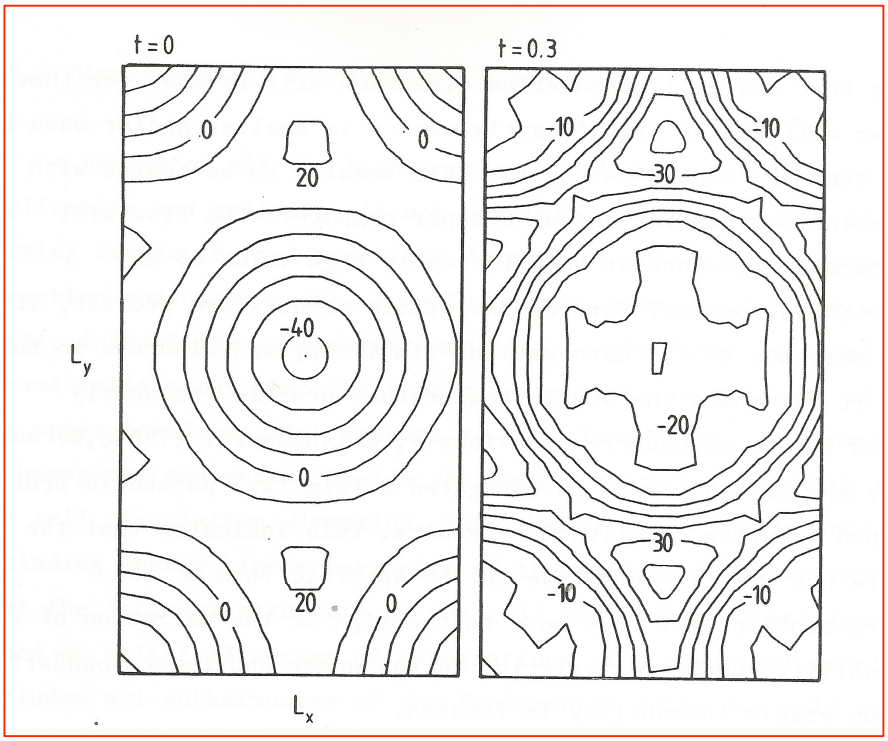

Figure 21. Vertical velocity halfway the convective layer in non-dimensional units (eq. 48) at the beginning (left panel) and at the end (t=0.3) (right panel) of a run with the higher order model. Ra=5000, Pr=5, a=1/(2√2) and $\overline{\Theta}_{001}$=2500 (van Delden, 1988).

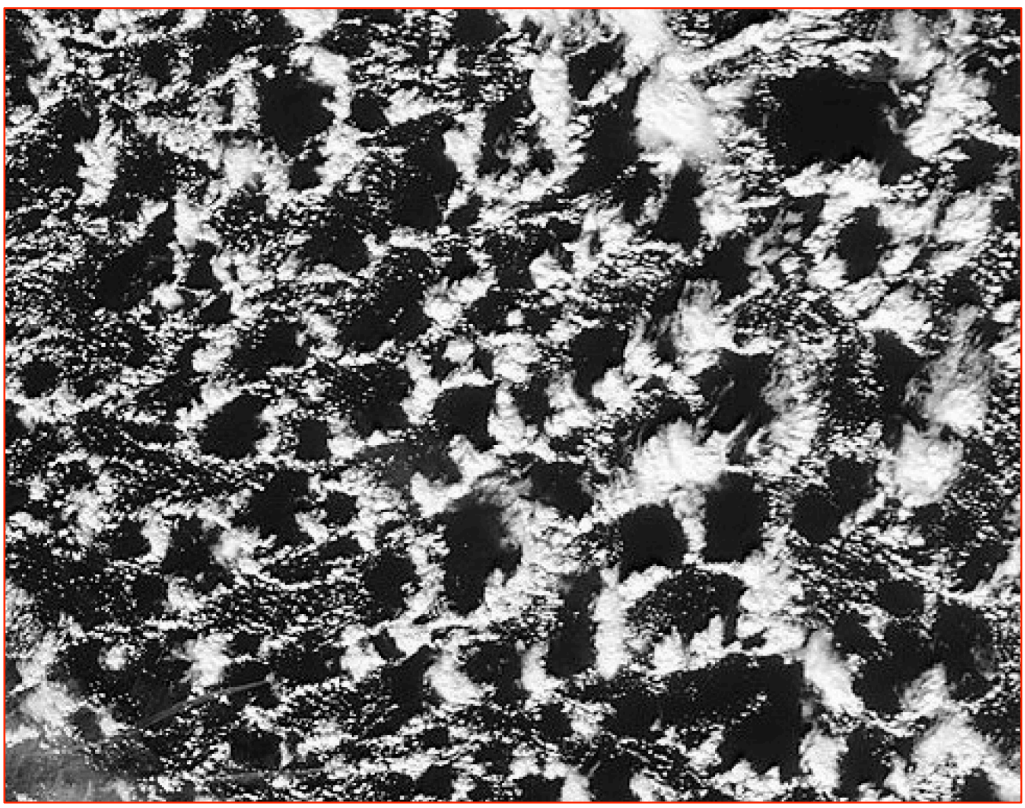

Figure 22: Open convection cells over the Atlantic Ocean near the Azores on 24 January 2006, 15:35 UTC. NASA MODIS Aqua satellite image with a resolution of 1 km. The open cell diameter is typically 30 km while H=2 km (Aspect ratio=30). The temperature difference between sea and air is 2-5°C and cloud cover fraction is 40%. (Source: Noteboom, 2007).

38. Exercises, part 5

(18)

Show that the steady state solutions of the Lorenz (1963) model are also solutions of the 12-component model of poloidal thermal convection (eqs. 163). Derive expressions for these solutions.

(19)

(a) Make a vertical cross section of the vertical velocity and the associated temperature distribution at $x=L_x/2$, as a function of y and z, for steady hexagonal convection according to the 12-component model of poloidal convection (eqs.163). The corresponding values of the Fourier coefficients are: W_{111}=-3.93, W_{021}=-3.93, W_{112}=0.22, W_{022}=0.22, Θ_{111}=-179.3, Θ_{021}=-179.3, Θ_{112}=-1.2, Θ_{022}=-1.2, Θ_{001}=564.8, Θ_{002}=672.8, Θ_{003}=-21.6, Θ_{004}=-0.1 (Ra=5000, $a=1/(2\sqrt{2})$ and $\overline{\Theta}_{001}$=500). Units are non-dimensional (eq. 48). Is this an up- or a down-hexagon?
(b) Make a plot of the associated horizontal mean temperature profile, as in **figure 19**.

(20)

The total kinetic energy is defined as

$$K \equiv \frac{1}{2}\int\left(u^2+v^2+w^2\right)d\sigma\,.$$

Here $d\sigma$ is a volume element. The integration extends over the region defined by eq. 123. The relation between the different velocity components in spectral space is given in eqs 140 and 141.
(a) Transform the above expression for the total kinetic energy to spectral space, assuming that the flow is poloidal.
(b) Show that total kinetic energy is conserved by the nonlinear terms in the low-order 12-component model of poloidal thermal convection (eqs. 163).

(21)
Apply the adiabatic elimination technique to the latter 4 model equations in the equation set (163), following the procedure that is presented in **section 25**. Assume that W_{111} and W_{021} are self-excited and that W_{112} and W_{022} are damped. The damped modes are slaved to the self-excited modes. Note that the positive relaxation coefficients for W_{111} and W_{021} are equal, as are the negative relaxation coefficients for W_{112} and W_{022}. Identify the steady state convection patterns and analyse their stability, using the resulting two equations (**figure 19**).

(22)
For this exercise you are given the python-code of the low-order model of poloidal convection, which integrates the twelve equations (163), and asked to install and run this code on your computer. As described on page 57, identify the basins of attraction in the plane, W_{111} versus W_{021}, of the three possible steady state solutions of the 12-component model (eqs. 163): rolls, up-hexagons, and down-hexagon. Do this for Pr=5, Ra=5000 and a=1/(2√2) and $\overline{\Theta}_{001}$=0.

(23)
Investigate the stability of the finite amplitude convective steady state solution of the Lorenz model (exercise 18) in the low-order model of poloidal convection as a function of Ra and Pr, by performing model-integrations in which the initial steady state solution is perturbed slightly, assuming that a=1/(2√2) and $\overline{\Theta}_{001}$=0.

39. References, part 5

Ball, Philip, 2009: **Shapes: Natures Patterns**. Oxford University Press, 312 pp.

D'Arcy Wentworth Thompson , 1942: **On Growth and Form**. **New edition**. Cambridge University Press. 1116 pp.

van Delden, A, 1988: On the flow-pattern of shallow atmospheric convection. **Contr.Atmosph.Phys**., **61**,169-186.

Noteboom, S. 2007: Open cell convection and closed cell convection. **KNMI-report**, De Bilt. (http://bibliotheek.knmi.nl/stageverslagen/stageverslag_Noteboom.pdf)

Palm, E. 1960: On the tendency towards hexagonal cells in steady convection. **J. Fluid Mech**., **8**, 183-192.

40. Appendix to part 5: Python-code of the spectral model of poloidal convection (basic version)

```
# LOW-ORDER MODEL OF POLOIDAL CONVECTION
# (SECTION 36 of Lecture notes on Thermal Convection for "Turbulence in Fluids")
# Numerical integration of equation-set 163 (lecture notes)
# Skeleton version of the script (no graphics)

# IMPORT MODULES
import numpy as np
import matplotlib.pyplot as plt
import math as M
from numpy import random

#-------------------------------------------------------------------------------------
# FUNCTION THAT COMPUTES TIME-DERIVATIVES

def
time_derivative(W111_,W112_,W021_,W022_,T111_,T112_,T021_,T022_,T001_,T002_,T003_,T004_,T_MEAN_001,Ra,Pr,a
):
 # SHORT NOTATION OF TOTAL WAVE NUMBERS (eqs. 142 and 143)
 pi = M.pi
 pi2 = M.pow(pi,2.0)
 k41 = (4.0*M.pow(ay,2.0)) + 1.0
 k44 = (4.0*M.pow(ay,2.0)) + 4.0
 a2 = M.pow(ay,2.0)

 fFT111 = -((3./2.)*pi*W111_*T022_) - ((3./2.)*pi*W021_*T112_) + (pi*T001_*W112_) - (2*pi*T002_*W111_) -
(3*pi*T003_*W112_) + (Ra*W111_) - (pi2*k41 * T111_)
 fFT112 = ((3./2.)*pi*W021_*T111_) + ((3./2.)*pi*W111_*T021_) + (pi*T001_*W111_) - (3*pi*T003_*W111_) -
(4*pi*T004_*W112_) + (Ra*W112_) - (pi2*k44 * T112_)
 fFT021 = -(3*pi*W111_*T112_) + (pi*T001_*W022_) - (2*pi*T002_*W021_) - (3*pi*T003_*W022_) + (Ra*W021_) -
(pi2*k41 * T021_)
 fFT022 = (3*pi*W111_*T111_) + (pi*T001_*W021_) - (3*pi*T003_*W021_) - (4*pi*T004_*W022_) + (Ra*W022_) -
(pi2*k44 * T022_)
 fFT001 = -(4*pi*W111_*T112_) - (4*pi*W112_*T111_) - (2*pi*W021_*T022_) - (2*pi*W022_*T021_) -
(pi2*(T001_-T_MEAN_001))
 fFT002 = (8*pi*W111_*T111_) + (4*pi*W021_*T021_) - (4*pi2*T002_)
 fFT003 = (12*pi*W111_*T112_) + (12*pi*W112_*T111_) + (6*pi*W021_*T022_) + (6*pi*W022_*T021_) -
(9*pi2*T003_)
 fFT004 = (16*pi*W112_*T112_) + (8*pi*W022_*T022_) - (16*pi2*T004_)
 fFW111 = -((3./2.)*pi*W022_*W111_) -((3./2.)*pi*W021_*W112_) +((4*a2*Pr/k41)*T111_) - (pi2*Pr*k41*W111_)
 fFW112 = ((3*pi*k41/k44)*W111_*W021_) +((4*a2*Pr/k44)*T112_) - (pi2*Pr*k44*W112_)
 fFW021 = -(3*pi*W112_*W111_) +((4*a2*Pr/k41)*T021_) - (pi2*Pr*k41*W021_)
 fFW022 =  (3*pi*(k41/k44)*W111_*W111_) +((4*a2*Pr/k44)*T022_) - (pi2*Pr*k44*W022_)

 return fFT111, fFT112, fFT021, fFT022, fFT001, fFT002, fFT003, fFT004, fFW111, fFW112, fFW021, fFW022
 #RETURNS TIME DERIVATIVES

# END OF FUNCTION ----------------------------------------
#-------------------------------------------------------------------------------------

# TIME-PARAMETERS
nrun_len = 200 # NUMBER OF RUNS (e.g. 200; see page 56 of the lecture notes)
dt=0.0005 # time step
nt_len = 50000  # number of time steps
t_len = nt_len * dt # total time of integration

# NON-DIMENSIONAL NUMBERS
Ra = 5000.0  # Rayleigh number
```

```
Pr = 5.0  # Prandtl number
T_MEAN_001 = 2500.0   # IMPOSED NON-LINEARITY STATIC TEMPERATURE PROFILE

# SCALE-PARAMETERS
a = 1/(2 * M.pow(2,0.5))  # ax = 2H/L
ay = a
ax = M.sqrt(3) * ay    #  p. 54 lecture notes

# APMPLITUDES OF FOURIER COEFFICEIENTS
W111 = np.zeros((nt_len, nrun_len), dtype='d')
W112 = np.zeros((nt_len, nrun_len), dtype='d')
W021 = np.zeros((nt_len, nrun_len), dtype='d')
W022 = np.zeros((nt_len, nrun_len), dtype='d')
T111 = np.zeros((nt_len, nrun_len), dtype='d')
T112 = np.zeros((nt_len, nrun_len), dtype='d')
T021 = np.zeros((nt_len, nrun_len), dtype='d')
T022 = np.zeros((nt_len, nrun_len), dtype='d')
T001 = np.zeros((nt_len, nrun_len), dtype='d')
T002 = np.zeros((nt_len, nrun_len), dtype='d')
T003 = np.zeros((nt_len, nrun_len), dtype='d')
T004 = np.zeros((nt_len, nrun_len), dtype='d')

# TIME-AXIS
t = np.zeros((nt_len), dtype='d')

# Counting number of a particular steady solution
nROLL= 0  # NUMBER OF TIMES: STEADY ROLL
nUP = 0   # NUMBER OF TIMES: STEADY UP-HEXAGON
nDOWN = 0  # NUMBER OF TIMES: STEADY DOWN-HEXAGON

# HEADER
print ("   RUN   MODE       Pr      Ra   T_MEAN_001  T111     T021     T112     T022     W111     W021
W112     W022     T001     T002     T003     T004 ")

# LOOP OVER nrun_len RUNS
for nrun in range(nrun_len):
 t[0] = 0.

 # INITIAL VALUES
 W111[0,nrun] = 0.0 + (random.randint(-1000,1000))/100.0
# (random.randint(-1000,1000))/100.0: return a random integer N such that -10 <= N <= +10.
 W112[0,nrun] = 0.0
 W021[0,nrun] = 0.0 + (random.randint(-1000,1000))/100.0
 T111[0,nrun] = 0.0
 T112[0,nrun] = 0.0
 T021[0,nrun] = 0.0
 T022[0,nrun] = 0.0
 T001[0,nrun] = 0.0
 T002[0,nrun] = 0.0
 T003[0,nrun] = 0.0
 T004[0,nrun] = 0.0


 # TIME-LOOP
 for nt in range(1,nt_len):
  t[nt] = nt * dt

  # FOURTH-ORDER RUNGE-KUTTA: step 1

  fFT111, fFT112, fFT021, fFT022, fFT001, fFT002, fFT003, fFT004, fFW111, fFW112, fFW021, fFW022 =
time_derivative(W111[nt-1,nrun],W112[nt-1,nrun],W021[nt-1,nrun],W022[nt-1,nrun],T111[nt-1,nrun],T112[nt-
```

```
1,nrun],T021[nt-1,nrun],T022[nt-1,nrun],T001[nt-1,nrun],T002[nt-1,nrun],T003[nt-1,nrun],T004[nt-
1,nrun],T_MEAN_001,Ra,Pr,a)

  T111_1 = T111[nt-1,nrun] + (fFT111 * dt/2)
  T112_1 = T112[nt-1,nrun] + (fFT112 * dt/2)
  T021_1 = T021[nt-1,nrun] + (fFT021 * dt/2)
  T022_1 = T022[nt-1,nrun] + (fFT022 * dt/2)
  T001_1 = T001[nt-1,nrun] + (fFT001 * dt/2)
  T002_1 = T002[nt-1,nrun] + (fFT002 * dt/2)
  T003_1 = T003[nt-1,nrun] + (fFT003 * dt/2)
  T004_1 = T004[nt-1,nrun] + (fFT004 * dt/2)
  W111_1 = W111[nt-1,nrun] + (fFW111 * dt/2)
  W112_1 = W112[nt-1,nrun] + (fFW112 * dt/2)
  W021_1 = W021[nt-1,nrun] + (fFW021 * dt/2)
  W022_1 = W022[nt-1,nrun] + (fFW022 * dt/2)

  # FOURTH-ORDER RUNGE-KUTTA: step 2

  fFT111, fFT112, fFT021, fFT022, fFT001, fFT002, fFT003, fFT004, fFW111, fFW112, fFW021, fFW022 =
time_derivative(W111_1,W112_1,W021_1,W022_1,T111_1,T112_1,T021_1,T022_1,T001_1,T002_1,T003_1,T004_1,T_MEAN
_001,Ra,Pr,a)

  T111_2 = T111[nt-1,nrun] + (fFT111 * dt/2)
  T112_2 = T112[nt-1,nrun] + (fFT112 * dt/2)
  T021_2 = T021[nt-1,nrun] + (fFT021 * dt/2)
  T022_2 = T022[nt-1,nrun] + (fFT022 * dt/2)
  T001_2 = T001[nt-1,nrun] + (fFT001 * dt/2)
  T002_2 = T002[nt-1,nrun] + (fFT002 * dt/2)
  T003_2 = T003[nt-1,nrun] + (fFT003 * dt/2)
  T004_2 = T004[nt-1,nrun] + (fFT004 * dt/2)
  W111_2 = W111[nt-1,nrun] + (fFW111 * dt/2)
  W112_2 = W112[nt-1,nrun] + (fFW112 * dt/2)
  W021_2 = W021[nt-1,nrun] + (fFW021 * dt/2)
  W022_2 = W022[nt-1,nrun] + (fFW022 * dt/2)

  # FOURTH-ORDER RUNGE-KUTTA: step 3

  fFT111, fFT112, fFT021, fFT022, fFT001, fFT002, fFT003, fFT004, fFW111, fFW112, fFW021, fFW022 =
time_derivative(W111_2,W112_2,W021_2,W022_2,T111_2,T112_2,T021_2,T022_2,T001_2,T002_2,T003_2,T004_2,T_MEAN
_001,Ra,Pr,a)

  T111_3 = T111[nt-1,nrun] + (fFT111 * dt)
  T112_3 = T112[nt-1,nrun] + (fFT112 * dt)
  T021_3 = T021[nt-1,nrun] + (fFT021 * dt)
  T022_3 = T022[nt-1,nrun] + (fFT022 * dt)
  T001_3 = T001[nt-1,nrun] + (fFT001 * dt)
  T002_3 = T002[nt-1,nrun] + (fFT002 * dt)
  T003_3 = T003[nt-1,nrun] + (fFT003 * dt)
  T004_3 = T004[nt-1,nrun] + (fFT004 * dt)
  W111_3 = W111[nt-1,nrun] + (fFW111 * dt)
  W112_3 = W112[nt-1,nrun] + (fFW112 * dt)
  W021_3 = W021[nt-1,nrun] + (fFW021 * dt)
  W022_3 = W022[nt-1,nrun] + (fFW022 * dt)

  # FOURTH-ORDER RUNGE-KUTTA: step 4

  fFT111, fFT112, fFT021, fFT022, fFT001, fFT002, fFT003, fFT004, fFW111, fFW112, fFW021, fFW022 =
time_derivative(W111_3,W112_3,W021_3,W022_3,T111_3,T112_3,T021_3,T022_3,T001_3,T002_3,T003_3,T004_3,T_MEAN
_001,Ra,Pr,a)

  T111_4 = T111[nt-1,nrun] - (fFT111 * dt/2)
```

```
  T112_4 = T112[nt-1,nrun] - (fFT112 * dt/2)
  T021_4 = T021[nt-1,nrun] - (fFT021 * dt/2)
  T022_4 = T022[nt-1,nrun] - (fFT022 * dt/2)
  T001_4 = T001[nt-1,nrun] - (fFT001 * dt/2)
  T002_4 = T002[nt-1,nrun] - (fFT002 * dt/2)
  T003_4 = T003[nt-1,nrun] - (fFT003 * dt/2)
  T004_4 = T004[nt-1,nrun] - (fFT004 * dt/2)
  W111_4 = W111[nt-1,nrun] - (fFW111 * dt/2)
  W112_4 = W112[nt-1,nrun] - (fFW112 * dt/2)
  W021_4 = W021[nt-1,nrun] - (fFW021 * dt/2)
  W022_4 = W022[nt-1,nrun] - (fFW022 * dt/2)

  # FOURTH-ORDER RUNGE-KUTTA: Aggregate step
  T111[nt,nrun] = (T111_1 + (2*T111_2) + T111_3 - T111_4)/3
  T112[nt,nrun] = (T112_1 + (2*T112_2) + T112_3 - T112_4)/3
  T021[nt,nrun] = (T021_1 + (2*T021_2) + T021_3 - T021_4)/3
  T022[nt,nrun] = (T022_1 + (2*T022_2) + T022_3 - T022_4)/3
  T001[nt,nrun] = (T001_1 + (2*T001_2) + T001_3 - T001_4)/3
  T002[nt,nrun] = (T002_1 + (2*T002_2) + T002_3 - T002_4)/3
  T003[nt,nrun] = (T003_1 + (2*T003_2) + T003_3 - T003_4)/3
  T004[nt,nrun] = (T004_1 + (2*T004_2) + T004_3 - T004_4)/3
  W111[nt,nrun] = (W111_1 + (2*W111_2) + W111_3 - W111_4)/3
  W112[nt,nrun] = (W112_1 + (2*W112_2) + W112_3 - W112_4)/3
  W021[nt,nrun] = (W021_1 + (2*W021_2) + W021_3 - W021_4)/3
  W022[nt,nrun] = (W022_1 + (2*W022_2) + W022_3 - W022_4)/3

 MODE=999
 if int(W111[nt,nrun])==0:
  MODE=0
  nROLL = nROLL + 1
 if (int(W111[nt,nrun])==int(W021[nt,nrun])) and (W021[nt,nrun]<0):
  MODE=1   #  down-hexagon
  nDOWN = nDOWN + 1
 if (int(W111[nt,nrun])==int(W021[nt,nrun])) and (W021[nt,nrun]>0):
  MODE=2   #  up-hexagon
  nUP = nUP + 1
 if (int(W111[nt,nrun])==int(-W021[nt,nrun])) and (W021[nt,nrun]<0):
  MODE=1   #  down-hexagon
  nDOWN = nDOWN + 1
 if (int(W111[nt,nrun])==int(-W021[nt,nrun])) and (W021[nt,nrun]>0):
  MODE=2   #  up-hexagon
  nUP = nUP + 1
  #END OF TIME-LOOP

 print
"%6.0f,%6.0f,%8.2f,%8.0f,%8.0f,%8.1f,%8.1f,%8.1f,%8.1f,%8.2f,%8.2f,%8.2f,%8.2f,%8.1f,%8.1f,%8.1f,%8.1f"%
(nrun,MODE,Pr,Ra,T_MEAN_001,T111[nt,nrun],T021[nt,nrun],T112[nt,nrun],T022[nt,nrun],W111[nt,nrun],W021[nt,
nrun],W112[nt,nrun],W022[nt,nrun],T001[nt,nrun],T002[nt,nrun],T003[nt,nrun],T004[nt,nrun])
 #END OF LOOP OVER MULTIPLE RUNS


print "   nRoll   nDOWN   nUP"
print "%6.0f,%6.0f,%6.0f"% (nROLL,nDOWN,nUP)
```

Answers to exercises

Exercise 1
The aspect ratio of observed convection cells (**figure 3**) is not exactly in agreement with the prediction made by Lord Rayleigh's theory. Give at least two reasons for this (slight) disagreement?

Answer to exercise 1
The most important four reasons are:

(1) In reality the boundary conditions are most likely not identical to those assumed by Lord Rayleigh (stress-free and perfectly conducting).

(2) In reality side boundaries cannot be avoided. The horizontal size of the fluid container also determines the total number of convection cells.

(3) Real convection cells have a finite-amplitude, while the amplitude of the disturbances in Rayleigh's theory is infinitesimally small.

(4) Another reason might be that ν is not constant because the viscous resistance to velocity shear in the fluid depends on the velocity shear in which case the fluid is called "**non-Newtonian**".

(5) If convection occurs in the atmosphere latent heat is released when water vapour condenses and also when water droplets freeze. This occurs only in the updraught. Latent heat release increases the buoyancy and hence the intensity of the updraught. The resulting asymmetry between the up- and downdraught enhances the aspect ratio of the convection cell.

Exercise 2
The instability criterion (41) is commonly expressed in terms of the so-called **Rayleigh number**, Ra, which is a non-dimensional number, defined as

$$\mathrm{Ra} \equiv \frac{g\alpha\Gamma H^4}{\kappa\nu}. \qquad (47)$$

What is the critical value of the Rayleigh number at the preferred horizontal wave-length? Plot the marginal value of the Rayleigh number as a function of the aspect ratio, L/H, where the Rayleigh number is the ordinate. Identify the region of instability in this graph. Will this curve shift upwards or downwards if no-slip conditions are imposed on the upper and lower boundaries, instead of stress-free conditions (section 4)?

Answer to exercise 2

The instability criterion is

$$\boxed{\Gamma > \frac{\nu\kappa k^6}{g\alpha l^2} = \frac{\nu\kappa}{g\alpha l^2}\left(l^2 + \left(\frac{\pi n}{H}\right)^2\right)^3}. \qquad (41)$$

This can also be expressed as

$$\mathrm{Ra} > \frac{H^4}{l^2}\left(l^2 + \left(\frac{\pi n}{H}\right)^2\right)^3 \equiv \mathrm{Ra}_{crit}.$$

The preferred wavelength is $L = 2\sqrt{2}H$ and $l = 2\pi/L$. Therefore,

$$\mathrm{Ra}_{crit} = 2\pi^4\left(\frac{1}{2} + n^2\right)^3.$$

With n=1 this becomes

$$\mathrm{Ra}_{crit} = \frac{27\pi^4}{4} \approx 657.$$

The curve will shift upwards if no-slip boundary conditions are imposed.
For n=2, the critical Rayleigh number is 17753!

Exercise 3
At which minimum Rayleigh number is a "mode" with n=2 unstable.

Answer to exercise 3

The minimum Rayleigh number at which a "mode" with n=2 is unstable is $108\pi^4 \approx 10520$.

Exercise 4

Express eqs. (29) and (30),

$$\boxed{\frac{\partial T'}{\partial t} = \Gamma w' + \kappa\left(\frac{\partial^2}{\partial x^2} + \frac{\partial^2}{\partial z^2}\right)T'} \qquad (29)$$

and

$$\boxed{\frac{\partial}{\partial t}\left(\frac{\partial^2}{\partial x^2} + \frac{\partial^2}{\partial z^2}\right)w' \approx g\alpha\frac{\partial^2 T'}{\partial x^2} + \nu\left(\frac{\partial^2}{\partial x^2} + \frac{\partial^2}{\partial z^2}\right)^2 w'} \qquad (30)$$

in dimensionless form, in terms of the following units

$$\{L\} = H;\ \{t\} = \frac{H^2}{\kappa};\ \{T\} = \frac{\kappa\nu}{g\alpha H^3}\ . \tag{48}$$

Verify that $\{t\}$ has the unit of time (seconds) and that $\{T\}$ has the units of temperature (degrees Kelvin). The new (non-dimensional) unit of time, t^*, is

$$t^* \equiv \frac{\kappa}{H^2} t\ . \tag{49}$$

The system of eqs. 29 and 30 contains 5 external parameters, which may determine the solution. In the non-dimensional form we discover that the solution depends on only two parameters: the Rayleigh number and a second non-dimensional number, which is commonly referred to as the "**Prandtl number**", Pr. Identify the Prandtl number.

Answer to exercise 4

If we define non-dimensional variables, indicated by an asterisk, as

$$\frac{H^2}{\kappa} t^* \equiv t; \frac{\kappa\nu}{g\alpha H^3} T^* \equiv T; \frac{\kappa}{H} w^* \equiv w; \frac{\partial}{\partial x^{*2}} \equiv \frac{1}{H^2}\frac{\partial}{\partial x^2}; \frac{\partial}{\partial z^{*2}} \equiv \frac{1}{H^2}\frac{\partial}{\partial z^2}\ .$$

we find, for the temperature equation (29),

$$\frac{\partial T'^*}{\partial t^*} = \mathrm{Ra} w'^* + \left(\frac{\partial}{\partial x^{*2}} + \frac{\partial}{\partial z^{*2}}\right) T'^*\ .$$

The non-dimensional form of eq. 30 is

$$\frac{\partial}{\partial t^*}\left(\frac{\partial}{\partial x^{*2}} + \frac{\partial}{\partial z^{*2}}\right) w'^* = \mathrm{Pr}\frac{\partial T'^*}{\partial x^{*2}} + \mathrm{Pr}\left(\frac{\partial}{\partial x^{*2}} + \frac{\partial}{\partial z^{*2}}\right)^2 w'^*,$$

with the **Prandtl number**,

$$\boxed{\mathrm{Pr} \equiv \frac{\nu}{\kappa}},$$

is the second non-dimensional parameter.

Exercise 5

Figure 5 shows a regime diagram of laboratory convection as a function of Ra and Pr, demonstrating that time dependent flow emerges when Ra is sufficiently large. Time-dependent turbulent flow emerges for lower Ra when Pr is small than when Pr is large. Which non-linear terms are responsible for this "early" onset of time-dependent flow at low Pr: those in eq. 57 (momentum advection) or those in eq. 58 (temperature advection)? Is the Lorenz model more applicable to low Pr convection or to high Pr convection?

Answer to exercise 5

The non-dimensional form of the governing equations is (see exercise 4) (dropping the primes)

$$\frac{dT^*}{dt^*} = \frac{\partial T^*}{\partial t^*} + u^*\frac{\partial T^*}{\partial x^*} + v^*\frac{\partial T^*}{\partial y^*} + w^*\frac{\partial T^*}{\partial z^*} = \mathrm{Ra}w^* + \left(\frac{\partial^2}{\partial x^{*2}} + \frac{\partial^2}{\partial z^{*2}}\right)T^*$$

$$\frac{d}{dt^*}\left(\frac{\partial^2}{\partial x^{*2}} + \frac{\partial^2}{\partial z^{*2}}\right)w^* = \left(\frac{\partial}{\partial t^*} + u^*\frac{\partial}{\partial x^*} + v^*\frac{\partial}{\partial y^*} + w^*\frac{\partial}{\partial z^*}\right)\left(\frac{\partial^2}{\partial x^{*2}} + \frac{\partial^2}{\partial z^{*2}}\right)w^*$$

$$= \mathrm{Pr}\frac{\partial^2 T^*}{\partial x^{*2}} + \mathrm{Pr}\left(\frac{\partial^2}{\partial x^{*2}} + \frac{\partial^2}{\partial z^{*2}}\right)^2 w^*$$

If we divide the second equation by Pr, we see that the non-linear advection terms vanish if we let Pr go to infinity. On the other hand the non-linearity dominates if Pr goes to zero. Therefore, the "early" onset of time-dependent flow at low Pr is due to the effect of advection of momentum, i.e. the non-linear terms in the second equation. The Lorenz model does not contain the effect of advection of momentum. Therefore, it is more applicable to high Pr convection.

Exercise 6

The Lorenz model has two other steady state solutions (next to the state of rest), corresponding to finite amplitude convection. Derive expressions for X, Y, and Z in these steady states. Write these expressions in terms of $r \equiv \sqrt{\left(Ra - Ra_c\right)}$ and a_x (hint: the steady state values of X, Y, and Z do not depend on Pr).

Answer to exercise 6

By putting the time-derivatives in eqs. 87-89 equal to zero we can deduce that there are three steady states, i.e.

$$(X,Y,Z) = (0,\ 0,\ 0)$$

$$(X,Y,Z) = (X_0,Y_0,Z_0) \equiv \left(\frac{r}{\sqrt{2}\pi^2\left(a^2+1\right)}, \frac{\pi\left(a^2+1\right)r}{\sqrt{2}a}, \frac{r^2}{2\pi}\right)$$

or

$$(X,Y,Z) = (X_0,Y_0,Z_0) \equiv \left(\frac{-r}{\sqrt{2}\pi^2\left(a^2+1\right)}, \frac{-\pi\left(a^2+1\right)r}{\sqrt{2}a}, \frac{r^2}{2\pi}\right)$$

The first steady state corresponds to the state of rest, while the second and third steady states correspond to cases of steady convection in which both the direction of the circulation and temperature anomaly are exactly opposite. In both cases this circulation has an identical effect on the horizontal mean temperature distribution, represented by Z.

Exercise 7

Show that the solution of the Lorenz model in phase space (i.e. as a function of X, Y and Z) for large t will either collapse to a point, to a line or to a two-dimensional surface (e.g. a torus) for all values of Ra, Pr and a_x. This means that the volume in phase space, spanned by the collection of trajectories corresponding to different initial states, will, as each point in phase space is displaced in accordance with eqs. 87-89, shrink to zero for large t. What is the associated e-folding time? In the words of Lorenz (1963) (p.135), *all trajectories ultimately become confined to a specific subspace having zero volume*. If the trajectories do not lie on a closed line or a torus in phase space, this subspace is referred as a "**strange attractor**", a term which was introduced by the French mathematician, David Ruelle, and the Dutch mathematician, Floris Takens, in 1971 (see Ruelle (2006) and section 9.3 in Strogatz (1994)).

Answer to exercise 7

In three-dimensional phase (X, Y, Z)-space the divergence of the "velocity" is *proportional* to the tendency of the volume, V, of the collection of trajectories, i.e.

$$\frac{1}{V}\frac{dV}{dt} = \frac{\partial}{\partial X}\left(\frac{dX}{dt}\right) + \frac{\partial}{\partial Y}\left(\frac{dY}{dt}\right) + \frac{\partial}{\partial Z}\left(\frac{dZ}{dt}\right) = -\pi^2(a^2+1)\mathrm{Pr} - \pi^2(a^2+1) - 4\pi^2 < 0\ .$$

Because (1/V)dV/dt is negative, the volume of a collection of trajectories in phase space decreases in time. The rate at which this volume decreases is proportional to the constant,

$$-\pi^2\left(\left(a^2+1\right)(\mathrm{Pr}+1)+4\right),$$

i.e. the rate increases with increasing a and increasing Pr.

Exercise 9

Linearise the Lorenz equations (87-89) around the steady finite amplitude convective state and express this linearised system as in eqs. 91 and 92. Determine the linear stability of the finite amplitude steady states as a function of Ra and a_x, for Pr=10 (this is the value of Pr that was chosen by Lorenz in 1963) by determining the eigenvalues of the corresponding matrix, M. Draw a regime diagram, with Ra as the ordinate and a_x as the abscissa, indicating regions where finite amplitude convection is steady and stable and regions where finite amplitude convection is not steady and unstable. This can be done numerically. Determine the minimum value of Ra and the corresponding value of a_x for which all steady states are linearly unstable and for which the model only has time-dependent solutions (for Pr=10). This exercise is given as homework.

Answer to exercise 9

We assume that the three variables can be written as a sum of the steady value plus a perturbation as,

$$X = X_0 + X';\ Y = Y_0 + Y';\ Z = Z_0 + Z',$$

where the subscript, 0, denotes the steady state value and the prime denotes the perturbation. We assume that

$$X_0 >> X';\ Y_0 >> Y';\ Z_0 >> Z',$$

We now substitute these assumptions into the governing equations 87-89:

$$\frac{dX'}{dt} = \frac{a\,\mathrm{Pr}}{\pi\left(a^2+1\right)}Y' - \pi^2\left(a^2+1\right)\mathrm{Pr}\,X';$$

$$\frac{dY'}{dt} = \pi a\,\mathrm{Ra}X' - \pi^2\left(a^2+1\right)Y' - 2\pi^2 a\left(Z'X_0 + X'Z_0 + X'Z'\right)$$

$$\approx \pi a\,\mathrm{Ra}X' - \pi^2\left(a^2+1\right)Y' - 2\pi^2 a\left(Z'X_0 + X'Z_0\right)$$

$$\frac{dZ'}{dt} = 4\pi^2 a\left(Y'X_0 + X'Y_0 + X'Y'\right) - 4\pi^2 Z'$$

The products of perturbations are neglected. The system of three linearised equations can now be written as,

$$\frac{d}{dt}\begin{pmatrix} X' \\ Y' \\ Z' \end{pmatrix} = M\begin{pmatrix} X' \\ Y' \\ Z' \end{pmatrix},$$

where

$$M = \begin{pmatrix} -\pi^2\left(a^2+1\right)\mathrm{Pr} & \dfrac{a\,\mathrm{Pr}}{\pi\left(a^2+1\right)} & 0 \\ \pi a\mathrm{R}a - 2\pi^2 a Z_0 & -\pi^2\left(a^2+1\right) & -2\pi^2 a X_0 \\ 4\pi^2 a Y_0 & 4\pi^2 a X_0 & -4\pi^2 \end{pmatrix}$$

with (see exercise 6)

$$X_0 = \pm\frac{r}{\sqrt{2}\pi^2\left(a^2+1\right)}\ ;\ Y_0 = \pm\frac{\pi\left(a^2+1\right)r}{\sqrt{2}a}\ ;\ Z_0 = \frac{r^2}{2\pi}\ .$$

The eigenvalues of *M* determine the stability of the circulation. The eigenvalues can be determined numerically as a function of *a*, Pr and Ra. Instability ensues if one eigenvalue has a positive real part.

The regime diagram has been determined with the following *Python-script*. The result is shown below.

```
import numpy as N
import matplotlib.pyplot as plt
import math as M
from scipy import linalg as LA

x_len = 500
y_len = 500
pi = M.pi
pi2 = M.pow(pi,2)
Pr = 10
ax = 0.0

Matrix = N.zeros((3,3), dtype='d')
Growthrate = N.zeros((y_len,x_len), dtype='d')
x_axis = N.zeros((x_len), dtype='d')
y_axis = N.zeros((y_len), dtype='d')
Ra0 = 0
for x in range(x_len):
 ax = ax + 0.01
 x_axis[x] = ax
 ax2 = (M.pow(ax,2)+1)
 Rac = M.pow(pi,4) * M.pow(ax2,3)/M.pow(ax,2)
 Ra = Ra0
  for y in range(y_len):
  Ra =  Ra+100
  r = 0
  if Ra>Rac: r = M.pow(Ra-Rac,0.5)
  y_axis[y] = Ra
  X0 = r / (M.pow(2,0.5)*M.pow(pi,2)*ax2)
  Y0 = pi * ax2 * r / (M.pow(2,0.5)*ax)
```

```
  Z0 = (Ra-Rac)/(2*pi)
  Matrix[0,0] = -pi2 * ax2 * Pr
  Matrix[0,1] = ax * Pr / ( pi * ax2 )
  Matrix[0,2] = 0.0
  Matrix[1,0] = (pi * ax * Ra) - (2 * pi2 * ax * Z0)
  Matrix[1,1] = -pi2 * ax2
  Matrix[1,2] = -2 * pi2 * ax * X0
  Matrix[2,0] = 4 * pi2 * ax * Y0
  Matrix[2,1] = 4 * pi2 * ax * X0
  Matrix[2,2] = -4 * pi2
  e_vals = LA.eigvals(Matrix)
  Growthrate[y,x] = (N.amax(e_vals)).real #maximum real part of eigenvalue
plt.figure(figsize=(8,6))
plt.axis([0,5,0,50000])
CS =plt.contour(x_axis,y_axis, Growthrate,levels=[-0.01], linewidths=2, linestyles='solid',
colors='black')
plt.xlabel('a=2H/L',fontsize=18) # label along x-axis
plt.ylabel('Rayleigh number',fontsize=18) # label along y-axis
plt.xticks(N.arange(0,5,0.5))
plt.savefig("Ex8[TurbulenceFluids]a")
plt.show()
```

The minimum value of Ra and the corresponding value of a_x for which two steady states, corresponding to finite amplitude convection, are linearly unstable (for Pr=10), are 15878 and 0.77, respectively.

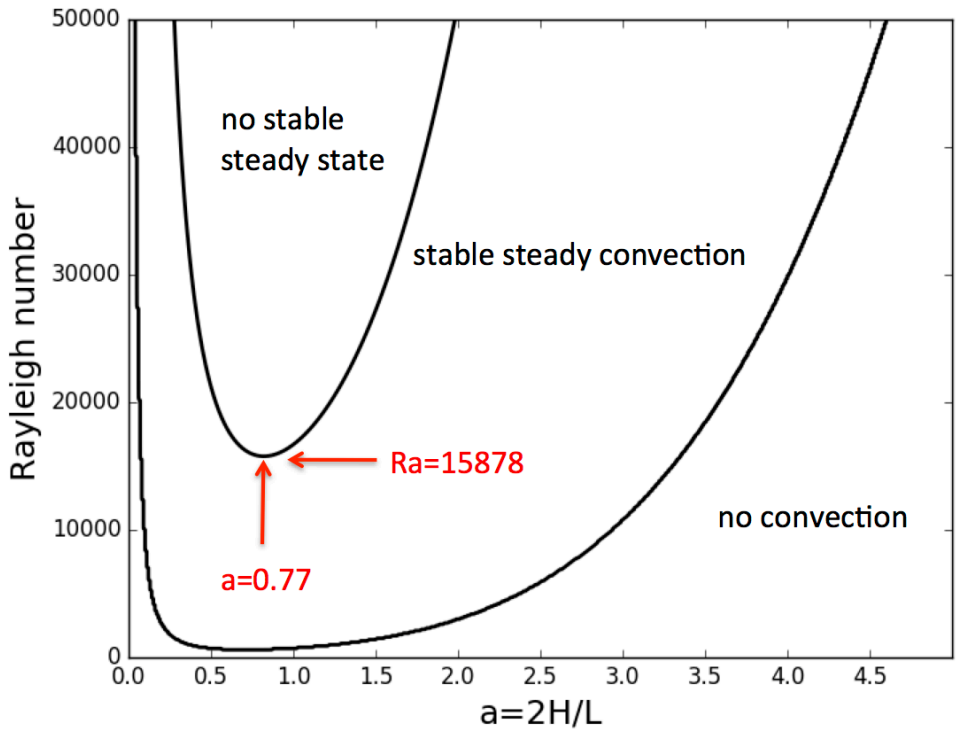

Exercise 10

The total kinetic energy (K) and the total potential energy (P), associated with the perturbations (eq. 6) in two-dimensional convection (in which v=0) are, respectively,

$$K = \frac{1}{2}\int\left(u^2 + w^2\right)d\sigma\ ; \tag{102}$$

$$P = -\frac{1}{2}\mathrm{Pr}\int\theta^2 d\sigma\,. \tag{103}$$

Express K and P in spectral space and show that $K+P$ is conserved **by the non-linear terms in the Lorenz model**.

Answer to exercise 10

Since $\nabla\psi \equiv \left(\frac{\partial\psi}{\partial x}, \frac{\partial\psi}{\partial z}\right)$

$$(\nabla\psi)^2 \equiv \nabla\psi\cdot\nabla\psi = \left(\frac{\partial\psi}{\partial x}\right)^2 + \left(\frac{\partial\psi}{\partial z}\right)^2 = u^2 + w^2,$$

and

$$\nabla\left(\psi\nabla\psi\right) = \psi\nabla^2\psi + \left(\nabla\psi\right)^2 = \psi\nabla^2\psi + u^2 + w^2,$$

and, because $\int\nabla(...)d\sigma = 0$,

$$K = -\frac{1}{2}\int\psi\nabla^2\psi d\sigma\,.$$

Inserting the Fourier expansion (67), using the definition definition (62) of the basis functions, and making use of the orthogonality relation (68) we get

$$K = \frac{1}{2}\sum_\gamma k_\gamma^2\Psi_\gamma^2$$

We define the kinetic energy in the component γ as

$$K_\gamma = \frac{1}{2}k_\gamma^2\Psi_\gamma^2\ .$$

Translating this to the Lorenz model we get

$$K = 2(a_x^2 + 1)X^2\,.$$

However, the only non-linear interactions in the Lorenz model are the interaction between (1,1) and (-1,1) (in eq. 88) and between (1,-1) (and 0,2) (in eq. 89) (the feedback) . Both interactions involve the temperature. In other words, only potential energy is transferred between different Fourier components (different scales). The equations containing these interactions are eqs. 88 and 89:

$$\frac{dY}{dt} = -2\pi^2 a_x XZ + \pi a_x RaX - \pi^2 (a_x + 1)Y \qquad (88)$$

$$\frac{dZ}{dt} = 4\pi^2 a_x XY - 4\pi^2 Z \qquad (89)$$

Therefore we need to define potential energy in terms of Y and Z.

Substituting the Fourier expansion (67) into the definition of potential energy (103) we get

$$P = -\frac{1}{2}\mathrm{Pr}\sum_{\gamma}\Theta_{\gamma}^2 \ .$$

Adding together the energy contents of all wave components we get

$$P = -\mathrm{Pr}\sum_{n=1}^{\infty}\Theta_{0,n}^2 - 2\mathrm{Pr}\sum_{l=1}^{\infty}\sum_{n=1}^{\infty}\Theta_{l,n}^2$$

Translating this to the Lorenz model we get

$$P = -\mathrm{Pr}(2Y^2 + Z^2) \ .$$

To check if energy is conserved by the non-linear terms we neglect the linear terms in eqs. 88 and 89:

$$\frac{dY}{dt} = -2\pi^2 a_x XZ \qquad (88b)$$

$$\frac{dZ}{dt} = 4\pi^2 a_x XY \ . \qquad (89b)$$

Now, when we multiply eq. 88b by 4PrY and eq. 89b by 2PrZ and add the two resulting equations we get

$$\frac{dP}{dt} = 0 \ .$$

Exercise 11

Use the expression for kinetic energy in spectral space, derived in **exercise 10**, to derive an expression for the kinetic energy in the steady state of finite amplitude convection in the Lorenz model. At which aspect ratio will the kinetic energy be a maximum if Ra=10000 and if Ra=20000? Is the equilibrium state of finite amplitude convection stable to small perturbations at these two combinations of values of the aspect and the Rayleigh number (use the result of exercise 8)? Is this aspect ratio at which kinetic energy is maximized larger or smaller than the preferred aspect ratio for onset of convection at the minimum critical Rayleigh number? What does this imply?

Answer to exercise 11

The kinetic in the Lorenz model is given by (see the answer to exercise 9),

$$K = 2\left(a_x^2 + 1\right)X^2$$

In the steady state of finite amplitude convection

$$X = X_0 = \pm \frac{r}{\sqrt{2}\pi^2\left(a_x^2 + 1\right)}$$

with

$$r \equiv \sqrt{\left(Ra - Ra_c\right)}$$

and

$$\mathrm{Ra_c} = \frac{\pi^4\left(a_x^2 + 1\right)^3}{a_x^2}.$$

Therefore:

$$K = \frac{\left(Ra - Ra_c\right)}{\pi^4\left(a_x^2 + 1\right)}$$

K is maximized for a_x=0.33 if Ra=10000 and for a_x=0.27 if Ra=20000. Finite amplite convection is stable to small perturbations at these parameter values. These values of a_x correspond a larger aspect ratio. The largest growth rate is found for smaller values of the aspect ratio. This implies that the preferred aspect ratio for large amplitude convection may be larger than the preferred scale at onset.

Exercise 13

For this exercise you need to know how to program a computer (in Mathematica, Python, MATLAB, C …).

(a) Integrate the Lorenz (1963) equations (eqs. 87-89) in time numerically through at least 5 non-dimensional time units. Approximate the time-derivatives with the fourth order (RK-4) Runge-Kutta scheme (**section 22** or https://en.wikipedia.org/wiki/Runge–Kutta_methods). Do this for the exact same values of a_x, Ra, Pr, which Lorenz used to illustrate the chaotic solution of his model, i.e. $a_x=1/(2^{1/2})$, $Ra=28Ra_c$ ($Ra_c=657$), Pr=10. The initial condition should lie close to steady state convection (insert a very small perturbation to this steady state).

(b) Locate local maxima of $Z(t)$, Z_n and plot Z_{n+1} as a function of Z_n, in other words reproduce the *Lorenz map* (see page 139 of Lorenz (1963), or p. 326-328 of Strogatz (1994)). According to the Lorenz map, the value of the next maximum (next peak in Z) is predictable.

(c) Now, plot the time between local maxima of $Z(t)$ as a function of time (e.g. the time half-way between two maxima). Discuss the plot.

(d) Perform a second integration with a slightly different initial condition, by weakly perturbing only one of the three variables. Plot a measure of the separation in phase space between the two solutions and estimate the associated Lyapunov-exponent, l (see p. 320-323 of Strogatz (1994)).

(e) Compare the "climate" of the two solutions, i.e. the time average of X, Y, and Z . You may have to extend your integration in time by many more than 5 non-dimensional time units to get a "stable" answer. What conclusions can you draw? Now, compare the "climate" of the absolute values of the two solutions, i.e. the time average of $|X|$, $|Y|$, and $|Z|$. What do you conclude from this?

(f) Model climate can also be characterised by the so-called "probability distribution function" ("pdf"). A plot of the "pdf" as a function of X and Y gives the probability of finding the Lorenz model state vector in any point in X-Y plane of phase space. Plot this "pdf" and interpret your result in the light of **(e).**

Answer to exercise 13

(a)

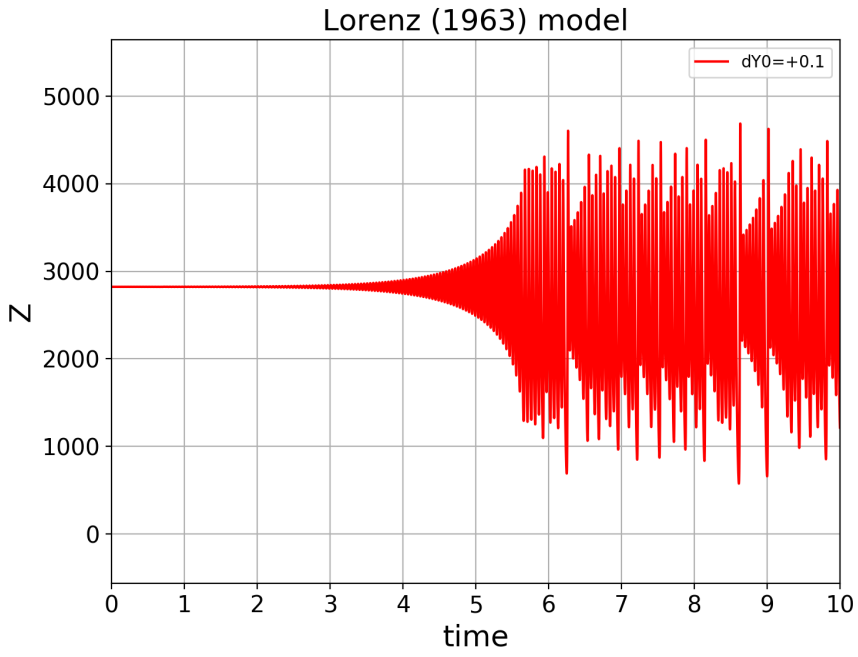

The initial condition for the first run (**run 1**) is (see exercise 6)

$$X = X_0;\ Y = Y_0 + 0.1;\ Z = Z_0.$$

Therefore, only Y is perturbed. Until t=5 the solution exhibits a constant period with an exponentially increasing amplitude. After t=5 it becomes non-periodic. The amplitude of the oscillation varies chaotically (figure above). The time between successive peaks also varies chaotically.

(b)

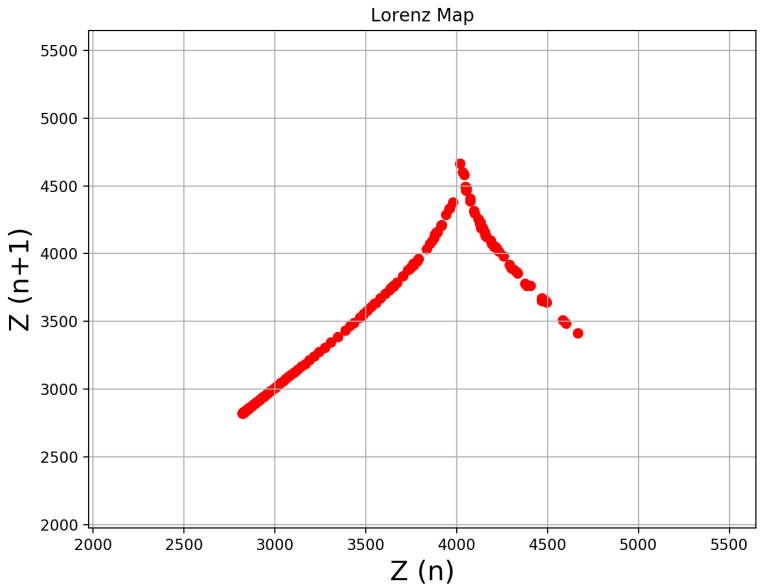

This "Lorenz map" is based on **run 1**, which was extended to 15 time units. The dots seem to lie on a line, implying that each peak-value is predictable from the previous peak value.

(c)

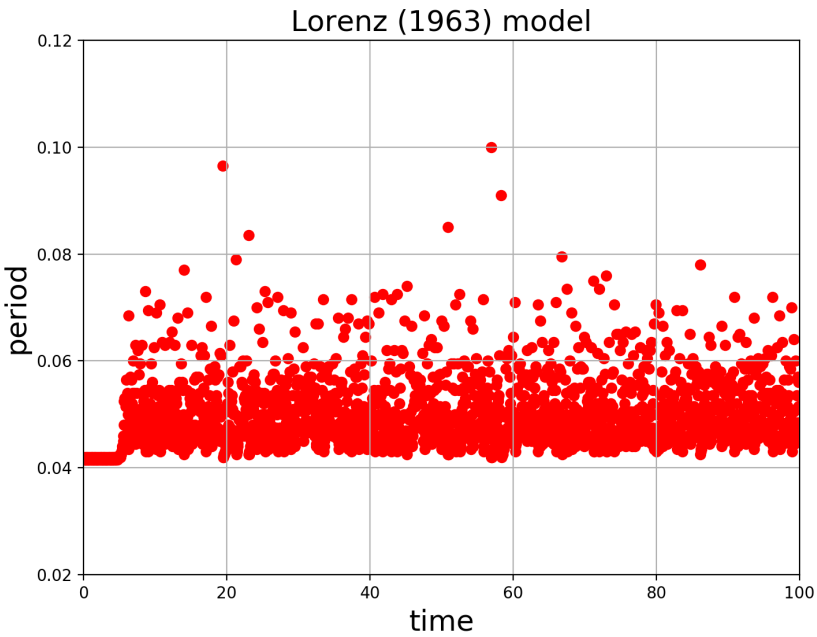

The time between successive peaks (plotted in the graph above) is constant initially, but varies erratically after t=5. Therefore, although the successive peak values themselves after t=5 are predictable, the time at which the next peak will occur is not predictable. This chaotic behaviour occurs after the solution has reached the limits of the "attractor" in phase space, as we will see in the next part of the exercise.

(d)

A **second run (run 2)** is performed with

$$X = X_0;\ Y = Y_0 + 0.2;\ Z = Z_0$$

as initial condition. The time evolution of Z in both integrations is shown in the graph below. The red line corresponds to integration shown in 10(a). The blue line corresponds to the time evolution in the second run, with a slightly different initial condition. The total time of integration is extended to 15 time units. In the first 5 time units the amplitude of the oscillation in the second run (blue) grows much faster than the amplitude of the oscillation in the first run (red).

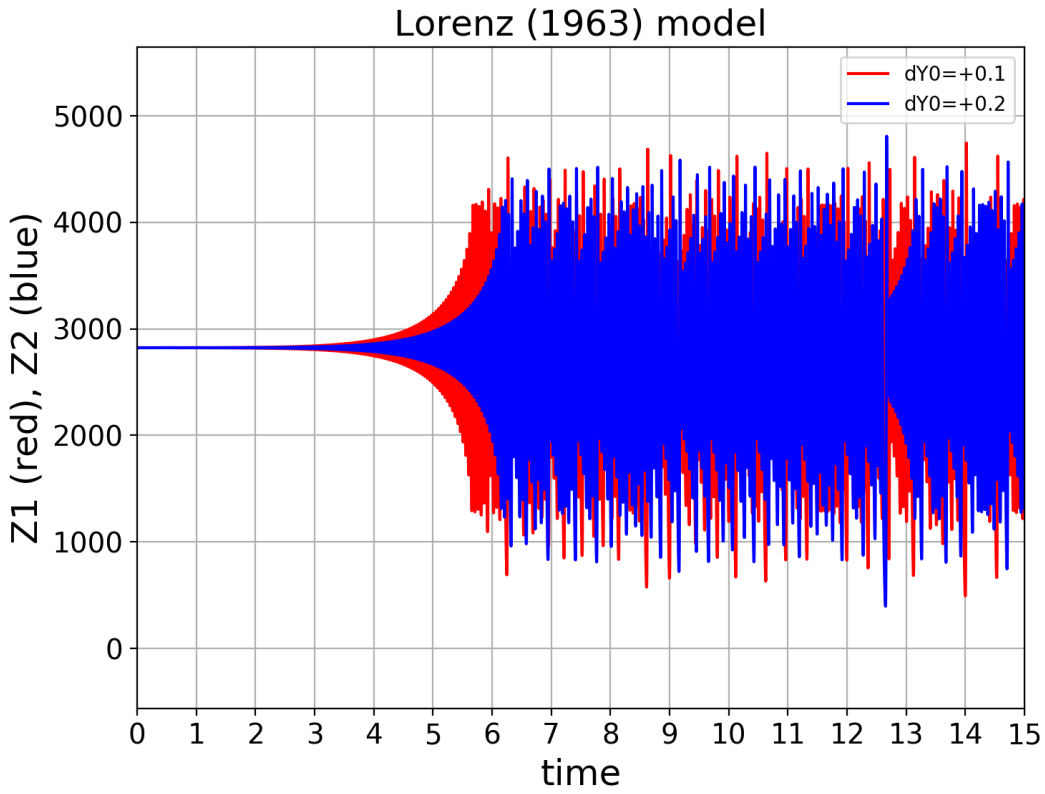

The graph on the next page shows the natural logarithm of δ as a function of time, where δ is defined as the distance between the two trajectories in three-dimensional phase space (with slightly different initial conditions) (see previous graph). The curve is similar to the schematic figure given in Strogatz (1994) (figure 9.3.5 on page 321). The Lyapunov exponent, λ, is estimated by fitting a straight line to the first part of the curve (e.g. between t=0 and t=4.0) and determining the slope of this line. This yields a slope, λ=1.33>0. This

means that the trajectories diverge exponentially. The divergence stops when the separation is comparable to the dimensions of the attractor.
Because the initial state in this case lies very close to the finite amplitude fixed point, it is also possible to determine the Lyapunov exponent from the matrix *M* in exercise 9. The Lyapunov exponent consists of three components, which correspond to the three eigenvalues of *M*. Each real part of each eigenvalue represents the Lyapunov exponent in one of the three directions in phase space.

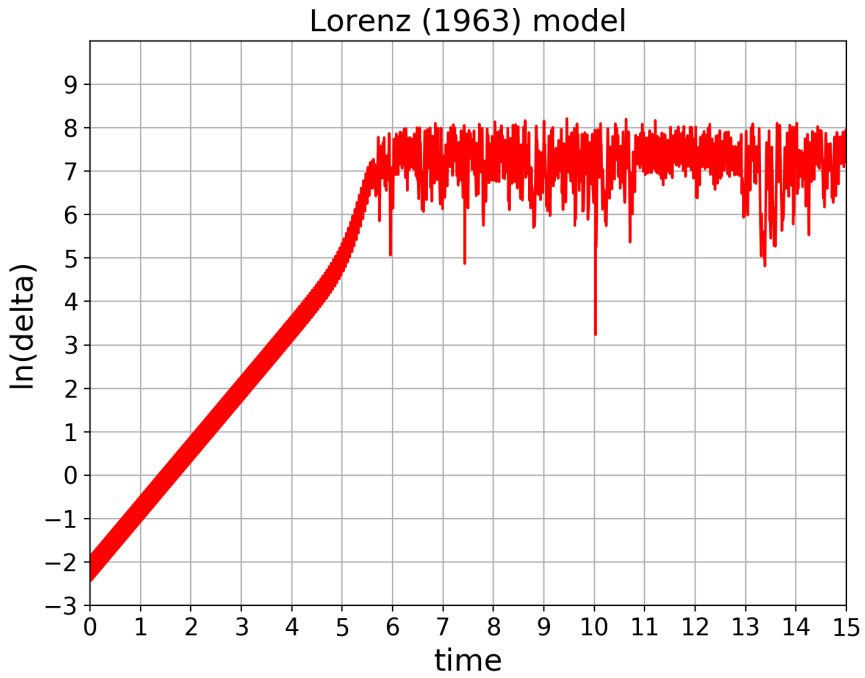

(e)
The steady values of of |*X*|, |*Y*| and |*Z*| are

$\mathbf{X_0}$	$\mathbf{Y_0}$	$\mathbf{Z_0}$
6.4	627.6	2823.2

The distance between the two trajectories in three-dimensional phase space increases exponentially in time during first 5 time units. After 5 tot 6 time units this distance oscillates around a quasi-constant value. The climate of the solution might best be determined by averaging the solution for, say, $t>7.5$. The "climate" of the two solutions, indeed, is quite similar when we take the average for $7.5<t<15$, as can be seen in the table below. Note that the climate does not coincide with the steady state!

The value of |*X*|, |*Y*| and |*Z*|, averaged over the last **7.5 time units** of both runs.

Run	**X**	**Y**	**Z**
1	4.85	513	2463
2	4.81	509	2455

Earth's climate is governed by non-linear equations. Therefore, it is very likely a chaotic system, with solutions similar to the chaotic solutions of the Lorenz equations, studied here. Can we derive some hope from this result for prediction of the statistics of Earth's climate in the coming decades?

Exercise 15

The Lorenz model represents the lowest order model of convection. It describes the growth, when the Rayleigh exceeds the critical Rayleigh, of the amplitude of one Fourier mode in both the stream function and the temperature, and the interaction of this Fourier mode with one additional Fourier mode, which represents the modification of the horizontal-mean temperature field by convection.

If the Rayleigh number exceeds the critical value for onset of convection for two Fourier modes $(l,n)=(1,1)$ and $(l,n)=(2,1)$: what will happen? The Lorenz model does **not** describe this situation in which more than one Fourier mode or wave is linearly unstable, or "self-excited".

If two modes grow, will this lead to a less ordered flow pattern? Observations indicate that this is mostly not the case (**figure 3**). It appears as if one Fourier mode predominates. Why is one discrete scale of motion selected?

These questions might be answered with an extension of Lorenz's (1963), in which two linearly unstable (self-excited) modes (or waves) with wave vectors, $(l,n)=(1,1)$ and $(l,n)=(2,1)$, are included inside the truncation. Which other modes would you include inside this truncated model? How many first order ordinary differential equations would this model have?

Answer to exercise 15

Because of the symmetry relations (eqs. 79-84), our attention is retricted to the upper right quadrant of two-dimensional wave number space. Due to the selection rule (eq. 74), the modes, which are excited by the interaction of (1,1) and (2,1), are (1,2) and (3,2). Therefore, to describe the interaction of the two basic modes, (1,1) and (2,1), we need to include (1,2) and (3,2). These wave modes are included inside the truncation of the Fourier expansion of the streamfunction and the temperature. This yields 8 nonlinear first order differential equations, describing the time evolution 8 amplitudes. In addition to this we need to include (0,2) and (0,4) in the Fourier expansion of the temperature. The modes, (0,1) and (0,3) are not included because these separately imply a non-zero average temperature perturbation. This yields a model consisting of 10 nonlinear first order differential equations.

(17)

For this exercise you are given the python-code of the 10-component model of two-dimensional convection, which integrates the twelve equations (105), and asked to install and run this code on your computer. Oscillations with a period in the range between 1 and 10 non-dimensional viscous time-units (H^2/ν) are observed in a layer of fluid with low Pr and Rayleigh numbers which are just super-critical to several times super-critical (Krishnamurti, 1973). The 10-component model also exhibits oscillations at low Pr (=0.1), with $a_x=1/2\sqrt{2}$ and for Rayleigh number 1.5 times supercritical.

(a) Can you qualitatively foresee the existence of these oscillations from eqs. 112 and 113?

(b) Investigate these oscillations in the 10-component model (105). Are the oscillations qualitatively in accord with your predictions based on eqs. 112 and 113?

(c) Do you get oscillations with periods similar to periods observed by Krishnamurti?

(d) Is this solution "chaotic"? If so, why?

(e) Make a scatter plot ("map") of the peak-values of A as a function of the previous peak-value of A. Compare this "map" with the Lorenz map (**figure 12**).

(f) Plot the time between successive peaks as a function of time half-way these peaks. What do you conclude from this?

Answer to exercise 17

(a)

The evolution of A, B, C and D in a model run with Pr =0.1, $a_x=1/2\sqrt{2}$ and for Ra 1.5 times supercritical yields the result shown in the graph below. The total time span of the integration is 500 time units. The amplitude of the oscillations in A (red line) varies between -0.05 and -0.11 units.

You can qualitatively foresee these oscillations form eqs. 112 and 113:

$$\frac{dA}{dt}=\left(\lambda_A+\mu_1 B^2\right)A;\ \frac{dB}{dt}=\left(\lambda_B+\mu_2 A^2\right)B,\ \mu_1>0 \text{ and } \mu_2<0.$$

Oscillations occur if $\lambda_A<0$ and $\lambda_B>0$: if B grows because $\lambda_B>0$, A will grow due to the term $\mu_1 B^2 A$, which, in turn will damp B due to the term $\mu_2 A^2 B$, which will arrest the growth of A, etc.

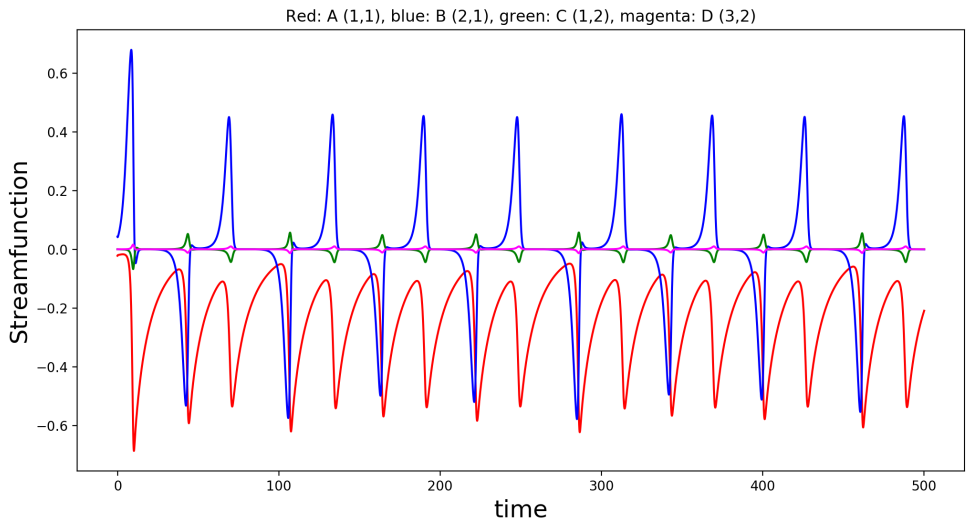

(b)
We see that, *A* grows when the amplitude of the linearly unstable mode (*B*) has reached exceeded threshold, after which *B* is damped by *A*, which, in turn makes *A* relax back to zero.
(c)
The period of the oscillations in *A* varies between 26 and 37 "conductive" time units. In terms of "viscous" time units, this would be 2.6 to 3.7 units, which is within the range of the measurements reported by Krishnamurti.
(d) The solution is "chaotic" because it depends on initial conditions. This is illustrated below. The initial conditions of these two solutions differ very little. On the left is the solution corresponding to the graph shown above. In particular, the mean value of *A*, differs appreciably (negative on the left and positive on the right).

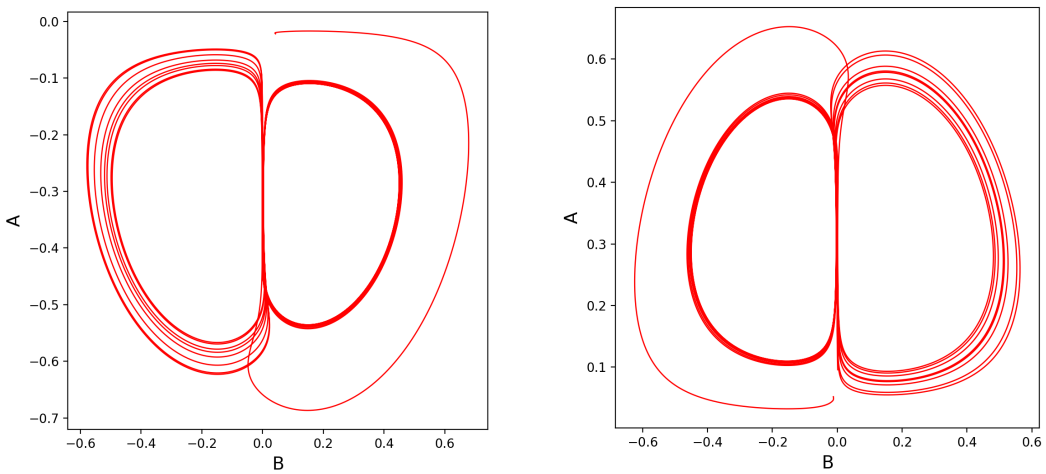

(e)
The map is shown below. The dots seem to lie on a smooth curve with no "thickness", as is the case with the Lorenz map (**section 19**). The amplitude of a peak can be predicted with knowledge of the amplitude of the previous peak!

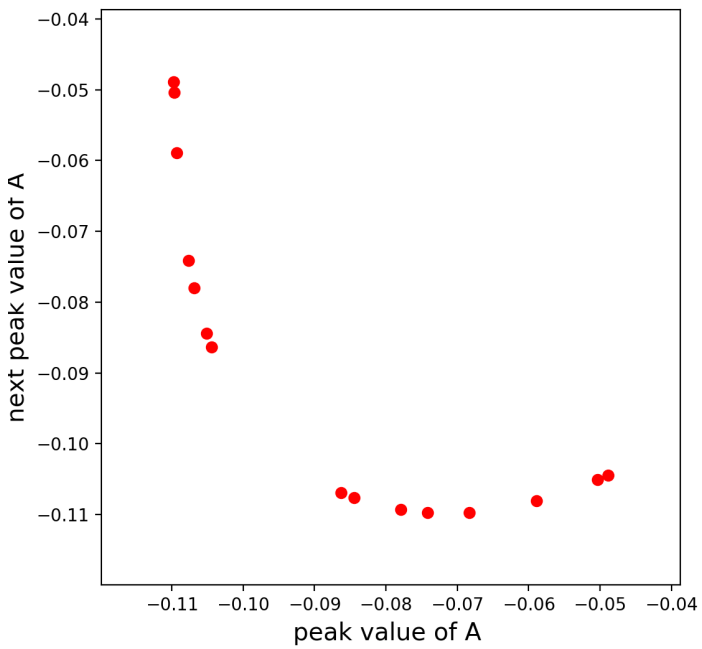

(f)

The scatter plot below shows the period (non-dimensional time units) between two peaks in chronological order for the integration lasting 500 time units. The statistics excludes the first two peaks. Conclusion: although the amplitude of the next peak may be predictable (**part e**), when it will occur is not predictable.

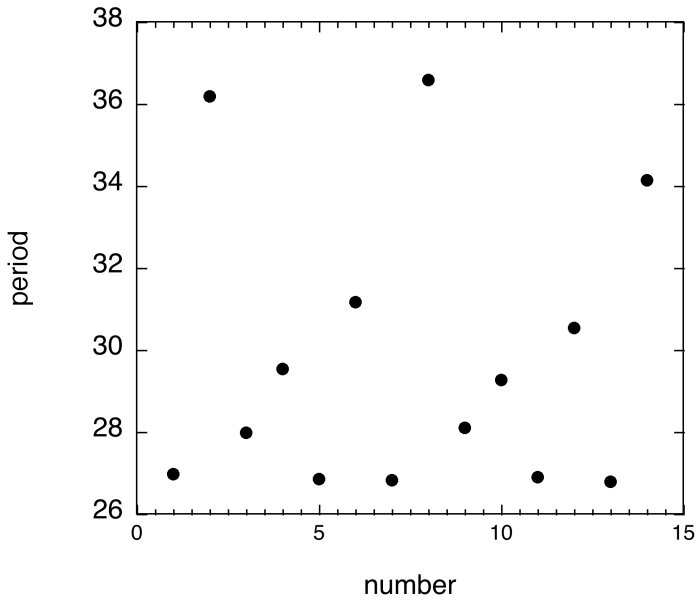

(18)
Show that the steady state solutions of the Lorenz (1963) model are also solutions of the 12-component model of poloidal thermal convection (eqs. 163). Derive expressions for these solutions.

Answer to exercise 18

The Lorenz model can be retrieved from the 12-component model equations bt putting all coefficients equal to zero, except W_{021}, Θ_{021} and Θ_{002}. If we use the short notation of the Lorenz model, i.e. $W_{021}=X$, $\Theta_{021}=Y$ and $\Theta_{002}=Z$, we obtain the follwing set of equations:

$$\frac{dX}{dt} = \frac{4a^2 \mathrm{Pr}}{4a^2+1} Y - \pi^2 \mathrm{Pr}(4a^2+1)X$$
$$\frac{dY}{dt} = -2\pi ZX + RaX - \pi^2(4a^2+1)Y$$
$$\frac{dZ}{dt} = 4\pi XY - 4\pi^2 Z$$

The steady states are found by putting the time-derivative equal to zero. The expression for the steady state value, X_0, of X is

$$X_0^2 = \frac{2a^2}{\pi^2(4a^2+1)^2}\left(Ra - \frac{\pi^4(4a^2+1)^3}{4a^2}\right) = \frac{2a^2}{\pi^2(4a^2+1)^2}\left(Ra - Ra_c\right),$$

The steady state value, Y_0, of Y is related to X_0 by

$$Y_0 = \frac{\pi^2(4a^2+1)^2}{4a^2} X_0,$$

Furthermore:

$$Z_0 = \frac{X_0 Y_0}{\pi}.$$

With the above, we find that

$$Z_0 = \frac{1}{2\pi}(Ra - Ra_c),$$

where

$$Ra_c \equiv \frac{\pi^4(4a^2+1)^3}{4a^2}.$$

(19)

(a) Make a vertical cross section of the vertical velocity and the associated temperature distribution at $x=L_x/2$, as a function of y and z, for steady hexagonal convection, according to the 12-component model of poloidal convection (eqs.163). The corresponding values of the Fourier coefficients are: W_{111}=-3.93, W_{021}=-3.93, W_{112}=0.22, W_{022}=0.22, Θ_{111}=-179.3, Θ_{021}=-179.3, Θ_{112}=-1.2, Θ_{022}=-1.2, Θ_{001}=564.8, Θ_{002}=672.8, Θ_{003}=-21.6, Θ_{004}=-0.1 (Ra=5000, $a=1/(2\sqrt{2}$ and $\overline{\Theta}_{001}$=500). Units are non-dimensional (eq. 48). Is this an up- or a down-hexagon?

(b) Make a plot of the associated horizontal mean temperature profile, as in **figure 19**.

Answer to exercise 19

(a)

In the cross-section below, red and blue shading represents temperature, normalised with Ra. The temperature ranges from -1.1 to 0, with red: >-0.5 and blue: <0.5. Contours represent vertical velocity. Contour interval: 5 non-dimensional units; solid: positive; dashed: negative. This is an up-hexagon.

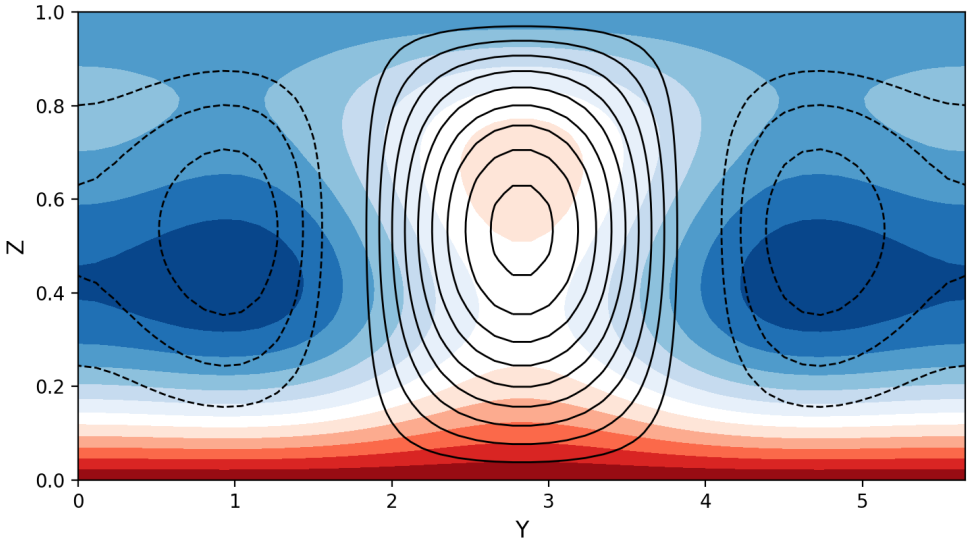

(b)

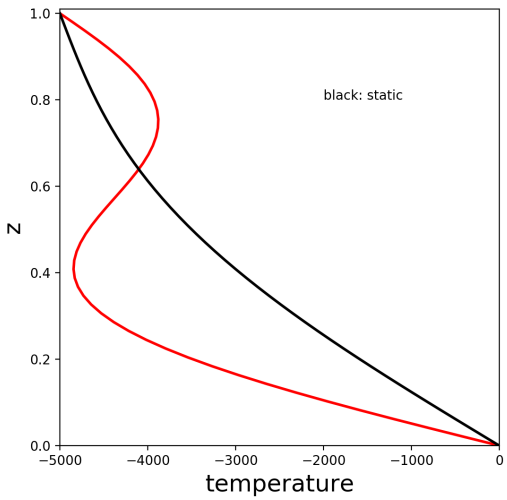

Red line: temperature profile corresponding to the up-hexagon (units: non-dimensional).

(20)
The total kinetic energy is defined as

$$K \equiv \frac{1}{2}\int\left(u^2+v^2+w^2\right)d\sigma\,.$$

Here $d\sigma$ is a volume element. The integration extends over the region defined by eq. 123. The relation between the different velocity components in spectral space is given in eqs 140 and 141.
(a) Transform the above expression for the total kinetic energy to spectral space, assuming that the flow is poloidal.
(b) Show that total kinetic energy is conserved by the nonlinear terms in the low-order 12-component model of poloidal thermal convection (eqs. 163).

Answer to exercise 20

(a) For simplicity we Fourier transform one of the three terms in the definition of *K*:

$$K \equiv \frac{1}{2}\int\left(w^2\right)d\sigma\,.$$

Substituting the Fourier series for *w* into this equation we find

$$K \equiv \frac{1}{2}\int\sum_\alpha W_\alpha S_\alpha \sum_\beta W_\beta S_\beta d\sigma = \frac{1}{2}\int\sum_\alpha W_\alpha S_\alpha \sum_\beta W_\beta S^*_{-\beta} d\sigma = \frac{1}{2}\int\sum_{\alpha,\beta} W_\alpha W_\beta S_\alpha S^*_{-\beta} d\sigma\,.$$

Because

$$\int S_\alpha S^*_{-\beta} d\sigma = \delta_{\alpha,-\beta}\,,$$

non-zero contributions to the integral are found only if α=-β. Therefore

$$K = \frac{1}{2}\sum_\alpha W_\alpha W_{-\alpha} = \frac{1}{2}\sum_\alpha -W^I_\alpha W^I_{-\alpha} == \frac{1}{2}\sum_\alpha\left(W^I_\alpha\right)^2\,.$$

Here we have used information from section 35 (eqs 160 and 156a).
The total kinetic is (dropping the superscript, *I*),

$$K = \frac{1}{2}\sum_\alpha\left\{\left(U_\alpha\right)^2+\left(V_\alpha\right)^2+\left(W_\alpha\right)^2\right\}\,.$$

Using the diagnostic relations derived form the continuity equation and the definition of the vertical component of the vorticity,

$$U_\alpha = -\frac{a_x n_\alpha l_\alpha}{q^2_\alpha} W_\alpha \text{ and } V_\alpha = -\frac{a_y n_\alpha m_\alpha}{q^2_\alpha} W_\alpha\,,$$

we obtain

$$\boxed{K = \frac{1}{2}\sum_{\alpha}\left\{\frac{k_\alpha^2}{\pi^2 q_\alpha^2}(W_\alpha)^2\right\}}.$$

(b) Remember that the sum over all wave vectors within the truncation of the model includes the negative wave numbers also. This means that if the wave vector (1,1,1) is included, then this means that (-1,-1,1), (-1,1,1), (-1,-1,1), (1,1,-1), (-1,-1,-1), (-1,1,-1), (-1,-1,-1) re also included. From eqs. 142 and 143 we find:

$$q_{111}^2 = q_{021}^2 = q_{112}^2 = q_{022}^2 = a_x^2 + a_y^2 = 4a^2$$

and

$$k_{111}^2 = k_{021}^2 = \pi^2(4a^2+1)\ ;\ k_{112}^2 = k_{022}^2 = \pi^2(4a^2+4).$$

Using the symmetry relations listed in section 35, the total kinetic energy in the twelve-component model of poloidal convection:

$$K = \frac{1}{2}\left(8\left(\frac{4a^2+1}{4a^2}\right)W_{111}^2 + 4\left(\frac{4a^2+1}{4a^2}\right)W_{021}^2 + 8\left(\frac{4a^2+4}{4a^2}\right)W_{112}^2 + 4\left(\frac{4a^2+4}{4a^2}\right)W_{022}^2\right)$$

The equations governing the spectral amplitudes of the vertical velocity are (eqs. 163)

$$\frac{dW_{111}}{dt} = -\frac{3}{2}\pi W_{022}W_{111} - \frac{3}{2}\pi W_{021}W_{112}$$
$$\frac{dW_{021}}{dt} = -3\pi W_{112}W_{111}$$
$$\frac{dW_{112}}{dt} = 3\pi\frac{4a^2+1}{4a^2+4}W_{111}W_{021}$$
$$\frac{dW_{022}}{dt} = 3\pi\frac{4a^2+1}{4a^2+4}W_{111}^2$$

The time evolution of the total kinetic is given by

$$\boxed{\begin{aligned}&\frac{dK}{dt} = 2\left(\frac{4a^2+1}{a^2}\right)\frac{dW_{111}^2}{dt} + \left(\frac{4a^2+1}{a^2}\right)\frac{dW_{021}^2}{dt} + 2\left(\frac{4a^2+4}{a^2}\right)\frac{dW_{112}^2}{dt} + \left(\frac{4a^2+4}{a^2}\right)\frac{dW_{022}^2}{dt}\\ &= -3\pi\left(\frac{4a^2+1}{a^2}\right)W_{022}W_{111}^2 - 3\pi\left(\frac{4a^2+1}{a^2}\right)W_{021}W_{112}W_{111} - 3\pi\left(\frac{4a^2+1}{a^2}\right)W_{112}W_{111}W_{021}\\ &+6\pi\left(\frac{4a^2+1}{a^2}\right)W_{111}W_{021}W_{112} + 3\pi\left(\frac{4a^2+1}{a^2}\right)W_{111}^2W_{022} = 0.\end{aligned}}$$

Total kinetic energy is conserved.

(21)
Apply the adiabatic elimination technique to the latter 4 model equations in the equation set (163), following the procedure that is presented in **section 25**. Assume that W_{111} and W_{021} are self-excited and that W_{112} and W_{022} are damped. The damped modes are slaved to the self-excited modes. Note that the positive relaxation coefficients for W_{111} and W_{021} are equal, as are the negative relaxation coefficients for W_{112} and W_{022}. Identify the steady state convection patterns and analyse their stability, using the resulting two equations (**figure 19**).

Answer to exercise 21

Following the procedure presented in section 25 we write the latter four equations in the eq. set (163) as follows.

$$\frac{dA}{dt} = -\frac{3}{2}\pi AD - \frac{3}{2}\pi BD + \lambda_A A$$
$$\frac{dB}{dt} = -3\pi AC + \lambda_B B$$
$$\frac{dC}{dt} = \chi AB - \frac{3}{2}\pi BD + \lambda_C C$$
$$\frac{dD}{dt} = \chi A^2 + \lambda_D D$$

where

$$A \equiv W_{111};\ B \equiv W_{021};\ C \equiv W_{112};\ D \equiv W_{022}\ ,$$

and

$$\chi \equiv 3\pi \frac{4a^2+1}{4a^2+4} > 0\,.$$

The linear terms in the original equations have been bundled together as a linear growth or damping term. Exponential growth occurs if the coefficient, λ, is positive, while exponential damping occurs if the coefficient, λ, is negative. The critical Rayleigh numbers for mode *A* and mode *B* are identical, because the total wave number, *k* (eq. 143), of these modes is identical. Therefore

$$\lambda_A = \lambda_B \equiv \lambda_1 > 0$$

if this critical Rayleigh number is exceeded. For $a=1/(2\sqrt{2})$, the critical Rayleigh number of modes *A* and *B* is 657 (see exercise 2). For this value of *a*,

$\chi=\pi$.

The critical Rayleigh numbers for mode *C* and mode *D* are identical, because the total wave number, *k*, of these modes is identical. The critical Rayleigh number for the modes with $n=2$ (=17753 if $a=1/(2\sqrt{2})$; see exercise 2) is much higher than the critical Rayleigh number for a mode with $n=1$ (=657 if $a=1/(2\sqrt{2})$). If the critical Rayleigh number of *C* and *D* is not exceeded

$\lambda_C = \lambda_D \equiv \lambda_2 < 0$.

Hence we can apply the Herman Haken's adiabatic elimination technique, which leads to

$$D = -\frac{\chi}{\lambda_2} A^2 \text{ and } C = -\frac{\chi}{\lambda_2} AB. \quad (1)$$

Substituting this into the equations for the time evolution of *A* and *B* yields

$$\frac{dA}{dt} = \left(-\mu A^2 - \mu B^2 + \lambda_1\right) A \ , \quad (2a)$$

$$\frac{dB}{dt} = \left(-2\mu A^2 + \lambda_1\right) B \ . \quad (2b)$$

With $\chi=\pi$,

$$\mu \equiv -\frac{3}{2}\frac{\pi^2}{\lambda_2} > 0 \text{ because } \lambda_2 < 0 \ .$$

The steady states are

(1) $A_0 = B_0 = 0$: rest-state;

(2) $A_0 = \pm\sqrt{\frac{\lambda_1}{\mu}}$; $B_0 = 0$; $C_0 = 0$; $D_0 = -\frac{\chi}{\lambda_2}\frac{\lambda_1}{\mu} > 0$: unknown (3D) pattern;

(3) $A_0 = \pm\sqrt{\frac{\lambda_1}{2\mu}}$; $B_0 = \pm\sqrt{\frac{\lambda_1}{2\mu}}$; $C_0 = \pm\frac{1}{2}\frac{\chi}{\lambda_2}\frac{\lambda_1}{\mu}$; $D_0 = -\frac{1}{2}\frac{\chi}{\lambda_2}\frac{\lambda_1}{\mu} > 0$: hexagonal (3D) pattern.

The rest-state (steady state number 1) is unstable to small perturbations in *A* and *B* if $\lambda_1>0$.

If *A* is perturbed while *B*=0, the system will settle into steady state number (2) in the list above. The perturbation in *A* will grow only if the perturbation is so small that

$$A^2 < \frac{\lambda_1}{\mu}.$$

If this condition is satisfied, a pattern will reach steady state number 2. In this steady state, *B* will remain equal to zero because

$$\frac{dB}{dt} = \left(-2\mu A^2 + \lambda_1\right) B = -\lambda_1 B$$

implying that *B* is damped since $\lambda_1>0$.

If the initial value of *A* is such that

$$A^2 > \frac{\lambda_1}{\mu} \ ,$$

the perturbation will relax back to the steady state value, $(\lambda_1/\mu)^{1/2}$, implying that the second steady state, in the list above, is stable.

A 2D (roll) convection pattern, with A=0, is possible, but not in a steady state, according to eqs 2a,b. This is because a perturbation in B, while A=0, will grow exponentially according to

$$\frac{dB}{dt} = \lambda_1 B,$$

because λ_1>0. If

$$B^2 > \frac{\lambda_1}{\mu}.$$

A will not grow, even if A is perturbed. The process that ultimately halts the exponential growth of B is captured by the equations for Θ_{021} and Θ_{002} (eqs. 163).

It is not possible to say something definite about the stability of steady state solution number 3.

(22)
For this exercise you are given the python-code of the low-order model of poloidal convection, which integrates the twelve equations (163), and asked to install and run this code on your computer. As described on page 56, identify the basins of attraction in the plane, W_{111} versus W_{021}, of the three possible steady state solutions of the 12-component model (eqs. 163): rolls, up-hexagons, and down-hexagon. Do this for Pr=5, Ra=5000 and a=1/(2√2) and $\overline{\Theta}_{001}$=0.

Answer to exercise 22

The scatter plot below shows the result of 1000 model integrations (eqs. 163), lasting 25 time units, with Ra=5000, Pr=5, a=1/(2√2) and $\overline{\Theta}_{001}$=0. The black circles with coloured crosses represent the steady states in terms of W_{111} and W_{021} at these parameter values, where red is a down hexagon, blue is an up-hexagon and green is a roll. The steady state of rest (W_{111}=W_{021}=0) is not indicated explicitly because it is linearly unstable. The **red dots** represent the initial values of W_{111} and W_{021} of runs, which have a **down-hexagon** as final stable steady state. The **blue dots** represent the initial values of W_{111} and W_{021} of runs, which have a **up-hexagon** as final stable steady state. The **green dots** represent the initial values of W_{111} and W_{021} of runs, which have a **roll convection pattern** as final stable steady state. The 1000 integrations lead to rolls in 386 cases, up-hexagons in 298 cases and down-hexagons in 315 cases. The fixed points associated with steady state hexagons appear to lie very close to the edge of their respective basins of attraction, bordering the basins of attraction of rolls. Sensitivity to initial conditons is greatest near the state of rest.

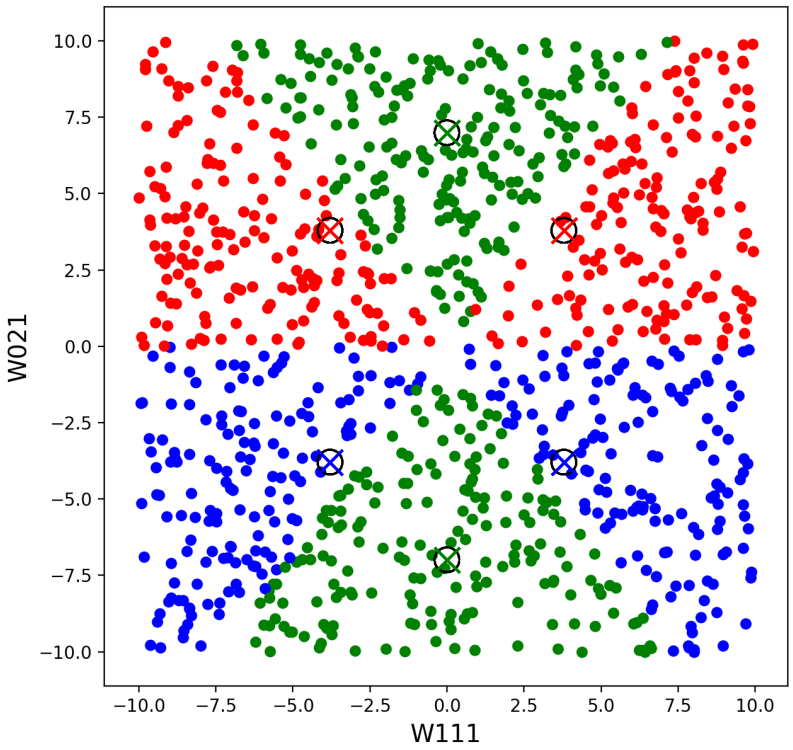

Below the result of repeating this mathematical experiment with a different value of $\overline{\Theta}_{001}$ (=500). The 1000 integrations lead to rolls in 477 cases, up-hexagons in 269 cases and down-hexagons in 252 cases. The "basins of attraction" of rolls (**green dots**) expand at the cost of the basins of attraction of down-hexagons (**red dots**).

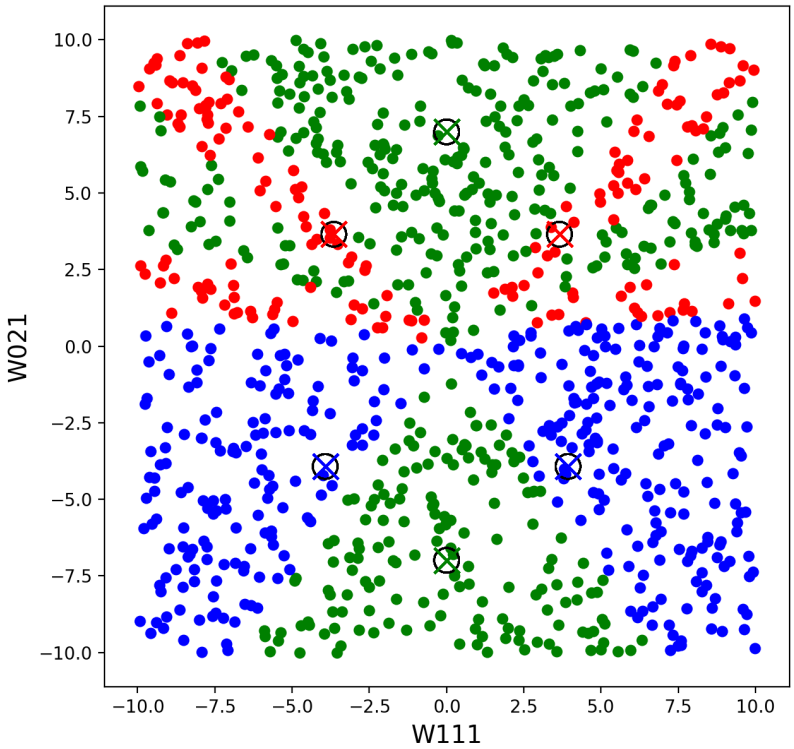

(23)
Investigate the stability of the finite amplitude convective steady state solution of the Lorenz model (exercise 18) in the low-order model of poloidal convection as a function of Ra and Pr, by performing model-integrations in which the initial steady state solution is perturbed slightly, assuming that a=1/(2√2) and $\overline{\Theta}_{001}$=0.

Answer to exercise 23

We use the result of exercise 18. The steady state convective solutions of the Lorenz model are

$$W_{021} = \frac{a}{\pi(4a^2+1)}\sqrt{2(\mathrm{Ra}-\mathrm{Ra}_c)};\ \Theta_{021} = \frac{\pi(4a^2+1)}{4a}\sqrt{2(\mathrm{Ra}-\mathrm{Ra}_c)};\ \Theta_{002} = \frac{W_{021}\Theta_{021}}{\pi}$$

$$W_{021} = \frac{-a}{\pi(4a^2+1)}\sqrt{2(\mathrm{Ra}-\mathrm{Ra}_c)};\ \Theta_{021} = \frac{-\pi(4a^2+1)}{4a}\sqrt{2(\mathrm{Ra}-\mathrm{Ra}_c)};\ \Theta_{002} = \frac{W_{021}\Theta_{021}}{\pi}$$

We substitute these expressions in the model as initial condition and then perturb the initial state slightly, and check what happens for different Ra and Pr when we integrate the model numerically. The initial state is perturbed by adding random numbers between -1 and +1 to the amplitudes, W_{021}, Θ_{021} and Θ_{002}. We calculate the distance in phase space between the perturbed initial condition and the fixed point, corresponding to the steady state. At the end of the integration we calculate the distance in phase space between the final state and the fixed point. The fixed point is unstable if the distance to the fixed point has increased. The fixed point is stable if the distance to the fixed point has decreased. The diagram below shows the result. A stable solution is indicated by circles; an unstable solution is indicated by red crosses. Note that Lorenz's (1963, p.136) result is recovered, namely that, when Pr=10, the finite amplitude convection is linearly unstable if $\mathrm{Ra}/\mathrm{Ra}_c$>24.74 (see also **exercise 9**).

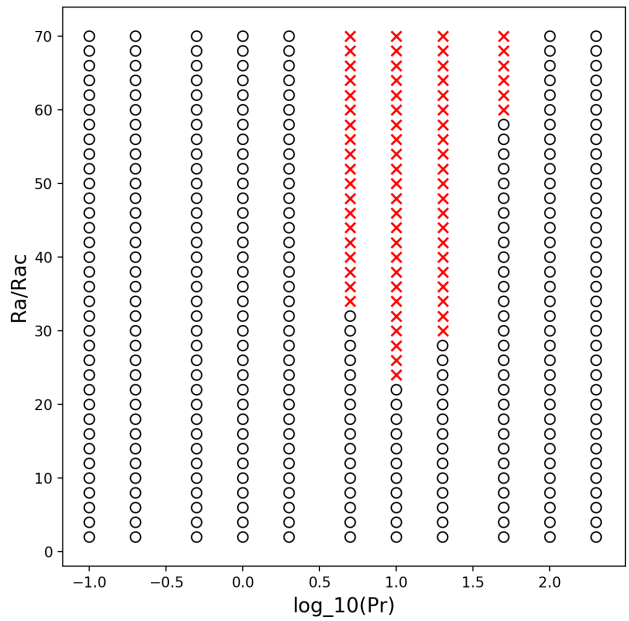

Next, the initial state is perturbed by adding random numbers between -1 and +1 to the amplitudes, Θ_{111}, W_{021}, Θ_{021} and Θ_{002}. Whereas in the previous calculation Lorenz's solution is perturbed only "from the inside", we are now perturbing the solution also "from the outside", i.e in the amplitude, Θ_{111}. The result is shown below. The region of instability is much larger.

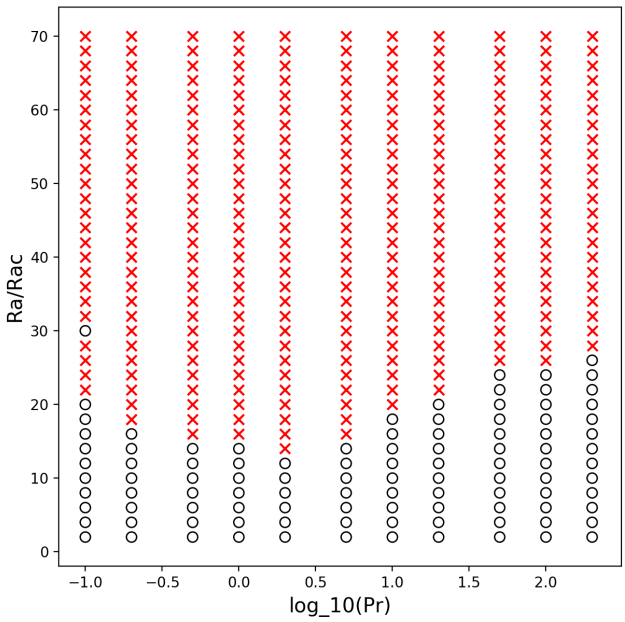

Finally we repeat this analysis, but now we also perturb W_{021} initially, next to Θ_{111}, W_{021}, Θ_{021} and Θ_{002}.

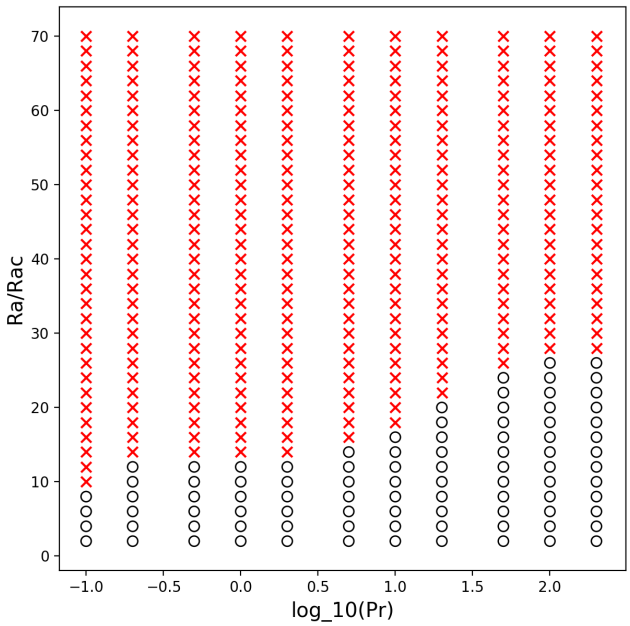

EXTRA QUESTIONS

(16) (homework)
In this exercise you are asked to perform a simulation with the ten-component model (equation set 105) and analyse the output by answering the questions below.
(a) Perform two simulations for Pr=0.1 and Pr=10, respectively with the following parameter values fixed by j=1, $a_x=1/2\sqrt{2}$, and Ra=20Ra$_c$.
Give the student the result of an integration of 10-component model at fixed Ra and Pr (0.1) (other parameters identical to simulation illustrated in **figure 14/15**)
Determine the growth(damping) rates or relaxation coefficients of the 4 modes at this Ra. Use these to determine the μ's and then integrate eqs. 109 and 110.

Question about hystereis …
(17)
Write a computer program, which numerically integrates eqs. 71 and 76 taking into account the symmetry relations listed in eqs. 79-82, and simulates the spectral energy cascade, which is described in section 10. Truncate the spectrum such that wave numbers for which $|l+n|\leq N$ are taken into account, where N varies from 2 to 10. Check energy conservation by the nonlinear interactions. Integrate the equations for $a_x=1/\sqrt{2}$, Pr=10 and Ra=28Ra$_c$. Interpret the result in the light of the discussion in section 10. (Use the RK-4 scheme, given is section 22).